千葉工業大学

博士学位論文

Theoretical study on the molecular mechanism of drug resistance in influenza A viruses

（A型インフルエンザウイルスの薬剤耐性の分子機構に関する理論的研究）

2022 年 3 月

Mohini Yadav

Acknowledgement

I would like to express my great appreciation and thanks to my supervisor Dr. Norifumi Yamamoto for guiding me on my scientific path with patience and kindness and always believing in me. My deep gratitude also goes to my second supervisor Dr. Gota Kawai for his continuous guidance and support. I would also like to sincerely thank my research collaborator, Dr. Manabu Igarashi, for his continuous guidance and support. I would also like to sincerely thank all my doctoral thesis evaluation committee members, Dr. Taiichi Sakamoto, Dr. Naozumi Teramoto, and Dr. Hidenori Matsuzawa, your encouraging words and thoughtful, detailed feedback have been very important to me. I would also like to sincerely thank Dr. Kaoru Onoe for his continuous support. I would also like to sincerely thank all my colleagues in the laboratory for being kind and always helping me.

My scientific endeavor as a doctoral student would not have been possible without my work being funded. Therefore, I would like to thank the Joint Usage/Research Center Program at Research Center for Zoonosis Control, Hokkaido University for providing financial support. I would also like to thank the TSUBAME Encouragement Program for Young/Female Users, Tokyo Institute of Technology for rewarding me with their scholarship to carry out molecular simulations on the TSUBAME supercomputer. I would also like to thank Watanuki International Scholarship Foundation for rewarding me with their scholarship. I would also like to thank Prof. Silvio Tosatto for providing the binary version of the RING 2.0 software.

A huge thank you goes to my parents and brother for love and support during my doctoral study in Japan, far from home. I would also like to thank all my extended family members and friends for their continuous love and support.

List of original publications included in the thesis

Yadav M, Igarashi M, Yamamoto N. 2021a. Dynamic residue interaction network analysis of the oseltamivir binding site of N1 neuraminidase and its H274Y mutation site conferring drug resistance in influenza A virus. *PeerJ* **9:**e11552 **DOI:**10.7717/peerj.11552

Yadav M, Igarashi M, Yamamoto N. 2021b. Theoretical insights into the molecular mechanism of I117V mutation in neuraminidase mediated reduction of oseltamivir drug susceptibility in A/H5N1 influenza virus. *PeerJ Physical Chemistry* **3:**e19 **DOI:**10.7717/peerj-pchem.19

Abstract

Influenza is a highly contagious respiratory illness caused by influenza virus. An influenza virus surface glycoprotein, neuraminidase (NA), plays a key role in the replication and transmission of influenza virus; thus, anti-influenza drugs that inhibit the function of NA have been developed. Currently, four types of NA inhibitors, oseltamivir (OTV), zanamivir, peramivir, and laninamivir are used in Japan for influenza treatment and prevention. On the other hand, in recent years, the emergence of influenza virus mutant strains resistant to NA inhibitors has been frequently reported. Previously, several studies have reported on the drug resistance mechanism of the influenza virus, but the detailed molecular mechanism of drug resistance in the influenza virus has not yet been clarified. In this study, the detailed molecular mechanism of drug resistance in two mutant strains of A/H5N1 influenza virus, H274Y mutant strain and I117V mutant strain, which reduces OTV susceptibility to NA as compared to wild type (WT), has been elucidated using molecular dynamics (MD) simulations.

In the study of the H274Y mutant strain, a new method, dynamic residue interaction network (dRIN) analysis based on MD simulations, has been developed to provide statistical insights into the residue interactions. The results of dRIN analysis revealed that the OTV binding site and H274Y mutation site of NA interact indirectly via the three interface residues connecting the two sites. After H274Y mutation, the interactions between residue 274 and the three interface residues significantly enhanced, resulting in significant reduction in interaction between OTV and its surrounding 150-loop residues. Thus, it was concluded that such changes in interactions between residues could cause the reduction in binding affinity of NA to OTV, resulting in OTV drug resistance in H274Y mutant strain of A/H5N1 influenza viruses.

In the study of the I117V mutant strain, the characteristics structural changes of NA associated with the I117V mutation were elucidated based on MD simulations. The MD simulations results revealed that after the I117V mutation, the secondary structure near the mutation site of NA changed, leading to the change in the interactions between residues at the OTV binding site of NA, causing the reduction in binding affinity of NA to OTV, resulting in reduced OTV susceptibility in I117V mutant strain of A/H5N1 influenza viruses.

Hence, in this study, the drug resistance mechanism of H274Y mutant strain and I117V mutant strain of A/H5N1 influenza virus was successfully elucidated using MD simulations. Finally, the dRIN analysis used in this study can be applied to a wide variety of systems, including individual proteins, protein-protein complexes, and protein-ligand complexes, to provide statistical insights into the residue interactions.

Table of Contents

Appendices

1. Introduction

1.1. Influenza virus

Influenza, also known as flu, is a highly contagious respiratory illness caused by influenza virus, resulting in mild to severe illness and sometimes even death (*Palese, 2004*).

1.1.1. Classification and Nomenclature

Influenza viruses belonging to the *Orthomyxoviridae* (formed from two Greek words, *orthos* (straight) and *myxa* (mucus)) virus family are enveloped, negative-sense, segmented, single-stranded RNA viruses (*Cox et al., 2010; Shaw & Palese, 2013*). So far, based on the core proteins, four types of influenza viruses have been identified, including influenza A virus (IAV), influenza B virus (IBV), influenza C virus (ICV), and influenza D virus (IDV) (*Hause et al., 2013; Hause et al., 2014; Ritchey et al., 1976*). IAV infect humans as well as various birds and mammals; the main reservoir is aquatic birds (*Parrish et al., 2015; Webster et al., 1992*). IBV and ICV infect pigs and humans (*Ran et al., 2015*). IDV infect pigs and cattles (*Hause et al., 2013; Hause et al., 2014*). IAV are categorized into subtypes based on the antigenicity of the surface proteins, Hemagglutinin (HA) and Neuraminidase (NA). So far, eighteen HA subtypes (H1-H18) and eleven NA subtypes (N1-N11) have been identified (*Schrauwen & Fouchier, 2014*).

For naming the strains of influenza viruses, the currently used nomenclature system includes, the virus type, the virus isolation host species (not mentioned if human), the location of virus isolation, the isolate number, the isolation year, and only for IAV, the subtype of HA and NA is mentioned in the brackets (e.g., A/Vietnam/1203/2004 (H5N1) and A/chicken/Bangli/BBVD-562/2007 (H5N1)) (*World Health Organization, 1980*).

1.1.2. Genome organization

The single stranded and negative sense RNA (complementary to mRNA) of IAV and IBV is segmented into 8 segments and are numbered from the longest to the shortest segment in descending order (segment 1 to 8) (*Palese & Shaw, 2007*). The complete genome of IAV and IBV contains ~13,600 nucleotides and ~14,600 nucleotides, respectively(*Shaw & Palese, 2013*). So far, the genome of IAV was found to encode fifteen different viral proteins, whereas the genome of IBV was found to encode eleven different viral proteins (*Krug & Fodor, 2013; Muramoto et al., 2013*).

The viral replication machinery components are encoded by 3 largest segments and the 5th largest segment, i.e., the RNA dependent RNA polymerase subunits, PB2 (encoded by segment 1), PB1 (encoded by segment 2) & PA (encoded by segment 3), and the nucleoprotein protein NP (encoded by segment 5). In IAV, two additional proteins, PB1-40 and PB1-F2 are also encoded by PB1 segment (segment 2) (*Chen et al., 2001; Wise et al., 2009*). In IAV, three additional proteins, PA-155, PA-X, and PA-N182 are also encoded by PA segment (segment 3) (*Jagger et al., 2012; Muramoto et al., 2013*). The viral surface glycoproteins are encoded by the 4th and 6th largest segments, i.e., hemagglutinin (HA) (encoded by segment 4) and neuraminidase (NA) (encoded by segment 6). In IBV, the NA segment (segment 6) also encodes for an additional protein, NB (*Jackson et al., 2011*). The M1 matrix protein and the ion channel protein (named M2 in IAV and BM2 in IBV) are encoded by the 7th largest segment (segment 7). However, the coding mechanism for the ion channel protein is different in IAV and IBV. The ion channel protein M2 is encoded by using a splice mechanism in IAV, whereas the ion channel protein BM2 is encoded by using an overlapping stop-start pentanucleotide in IBV (*Krug & Fodor, 2013*). The interferon-antagonist non-structural protein 1 (NS1) is encoded by smallest segment (segment 8) using an unspliced mRNA (*Dauber et al., 2004; García-Sastre, 2001; Kochs et al., 2007*). The nuclear export protein (NEP, previously known as non-structural protein 2 (NS2)) is encoded by segment 8 using a spliced mRNA (*Briedis & Lamb, 1982; Lamb et al., 1980*).

The conserved nucleotides present at both ends of the viral RNAs (vRNAs) act as promoters for replication and transcription. The viral RNA dependent RNA polymerase complex transcribes the negative-sense vRNAs into capped and polyadenylated mRNAs. During replication, the viral RNA dependent RNA polymerase complex synthesizes a positive-sense vRNA copy (called cRNA) that is used as a template to synthesize vRNAs for the propagation of the virus. The replication and transcription of influenza viruses occur in the infected host cell nucleus, unlike most other negative-sense RNA viruses.

1.1.3. Virion structure

The IAV and IBV have remarkably similar infectious virus particles, also known as a virion. Although influenza virion is pleomorphic, it usually has a spheroidal form (~100 nm in diameter) or a filamentous form (1μm or longer) (*Nayak et al., 2013; Shaw & Palese, 2013*).

The IAV schematic diagram is shown in Figure 1.1. Both IAV and IBV contains an envelope, a layer of matrix protein, and a ribonucleoprotein (RNP) core (*Nayak et al., 2013*).

The host cell derived lipid bilayer membrane forms the envelope (*Nayak et al., 2004*). A layer of spikes protruding radially from the viral surface is the most distinguishing feature of IAV and IBV. These spike-like structures correspond to the surface proteins, HA (rod shaped spikes) and NA (mushroom shaped spikes), which protrude about 10 to 14 nm from the surface of the virus (*Murti & Webster, 1986*). On spheroidal-shaped virions, ~500 HA and ~100 NA spikes are there (5:1 HA/NA ratio), whereas virions having filamentous form contain much more spikes. Although both HA and NA are found across the virus surface, the NA clusters appear to be found at the point where budding virus particles exit from host cells (*Russell et al., 2013*). Apart from HA and NA, other proteins are also inserted into the virus envelope; in IAV, ion channel protein M2, whereas in IBV, NB protein, and ion channel protein BM2 (*Shaw & Palese, 2013*). The M1 matrix protein, the most abundant protein of influenza virus, forms the matrix layer underneath the envelope of virus to provide shape and stability to the viral envelope (*Wrigley, 1979*). As M1 interacts with both the cytoplasmic tails of the membrane proteins and the nucleoprotein protein (NP) and viral RNA (vRNA), it is suggested to be a vital link between the viral envelope and the inner core components (*Shaw & Palese, 2013*). The viral genome (eight segments of vRNA) is contained in the core of the virion. Each vRNA segment is bound to the viral RNA dependent RNA polymerase subunits (PA, PB1 & PB2) and with multiple copies of NP, leading to formation of RNP complex (*Cox et al., 2010*). The vRNA forms a helical hairpin structure after being wrapped around by multiple copies of NP and it is bound at one end by the viral RNA dependent RNA polymerase subunits (PA, PB1 & PB2) (*Shaw & Palese, 2013*). In small amounts, NEP/NS2 is also present in the core of the virion and is probably connected to M1 (*Paterson & Fodor, 2012*).

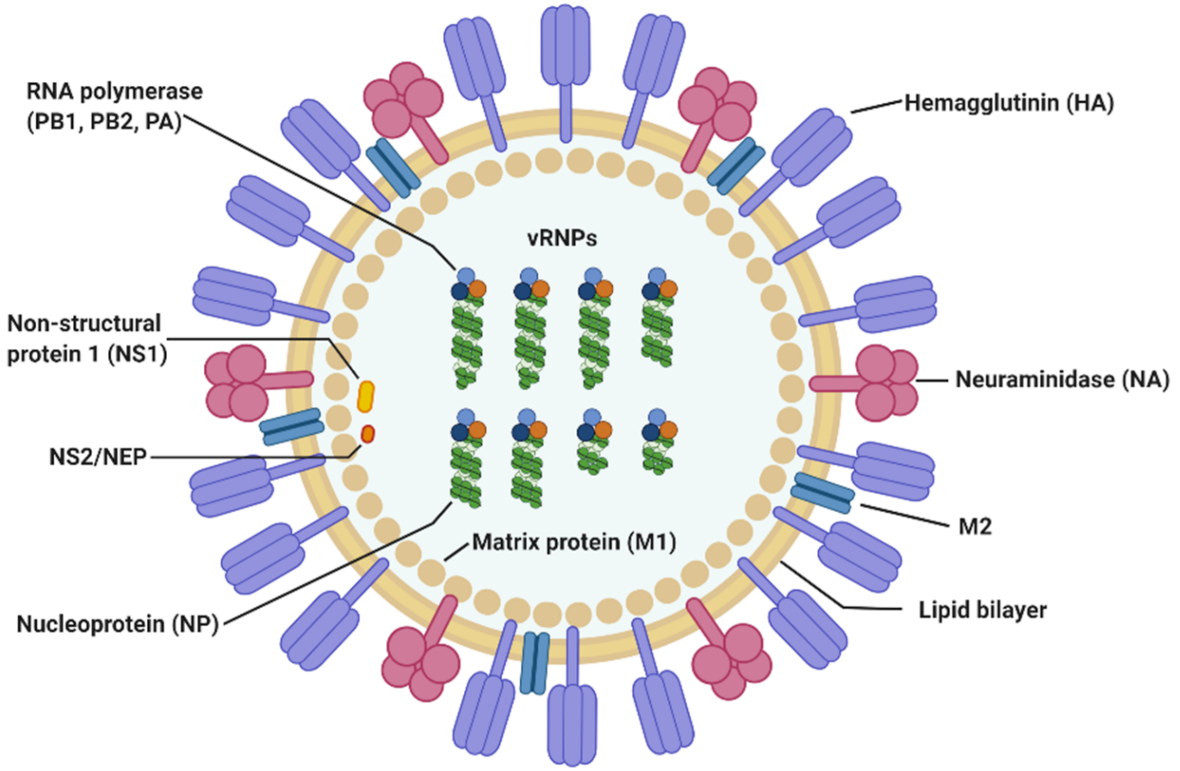

Figure 1.1: The influenza A virus schematic diagram (from *Jung & Lee, 2020*). Figure extracted directly from the original article by *Jung & Lee* (*2020*), without modifications (CC BY 4.0 license, https://creativecommons.org/licenses/by/4.0).

1.1.4. Replication process

In the first stage of influenza virus infection, HA binds to the surface receptor of the host cell containing terminal α-2,3-linked or α-2,6-linked sialic acid residues (*Skehel & Wiley, 2000*). Avian influenza virus tends to bind to α-2,3-linked sialic acid residues, human influenza virus tends to bind to α-2,6-linked sialic acid residues and swine influenza virus binds to both (*Steinhauer & Wharton, 1998; Suzuki et al., 2000*). HA mutations can change the preference of terminal sialic acid residues and thus enable virus transmission to a new host (*Matrosovich et al., 2000; Stevens et al., 2006*). After binding, the virus enters the host cell via receptor-mediated endocytosis, either clathrin-dependent or clathrin-independent or micropinocytosis (*Chen & Zhuang, 2008; de Conto et al., 2011; de Vries et al., 2011; Lakadamyali et al., 2004; Lakadamyali et al., 2006; Sieczkarski & Whittaker, 2002*).

After entering the host cell, the acidic environment of the endocytic vesicle causes the opening of the M2 ion channel, enabling the transfer of H+ ions into the virus (*Bui et al., 1996; Pinto et al., 1992*). The low pH causes the change in HA conformation, exposing the fusion

peptide that enables the fusion of viral envelope and the endosomal membrane, resulting in the release of RNP complexes into the host cell cytoplasm (*Wiley & Skehel, 1987*). These RNP complexes are then translocated to the host cell nucleus (*Babcock et al., 2004; Kemler et al., 1994*). The nuclear localization signal (NLS) is contained in all proteins (PA, PB1, PB2 & NP) involved in the formation of the RNP complex, which enables the binding to the proteins of the host cell's nuclear import machinery and enters the host cell nucleus (*Boulo et al., 2007*).

After the entry of the RNP complex into the host cell nucleus, the RNA dependent RNA polymerase complex helps in the transcription and replication of the negative sense vRNA, leading to the formation of 3 types of RNA, the complementary positive-sense RNA (cRNA) that serves as a template to form more vRNA, the negative-sense small viral RNA (svRNA) that regulates the switch from transcription to replication (*Perez et al., 2010; Umbach et al., 2010*) and the viral mRNA that are translocated to the host cell cytoplasm for translation. After translation of mRNA to the viral proteins, the viral proteins that are necessary for transcription and replication processes are imported again into the host cell nucleus, and then for packaging, the progeny RNP complexes are translocated to the host cell cytoplasm with the help of NEP and M1. The M2, HA, and NA proteins are transported via the *trans*-Golgi secretory pathway, and the matured viral proteins are released at the host cell membrane region where the progeny virions are assembled with the help of M1. After that, the progeny virions bud out of the host cells. The exit of the progeny virions from the host cells is mediated via NA, which cleaves the bond between the surface receptor of the host cell and the terminal sialic acid residue.

1.2. Influenza virus neuraminidase

Influenza virus neuraminidase (NA) is the key protein for the purpose of this study, as it is targeted by neuraminidase inhibitors.

1.2.1. Structure

The mushroom-shaped surface glycoprotein NA is embedded in the influenza virus envelope. It accounts for about 10-20% of all surface glycoproteins on the influenza virus envelope, with an averaged sized influenza virion of 120 nm having approximately 300-400 HA spikes and 40-50 NA spikes (*Moules et al., 2010; Varghese et al., 1983; Ward et al., 1983*). It is a homo-tetramer, with each monomer of about 470 amino acids folding into 4 distinct structural domains - the catalytic head, the stalk, the transmembrane region, and the cytoplasmic tail

(Figure 1.2). According to cryo-electron tomography (CT) studies, NA homo-tetramer exists as isolated spikes or in local clusters on the influenza virus envelope along with HA (*Harris et al., 2006*). Depending on the stalk length, NA may project slightly less or more above the influenza virus envelope as compared to HA, which may have an impact on the overall enzymatic activity of the influenza virus (*Harris et al., 2006; Matsuoka et al., 2009*).

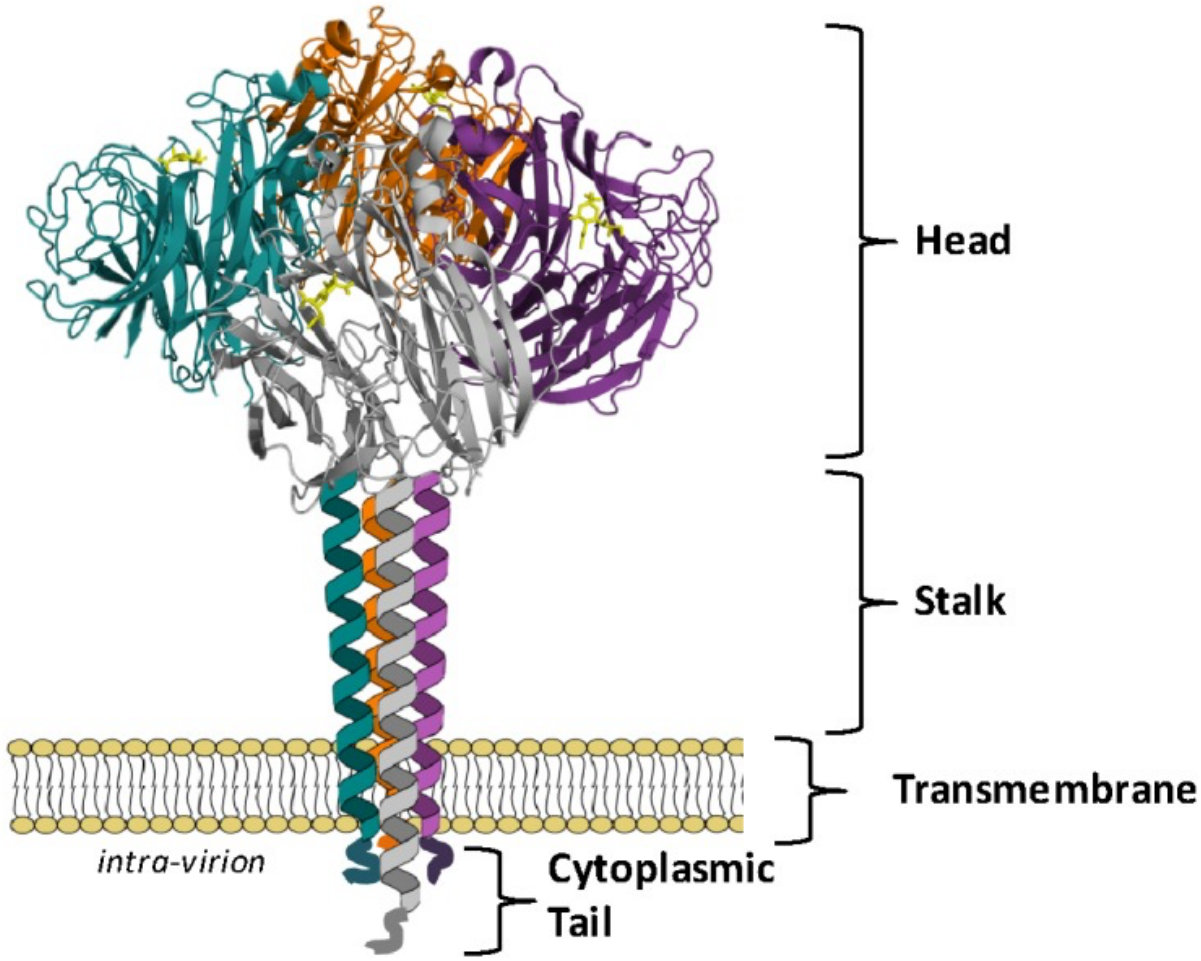

Figure 1.2: The influenza virus neuraminidase schematic diagram (from *McAuley et al., 2019*). Figure extracted directly from the original article by *McAuley et al.* (*2019*), without modifications (CC BY 4.0 license, https://creativecommons.org/licenses/by/4.0).

The N-terminal cytoplasmic tail consists of a highly conserved sequence of six polar amino acids (MNPNQK) across all IAV NA subtypes (*Blok & Air, 1982*). It plays a key role in the incorporation of NA into progeny virions but is not necessary for the replication of the influenza virus (*Cox et al., 2010*). The hydrophobic transmembrane region helps in the attachment of NA to the envelope of the influenza virus (*Bos et al., 1984*), having a variable sequence of about 7-29 amino acids and may form a transmembrane alpha helix (*Air, 2012;*

Blok & Air, 1982). The combined signal peptide-anchor function of this transmembrane region directs NA through the endoplasmic reticulum and retains it in the influenza virus membrane (*Air, 2012*). The stalk is the most variable among all NA structural domains, varying in sequence as well as in length, both among and within IAV NA subtypes (*Colman, 1989*). The stalks of most NAs consist of ~50 amino acids, but in N1 and N2 NA deletions of upto 18 amino acids have been found (*Air, 2012*). The variations in the length of the stalk are suggested to regulate the distance between the catalytic head and the host cell surface receptors (*da Silva et al., 2013*). However, the structure of the stalk is still unknown. The C-terminal catalytic head, which is both enzymatically and antigenically active, consists of ~390 amino acids and has the largest number of conserved amino acids among all NA structural domains (*Sylte & Suarez, 2009*).

In the center of the catalytic head, the NA active site is located as a deep pocket. The NA active site consists of nineteen conserved residues - eight functional residues [R118, D151, R152, R224, E276, R292, R371, and Y406; N2 numbering] and eleven framework residues [E119, R156, W178, S179, D198, I222, E227, H274, E277, N294, and E425; N2 numbering] (*Colman et al., 1983; Colman et al., 1993*). The homo-tetramer form of NA is considered optimal for catalytic activity, and NA mutations that destabilize the homo-tetramer form cause the reduction of catalytic activity (*Fujisaki et al., 2012; McKimm-Breschkin et al., 1996; McKimm-Breschkin et al., 2013a*). Although NA monomers alone are considered to have no catalytic activity (*Air, 2012*), there have been reports of catalytic activity in soluble recombinant influenza NA monomer expressed in yeast and mammalian cells with properties comparable to the homo-tetramer NA (*Nivitchanyong et al., 2011; Yongkiettrakul et al., 2009*). The NA active site is the target of neuraminidase inhibitors because of its highly conserved structure and its vital role in the infection and spread of the influenza virus.

1.2.2. Group specific structural features

The currently known IAV NA subtypes (N1-N11) are clustered into three distinct phylogenetic groups, group 1 (N1, N4, N5, N8), group 2 (N2, N3, N6, N7, N9), and influenza A-like group 3 (N10, N11) (*Russell et al., 2006; Wu et al., 2014*). By comparing the crystal structures of group 1 and group 2 NAs, it was revealed that 150-loop (residues 147-152; N2 numbering), which is present near the NA active site, is able to exist in at least two conformations: an open conformation, which results in the formation of an additional cavity (150-cavity) near the NA active site and a closed conformation, which results in lack of 150-cavity (*Russell et al., 2006*). Crystal structures of group 1 NA appear to have 150-cavity that closes upon ligand

binding (*Russell et al., 2006*). Crystal structures of group 2 NA appear to lack 150-cavity. Atypical to group 1 NA, crystal structure of A(H1N1)pdm09 NA appear to lack 150-cavity (*Li et al., 2010*). The influenza A-like group 3 consists of bat-derived N10 and N11, due to the lack of sialidase activity, they are considered NA-like (*Tong et al., 2013; Wu et al., 2014; Zhu et al., 2012*). Crystal structures of influenza A-like group 3 NA revealed that in N10 and N11, most of the conserved active site residues are mutated, and therefore it lacks sialidase activity (*Tong et al., 2013; Wu et al., 2014; Zhu et al., 2012*).

1.2.3. Function

In the last stage of viral infection, NA act as a scissor to remove terminal α-2,3-linked or α-2,6-linked sialic acid residues from the surface receptors of the host cells to facilitate the exit of progeny virions, thus enabling the spread of progeny virions to surrounding host cells (*Garman & Laver, 2005*). As the function of HA is opposite to NA, the two surface glycoproteins must maintain an optimal balance between their receptor-binding and receptor-destroying activities, this HA-NA balance is crucial for the efficient replication of virus (*Wagner et al., 2002*). The NA also has sialidase activity on the mucus lining the respiratory tract epithelium (rich in sialic acid), cleansing the environment, and enabling virion access to host cells, promoting viral infection (*Matrosovich et al., 2004; Yang et al., 2014*). The NA of human H3N2 viruses also causes NA-dependent hemagglutination of red blood cells (*Hooper & Bloom, 2013; Lin et al., 2010; Mohr et al., 2015*). The NA may help in facilitating virus entry and enhancing late endosome/lysosome trafficking (*Shaw & Palese, 2013*). The NA is also a molecular target for developing novel NA inhibitors and antibodies.

1.2.4. Neuraminidase inhibitors

NA inhibitors are designed based on the sialic acid substrate, competing to bind to the active site of NA and having higher binding affinity as compared to the sialic acid. In the last stage of influenza virus infection, NA act as a scissor to cleave terminal α-2,3-linked or α-2,6-linked sialic acid residues from the surface receptors of the host cell to facilitate the exit of progeny virions, thus enabling the spread of progeny virions to surrounding host cells (*Garman & Laver, 2005*). However, NA inhibitors bind to the active site of NA and block this sialidase activity, resulting in preventing the exit of progeny virions from host cells, thus disabling the spread of progeny virions to surrounding host cells (*Moscona, 2005*). Currently, four types of NA inhibitors are used for influenza treatment in Japan: Oseltamivir phosphate (Tamiflu®,

Hoffmann-La Roche AG) (*Kim et al., 1997*); Zanamivir (Relenza®, GlaxoSmithKline Inc.) (*von Itzstein et al., 1993*); Laninamivir octanoate (Inavir®, Daiichi Sankyo) (*Koyama et al., 2010*); and Peramivir (Rapivab®, BioCryst Pharmaceuticals Inc.) (*Babu et al., 2000*). Among these, Tamiflu, Relenza, and Rapivab are FDA-approved drugs used worldwide for influenza treatment. Figure 1.3 shows the sialic acid and NA inhibitors chemical structure.

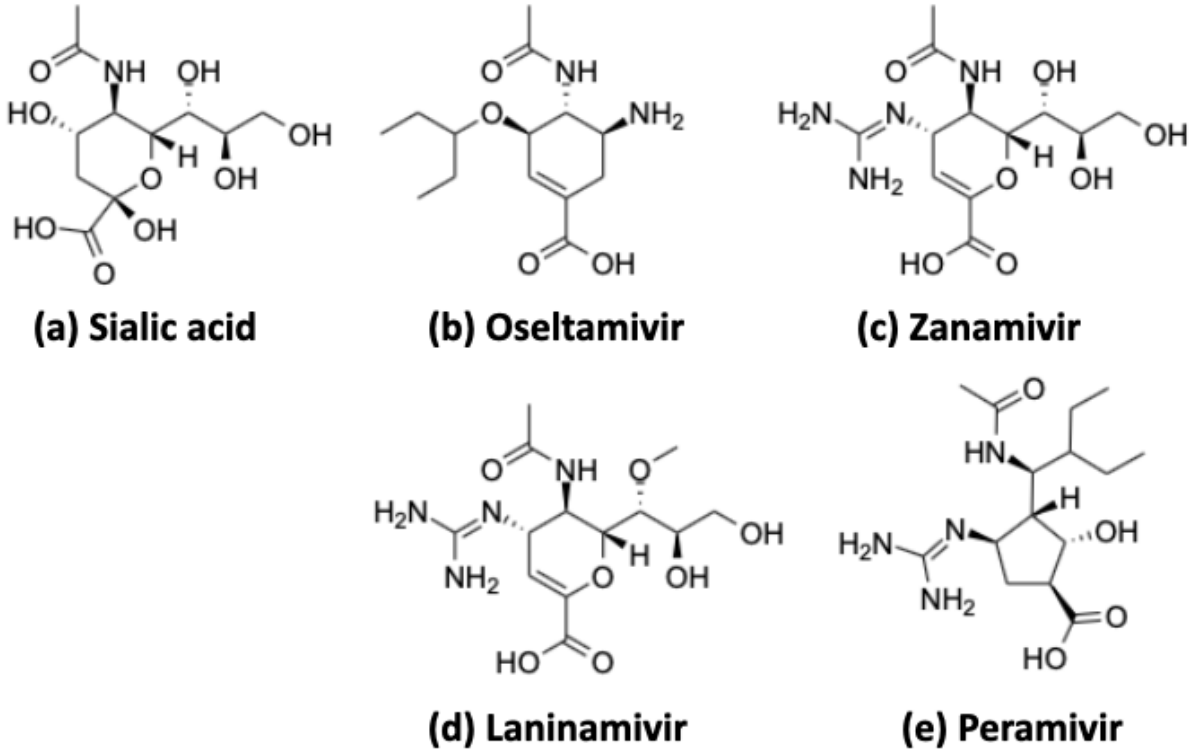

Figure 1.3: Sialic acid and neuraminidase inhibitors, oseltamivir, zanamivir, laninamivir & peramivir, chemical structure drawn using ChemDraw JS web server (https://chemdrawdirect.perkinelmer.cloud/js/sample/index.html).

1.3. Oseltamivir resistance

From 1999 to 2002, first reports of reduced sensitivity to oseltamivir (OTV) due to H274Y mutation in influenza virus NA were made, but these resistant viruses were rarely isolated (*Hurt et al., 2004; Monto et al., 2006*). OTV resistant influenza viruses were not isolated in 2004-2005 influenza season and isolation rates were very low in 2005-2006 influenza season (0.4%) and in 2006-2007 influenza season (0.6%) (*Escuret et al., 2008*). Based on *in vivo* studies, it was reported that since OTV resistance was causing reduction in viral fitness, it would not become an important clinical issue (*Ives et al., 2002*). However, in 2007-2008 influenza season in Europe, the emergence of resistance to OTV due to NA H274Y mutation in H1N1

viruses spread quickly and this OTV resistant strain became predominant worldwide within months (*Hurt et al., 2012a; Li et al., 2015*). Unlike previous H274Y mutant strains in which viral fitness was reduced, the overall viral fitness was retained in these viruses because of permissive mutations in NA, including R194G, R222Q and V234M (*Bloom et al., 2010; Butler et al., 2014*). In 2008-2009 influenza season, OTV resistance was detected in a large number of seasonal H1N1 influenza viruses, in some cases exceeding 90% (*Dharan et al., 2009*). The landscape of OTV resistance was changed after the emergence of A(H1N1)pdm09 influenza viruses, with <1.5% resistance detected initially (*Hurt et al., 2012a*). Along with H274Y mutation in NA, secondary mutations, such as I223K, I223R, and G147R, were also detected in A(H1N1)pdm09 viruses (*Gubareva et al., 2017; Takashita et al., 2016; Takashita et al., 2020*). By 2011, OTV resistance was found in 1.6% A(H1N1)pdm09 viruses worldwide. In 2014-2015 influenza season, OTV resistance was found in 0.5 to 3.4% A(H1N1)pdm09 viruses (*Gubareva et al., 2017; Lina et al., 2018*).

This study focuses on H274Y and I117V mutations in NA in A/H5N1 avian influenza viruses causing reduction in sensitivity to OTV.

1.3.1. H274Y mutation

As residue 274 is a part of framework residues of NA active site, it does not interact directly with OTV (*Russell et al., 2006*). In comparison with wild type NA-OTV complex, the crystal structure of H274Y mutant NA-OTV complex has a subtle conformational change in which the carboxylate side chain of E276 near the residue 274 is shifted towards the NA active site (*Collins et al., 2008*). Since E276 is a part of functional residues of NA active site and interacts directly with OTV, a conformational change caused by the H274Y mutation disrupts favorable interactions between OTV and NA active site residues, leading to reduction in OTV binding affinity to NA, thereby causing OTV drug resistance in influenza virus. The theoretical insights into OTV drug resistance mechanism of influenza virus have been provided by using molecular dynamics (MD) simulations (*Li et al., 2012; Malaisree et al., 2009; Nguyen et al., 2011; Park & Jo, 2009; Ripoll et al., 2012; Vergara-Jaque et al., 2012; Wang & Zheng, 2009; Woods et al., 2012; Woods et al., 2013; Yusuf et al., 2016*). For example, *Malaisree et al.* (*2009*) showed using MD simulations that due to H274Y mutation, the phenyl ring of tyrosine rotates by 45° and leads to 115° rotation of the carboxylate group of E276, thereby resulting in reduced pocket size and hydrophobicity; due to such changes in NA active site, OTV pentyloxy group rotates by 125°, leading to ~5 kcal mol^{-1} increase in the binding free energy of NA to OTV

(*Malaisree et al., 2009*). Therefore, previous studies have used MD simulations to investigate conformational changes at NA active site. However, studies that focus only on the end point of the protein-ligand interaction based on three-dimensional structures may be insufficient to explain the mutations impact on drug resistance. Hence, it is still unclear whether the correlation between the active site of NA and its H274Y mutation site causes the reduction in binding affinity of NA to OTV.

1.3.2. I117V mutation

As residue 117 is not a part of the NA active site, there is no direct interaction between residue 117 and OTV. *In vivo* and *in vitro* studies have reported that OTV susceptibility to NA was reduced after I117V mutation (*Chen et al., 2010; Creanga et al., 2017; Hurt et al., 2007; Ilyushina et al., 2010; Kode et al., 2019; McKimm-Breschkin et al., 2007; McKimm-Breschkin et al., 2013b; Takano et al., 2013*). By using molecular dynamics (MD) simulations, several computational studies have investigated the molecular mechanism of reduction in OTV susceptibility to I117V mutant NA (*Mhlongo & Soliman, 2015; Takano et al., 2013*). *Takano et al.* (*2013*) investigated the effect of NA I117V mutation on OTV susceptibility *in vivo, in vitro*, and *in silico*. According to their experimental results, after I117V mutation in NA, OTV susceptibility to NA reduced slightly *in vitro* and dramatically *in vivo*. Furthermore, using a single 2.5 ns MD trajectory, they investigated the molecular mechanism of reduction in OTV susceptibility to I117V mutant NA. According to their computational results, the decrease in OTV binding affinity to I117V mutant NA is caused by the loss of hydrogen bond interaction between OTV carboxyl group and the side chain of R118 of NA. *Mhlongo & Soliman* (*2015*) investigated the molecular mechanism of reduction in OTV susceptibility to I117V mutant NA by analyzing four distinctive 25 ns MD trajectories. According to their computational results, the OTV orientation in the NA active site is disrupted after the I117V mutation because of the loss of hydrogen bond interaction between OTV amino group and the side chain of E119 of NA, causing reduction in OTV binding affinity to NA. In these previous computational studies, the production trajectory of MD simulations was too short to reach reliable statistical result. Moreover, they only focused on analyzing the changes in the direct interactions between OTV and active site residues of NA. However, the molecular mechanism of how the NA II17V mutation, which is not included in the NA active site, could affect the intermolecular interaction with OTV is still unclear.

2. Development of Dynamic Residue Interaction Network (dRIN) analysis

2.1. Introduction to Residue Interaction Network (RIN) analysis

In a protein, the covalent and non-covalent interactions between amino acid residues are necessary for stabilizing its three-dimensional structure and determining the necessary functions of living organisms. Residue interaction network (RIN) helps in visualizing interactions within a protein's spatial structure as a simplified graph with nodes (residues) and edges (interaction between residues). Based on how the interactions between amino acid residues are calculated, various types of RIN can be formed. The most common method to construct RIN is by calculating the Euclidean distance between C_{α}s or C_{β}s of different amino acid residues, and if the distance is less than a given threshold, the interaction exists; this is also known as contact map (*Brown et al., 2017; Sethi et al., 2009*). Another method to construct RIN is to calculate all non-covalent interactions between amino acid residues (*Martin et al., 2011; Piovesan et al., 2016; Shcherbinin & Veselovsky, 2019; Wolek et al., 2015*), resulting in the formation of a multigraph in which multiple edges connects two nodes, where each edge indicates a specific type of non-covalent interaction, such as hydrogen bond, van der Waals (vdW) interaction, salt bridge, π-π stacking interaction, or π-cation interaction, or other non-covalent interactions. As compared to simple graphs constructed using distance thresholds, multigraph contains more information as two nodes are connected by multiple edges, each edge representing a specific type of interaction. But the presence of multiple edges between two nodes makes it difficult to apply common algorithm and metrices used for characterizing and analyzing simple graphs (*Brandes, 2008*).

Currently, most approaches of RIN are static, constructed by using a single three-dimensional structure of protein and does not consider the dynamic characteristics of proteins, such as non-covalent interactions formation and annihilation. For revealing the ensemble-averaged and dynamic characteristics of residue interactions, several studies have used dynamic version of RIN, built from a set of multiple three-dimensional structures of protein obtained from MD simulations (*Bhattacharyya et al., 2013; Brown et al., 2017; Contreras-Riquelme et al., 2018; Pasi et al., 2012; Serçinoğlu & Ozbek, 2018; Tiberti et al., 2014*). Both the static and dynamic RIN have been applied in many types of analysis, including drug resistance (*Bhakat et al., 2014; Xue et al., 2013; Xue et al., 2014; Zhang et al., 2019*), allosteric behavior (*Sethi et al., 2009*), and protein stability (*Brinda & Vishveshwara, 2005; Giollo et al., 2014*).

2.2. Dynamic Residue Interaction Network (dRIN) analysis

2.2.1. Introduction

In this study, to provide statistical insights into the residue interactions, the original static residue interaction network (RIN) is extended to construct dynamic residue interaction network (dRIN) using multiple three-dimensional structures of individual protein, protein-protein complex or protein-ligand complex obtained from molecular dynamics (MD) simulations. Figure 2.1 shows the simplified representation of RIN and dRIN analysis.

The RIN analysis is used to analyze a single three-dimensional structure of individual protein, protein-protein complex or protein-ligand complex obtained from NMR spectroscopy or X-ray crystallography and thus it disregards the dynamic properties of individual protein, protein-protein complex, or protein-ligand complex, including non-covalent interactions formation and annihilation. Hence, RIN analysis can only provide static information about the interaction between residues.

The dRIN analysis is used to analyze the multiple three-dimensional structures of individual protein, protein-protein complex or protein-ligand complex obtained from MD simulations, thus it can characterize the dynamic aspects of residue interactions with respect to time. Hence, dRIN analysis can provide information about the interaction between residues, the occupancy of the residue interactions (the percentage of frames with interactions between residues in the MD simulation), and it can characterize the dynamic properties of residue interaction with respect to time when combined with dynamic cross correlation (DCC) method.

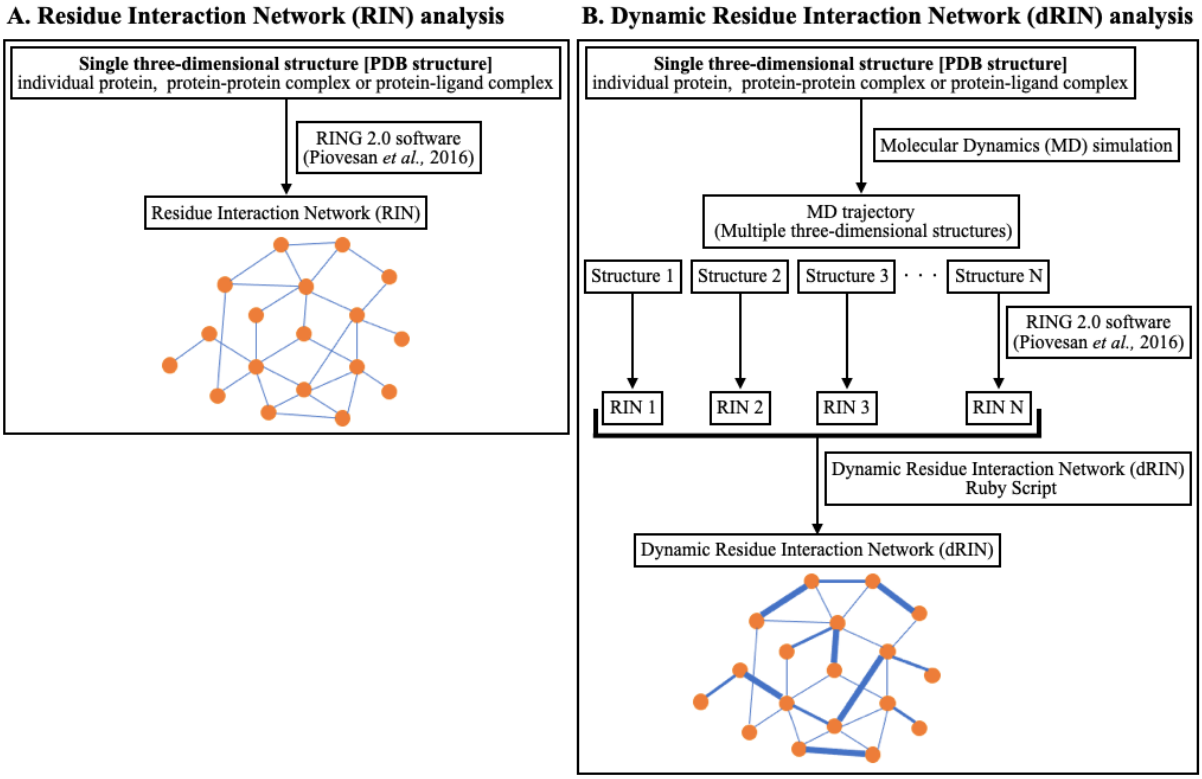

Figure 2.1: Simplified representation of (A) residue interaction network (RIN) analysis and (B) dynamic residue interaction network (dRIN) analysis. In graphical representation of RIN and dRIN, the node (orange) represents residue and the edge (blue) represents interaction between residues. The RIN analysis provides information about interactions between residues but do not provide any information about the occupancy of residue interactions. The dRIN analysis provides information about interactions between residues as well as the occupancy of residue interactions (indicated by the thickness of the edges).

The dRIN analysis used in this study classifies the residue-residue and residue-ligand interactions into specific types, including hydrogen bond, van der Waals (vdW) interaction, disulfide bridge, salt bridge, π-π stacking interaction, and π-cation interaction, using the RING 2.0 software (*Piovesan et al., 2016*). The RING 2.0 software criteria to determine different types of interactions is as follows:

1. Hydrogen bonds

In RING 2.0 software (*Piovesan et al., 2016*), hydrogen bond calculation is based on DSSP algorithm (*Kabsch & Sander, 1983*). Hydrogen bonds (Figure 2.2a) are defined by two rules: 1) the distance between the donor atom and the acceptor atom is less than or equal to 3.5 Å;

and 2) the angle formed by the donor atom, the hydrogen of the donor atom, and the acceptor atom is less than or equal to 63°. The valid donor and acceptor atoms considered by the RING 2.0 software are as follows:

Donors

main chain NH; Arginine NE, NH1, NH2; Asparagine ND2; Histidine NE2, ND1; Serine OG; Tyrosine OH; Cysteine SG; Threonine OG1; Glutamine NE2; Lysine NZ; Tryptophan NE1

Acceptors

Main chain C; Asparagine OD1; Glutamine OE1; Methionine SD; Aspartic acid OD1, OD2; Glutamic acid OE1, OE2; Serine OG; Threonine OG1; Histidine ND1; Tyrosine OH

2. Van der Waals (vdW) interactions

In RING 2.0 software (*Piovesan et al., 2016*), vdW interactions are identified by calculating the distance between the surface of two atoms (subtracting their vdW radii) (Figure 2.2b). The distance threshold is 0.5 Å. The RING 2.0 software considers only carbon-carbon and carbon-sulfur atom pairs for a valid vdW interaction. The RING 2.0 software also considers special vdW interactions involving nitrogen and oxygen side chain atoms of glutamine (NE2, OE1) and asparagine (ND2, OD1).

3. Disulfide bridges

Disulfide bridges are covalent bonds and found within a very constant distance (Figure 2.2c). The RING 2.0 software (*Piovesan et al., 2016*) identifies disulfide bridges when the distance between SG atoms of cysteine pairs is less than or equal to 2.5 Å.

4. Salt bridges

Salt bridges (ionic interactions) occur between residues with opposite charges (Figure 2.2d). The RING 2.0 software (*Piovesan et al., 2016*) identifies salt bridge when the distance between the mass centers of the charged groups is less than or equal to 4.0Å. The valid positively and negatively charged residues considered by the RING 2.0 software are as follows:

Positively charged residues: Arginine, Histidine, Lysine

Negatively charged residues: Aspartic acid, Glutamic acid

5. π-π stacking interactions

π-π stacking interactions occur between aromatic residues, histidine, tyrosine, tryptophan, and phenylalanine (Figure 2.2e). The RING 2.0 software (*Piovesan et al., 2016*) identifies the π-π stacking interaction when the distance between the two ring barycenters is less than or equal to 6.5 Å and adopts one of the following orientations (Figure 2.3): parallel (P), lateral (L), normal (N), tilted face to edge (T-FE) and tilted edge to face (T-EF).

6. π-cation interactions

π-cation interactions occur between positively charged amino acid residues and an aromatic side chain (Figure 2.2f). The RING 2.0 software (*Piovesan et al., 2016*) considers only arginine and lysine as positively charged amino acid residues for a valid π-cation interaction. Histidine is not considered because depending on its protonation state, it can act both as a cation and as a π-system. In RING 2.0 software, π-cation interactions are defined by two rules: 1) the distance between the mass center of the positively charged group and any atom of the π-system must be less than or equal to 5.0 Å; and 2) the angle between the distance vector and the aromatic ring plane must guarantee that the mass center of the cation lies above or below the ring area. Also, the RING 2.0 software calculates orientation of arginine according to the dihedral angle formed between the aromatic ring plane and the cationic guanidine group and allows only parallel (P), lateral (L) and normal (N) orientations (Figure 2.3).

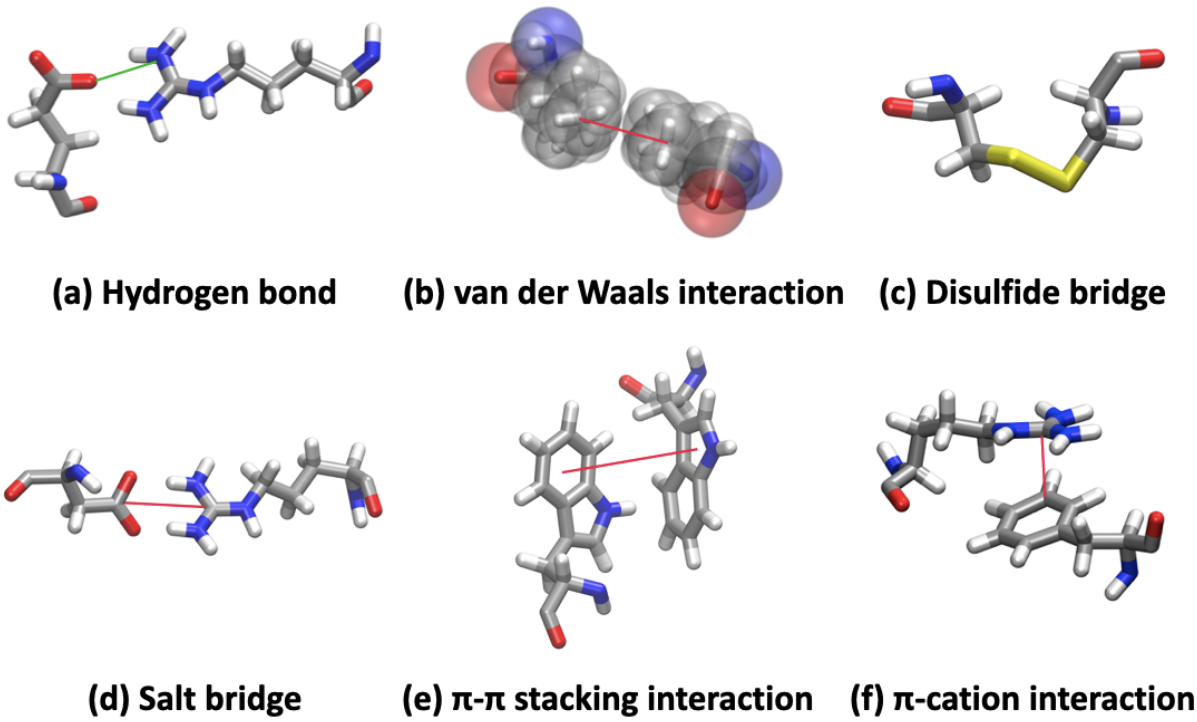

Figure 2.2: Types of residue interactions.

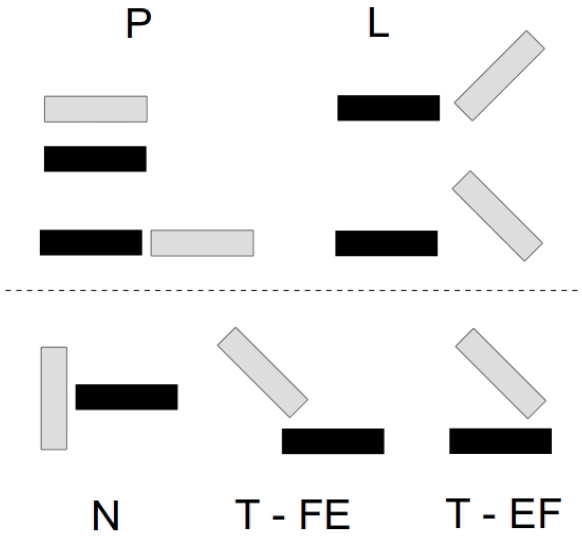

Figure 2.3: Definition of orientation in RING 2.0 software (*Piovesan et al., 2016*) - Parallel (P), Lateral (L), Normal (N), Tilted Face to Edge (T-FE), and Tilted Edge to Face (T-EF) (from *Piovesan et al., 2016*). π-π stacking interactions can adopt P, L, N, T-FE, and T-EF conformations. π-cation interactions between arginine and aromatic ring can adopt P, L and N conformations. Figure extracted directly from the original article by *Piovesan et al.* (*2016*), without modifications (CC BY-NC 4.0 license, https://creativecommons.org/licenses/by-nc/4.0/).

2.2.2. Methodology

In dRIN analysis, residue interactions are analyzed for multiple three-dimensional structures of individual protein, protein-protein complex, or protein-ligand complex obtained from MD simulations. In dRIN analysis, residue-ligand interactions are included in the residue interactions. The residue-residue and residue-ligand interactions are classified into specific types, including hydrogen bond, van der Waals (vdW) interaction, disulfide bridge, salt bridge, π-π stacking interaction, and π-cation interaction, using the RING 2.0 software (*Piovesan et al., 2016*). The hydrogen bonds between ligand and residues in the protein-ligand complex are detected using the CPPTRAJ program (*Roe & Cheatham, 2013*) in the AMBER 20 package (*Case et al., 2020*), as the RING 2.0 software misses them. Even though the RING 2.0 software detects various types of interactions per residue pair, only one interaction per interaction type is considered. The dRIN analysis further examine the interactions between residues that are not included in the attractive interactions detected by the RING 2.0 software but are in close contact with one another. In dRIN analysis, two residues are identified as being in close contact, if $d_{ij} - (\sigma_i + \sigma_j) < 0.4$ Å, where d_{ij} denotes the interatomic distance between the *i*- and *j*-th atoms in the two residues and σ_i is the vdW radius of the *i*-th atom. Several molecular structure visualization and analysis programs, including UCSF Chimera software (*Pettersen et al., 2004*), have adopted this definition of close contact. By repeating the above procedure, the dRIN is formed using the sets of residue interactions and close contacts obtained from the MD simulations for the individual protein, protein-protein complex, or protein-ligand complex. The occupancy of residue interactions is calculated as the percentage of frames with interactions between residues in the MD simulation. The dRIN analysis is implemented using the ruby script (Appendix C.1). To graphically visualize the dRIN, with nodes (residues) and edges (interactions between residues), various software can be used, such as the Cytoscape software (*Shannon et al., 2003*), and it can also be visualized using Matplotlib library for Python programming language (*Hunter, 2007*).

3. “Dynamic residue interaction network analysis of the oseltamivir binding site of N1 neuraminidase and its H274Y mutation site conferring drug resistance in influenza A virus”

3.1. Abstract

The His-to-Tyr mutation at position 274 (H274Y) in N1 neuraminidase (NA) is found in oseltamivir (OTV) drug resistant influenza viruses. However, the molecular mechanism by which the OTV binding affinity is reduced by the NA H274Y mutation has not been fully elucidated. In this study, the correlation between the OTV binding site and H274Y mutation site of NA is investigated using dynamic residue interaction network (dRIN) analysis based on molecular dynamics (MD) simulation. The results of dRIN analysis revealed that the interaction between OTV binding site of NA and its H274Y mutation site is mediated by three interface residues connecting the two sites. Due to H274Y mutation, the interaction between residue 274 and the three interface residues in NA significantly increased, resulting in significant decrease in the interaction between OTV and its surrounding 150-loop residues. Such changes in residue interactions could result in the reduction of OTV binding affinity to NA, causing OTV drug resistance in influenza viruses. To conclude, using dRIN analysis, we succeeded in understanding the characteristic changes in residue interactions caused by H274Y mutation, which can elucidate the molecular mechanism of drug resistance of OTV in influenza viruses. Finally, the dRIN analysis used in this study can be applied to a wide range of systems, including individual proteins, protein-protein complexes, and protein-ligand complexes, to characterize the dynamic characteristics of the residue interactions.

3.2. Introduction

Influenza, commonly known as flu, is a highly contagious respiratory illness caused by influenza virus, resulting in mild to severe illness and sometimes even death (*Palese, 2004*). Influenza virus has two surface glycoproteins, hemagglutinin (HA) and neuraminidase (NA), playing important roles in the influenza virus replication process (*Gamblin & Skehel, 2010*). HA binds to the terminal sialic acid of the surface receptor of the host cell and facilitates entry of virus into the host cell via endocytosis. In the last stage of infection, NA facilitates the exit of progeny virions from the host cell by cleaving the bond between terminal sialic acid and the surface receptor of the host cell, thus enabling the spread of progeny virions to surrounding host cells. Both HA and NA are used as molecular target for the development of novel anti-influenza

drugs. Indeed, NA inhibitors that inhibit the interaction between NA and terminal sialic acid of the host cell surface receptor have been developed (*Moscona, 2005*).

For influenza treatment and prevention, one of the widely used anti-NA drugs is Oseltamivir (OTV) (*Kim et al., 1997*). However, the emergence of OTV drug resistant influenza viruses has raised concerns worldwide (*de Jong et al., 2005*). For example, in the 2007-2008 influenza season, OTV drug resistant influenza viruses emerged globally, and within a year, these OTV drug resistant influenza viruses became the cause of most seasonal H1N1 influenza infection cases (*Moscona, 2009*). The His-to-Tyr mutation at position 274 in NA (H274Y) is the characteristic feature of these OTV drug resistant influenza viruses (*Gubareva et al., 2001; Hurt et al., 2009; Ives et al., 2002; Wang et al., 2002*). NA active site consists of nineteen conserved residues - eight functional residues [R118, D151, R152, R224, E276, R292, R371, and Y406; N2 numbering] and eleven framework residues [E119, R156, W178, S179, D198, I222, E227, H274, E277, N294, and E425; N2 numbering] (*Colman et al., 1983; Colman et al., 1993*). Residue 274 is a part of NA active site framework residues and does not interact directly with OTV (*Russell et al., 2006*). In comparison with the wild type NA-OTV complex, the crystal structure of H274Y mutant NA-OTV complex has a subtle conformational change in which the carboxylate side chain of E276 near the residue 274 is shifted towards the NA active site (*Collins et al., 2008*). Since E276 is a part of NA active site functional residues and interacts directly with OTV, a conformational change caused by the H274Y mutation disrupts favorable interactions between OTV and NA active site residues, leading to reduction in OTV binding affinity to NA, thereby causing OTV drug resistance in influenza virus.

The theoretical insights into OTV drug resistance mechanism of influenza virus have been provided by using molecular dynamics (MD) simulations (*Li et al., 2012; Malaisree et al., 2009; Nguyen et al., 2011; Park & Jo, 2009; Ripoll et al., 2012; Vergara-Jaque et al., 2012; Wang & Zheng, 2009; Woods et al., 2012; Woods et al., 2013; Yusuf et al., 2016*). For example, *Malaisree et al.* (*2009*) showed using MD simulations that due to H274Y mutation, the phenyl ring of tyrosine rotates by 45° and leads to the 115° rotation of the carboxylate group of E276, thereby resulting in reduced pocket size and hydrophobicity; due to such changes in NA active site, OTV pentyloxy group rotates by 125°, leading to ~5 kcal mol^{-1} increase in the binding free energy of NA to OTV (*Malaisree et al., 2009*). Therefore, previous studies have used MD simulations to investigate conformational changes at active (binding) site of NA. However, studies that focus only on the end point of the protein-ligand interaction based on three-dimensional structures may be insufficient to explain the mutations impact on drug

resistance. Hence, it is still unclear whether the correlation between the OTV binding site of NA and its H274Y mutation site causes the reduction in binding affinity of NA to OTV.

Residue interaction network (RIN) has previously been used to describe the spatial architecture of protein as a network of residue interactions (*Csermely et al., 2013; di Paola et al., 2013; Shcherbinin & Veselovsky, 2019; Yan et al., 2014*). The three-dimensional structure of protein is stabilized by covalent and non-covalent interactions between amino acid residues, and it determines the necessary functions of living organisms. RIN helps in visualizing interactions within a protein's spatial structure as a simplified graph with nodes (residues) and edges (interaction between residues). Based on how the interactions between amino acid residues are calculated, various types of RIN can be formed (*Csermely et al., 2013; di Paola et al., 2013; Shcherbinin & Veselovsky, 2019; Yan et al., 2014*). One of the widely used methods of RIN is to identify the various types of physiochemical interactions among residues based on certain criteria (*Piovesan et al., 2016; Shcherbinin & Veselovsky, 2019*). Most RIN methods used currently are static, based on a single three-dimensional structure of protein and not considering the dynamic characteristics of proteins, such as non-covalent interactions formation and annihilation. For revealing the ensemble-averaged and dynamic characteristics of residue interactions, several studies have used dynamic version of RIN (dRIN), built from a set of multiple three-dimensional structures of protein obtained from MD simulations (*Bhattacharyya et al., 2013; Brown et al., 2017; Contreras-Riquelme et al., 2018; Pasi et al., 2012; Serçinoğlu & Ozbek, 2018; Tiberti et al., 2014*). Both the static and dynamic version of RIN have been applied in many types of analysis, including drug resistance (*Bhakat et al., 2014; Xue et al., 2013; Xue et al., 2014; Zhang et al., 2019*), allosteric behavior (*Sethi et al., 2009*), and protein stability (*Brinda & Vishveshwara, 2005; Giollo et al., 2014*). *Buthelezi et al.* (*2020*) recently used RIN analysis to provide insights into the drug resistance mechanism of influenza viruses with NA H274Y mutation; however, they only used static RINs built using representative average structures obtained from MD simulations to analyze the changes in residue interactions caused by the mutation (*Buthelezi et al., 2020*). Overall, the drug resistance mechanism by which the NA H274Y mutation of influenza virus affects the dynamic characteristics of residue interactions is still unclear.

In this study, we used dRIN analysis to investigate the changes in residue-residue and residue-ligand interactions due to H274Y mutation in influenza virus NA bound to OTV. The approach used in this study extends the original static version of RIN to construct dynamic version of RIN (dRIN) using multiple three-dimensional structures of protein obtained

from MD simulations, to provide statistical insights into residue interactions. Here, we succeeded in clarifying the correlation between OTV binding site and H274Y mutation site of N1 NA conferring drug resistance in influenza virus. This study provides novel theoretical insights into the molecular mechanism of OTV drug resistance caused by NA H274Y mutation of influenza virus.

3.3. Methods

3.3.1. Initial structures

The Amber 20 package was used for structure preparation and MD simulations (*Case et al., 2020*). The Protein Data Bank (PDB) was used to obtain the crystal structures of wild type (WT) avian influenza virus A/H5N1 NA-OTV complex (PDB ID: 2HU4) and H274Y mutant NA-OTV complex (PDB ID: 3CL0) (*Collins et al., 2008; Russell et al., 2006*) and a single monomer was used for modeling. One calcium ion is present in H5N1 NA, which is required for structural stability (*Smith et al., 2006*). In the crystal structure of H5N1 NA registered as 2HU4, no calcium ion was present, thus the coordinates of the calcium ion were determined from the related structure registered as 3CL0. The PDB2PQR server was used to determine the protonation state of Histidine at pH 7 in the modeled complex (*Dolinsky et al., 2004*), and the other ionized residues (Arginine, Lysine, Aspartic acid, and Glutamic acid) were treated as charged entities. The missing hydrogen atoms of proteins and OTV were added using the LEaP module in Amber 20 package. Eight disulfide bonds are present in H5N1 NA. The "bond" command was executed in the tLEaP program to form a covalent bond between the SG atoms of the proximate cysteine residues for each disulfide bond. For proteins, the FF14SB force field of AMBER was used (*Maier et al., 2015*). For OTV, the Generalized AMBER Force Field (GAFF) was used (*Wang et al., 2004*). The restrained electrostatic potential fitting procedure was used to determine the OTV partial atomic charges (*Bayly et al., 1993*), based on HF/6-31G(d) level of quantum chemistry calculations using Gaussian 16 program (*Frisch et al., 2016*). The WT NA-OTV and H274Y mutant NA-OTV complexes were dissolved in a truncated octahedral box of TIP3P water molecules with a distance of at least 10 Å around them. The total charge of the complexes was neutralized by adding sodium counter ions.

3.3.2. Molecular Dynamics (MD) simulations

The energy minimization of each system was performed using the steepest descent method for first 500 steps, followed by the conjugate gradient method for next 4,500 steps, with a harmonic

restraint weight of 10 kcal mol^{-1} $Å^{-2}$ on the complexes, except for hydrogen atoms. After energy minimization, each system was gradually heated to 300K over a period of 200 ps in the *NVT* ensemble. The PMEMD module of Amber 20 package was used to perform all MD simulations. The weak-coupling algorithm was used to regulate temperature (*Berendsen et al., 1984*). The SHAKE algorithm was used to constrain all bond lengths including hydrogen atoms (*Ryckaert et al., 1977*), allowing an MD time-step of 2 fs to be used. Periodic boundary conditions were adopted. For non-bonded interactions, a cut-off of 8 Å was used. The particle-mesh Ewald method was used to treat long range electrostatics (*Darden et al., 1993*). After heating, MD simulation was performed for 80 ns in the *NpT* ensemble at a pressure of 1.0 atm and a temperature of 300K. The Berendsen barostat was used to maintain pressure. The production phase to be analyzed was the last 40 ns of MD simulations, which was determined based on the root mean square displacement (RMSD) for the protein backbone atoms with respect to the initial structure along the simulation time. Figure 3.1 shows the time series of RMSD for the protein backbone atoms in the WT and H274Y mutant NA. After 40 ns, the changes in RMSD were almost constant, indicating that the MD simulations properly converged in the region of 40-80 ns.

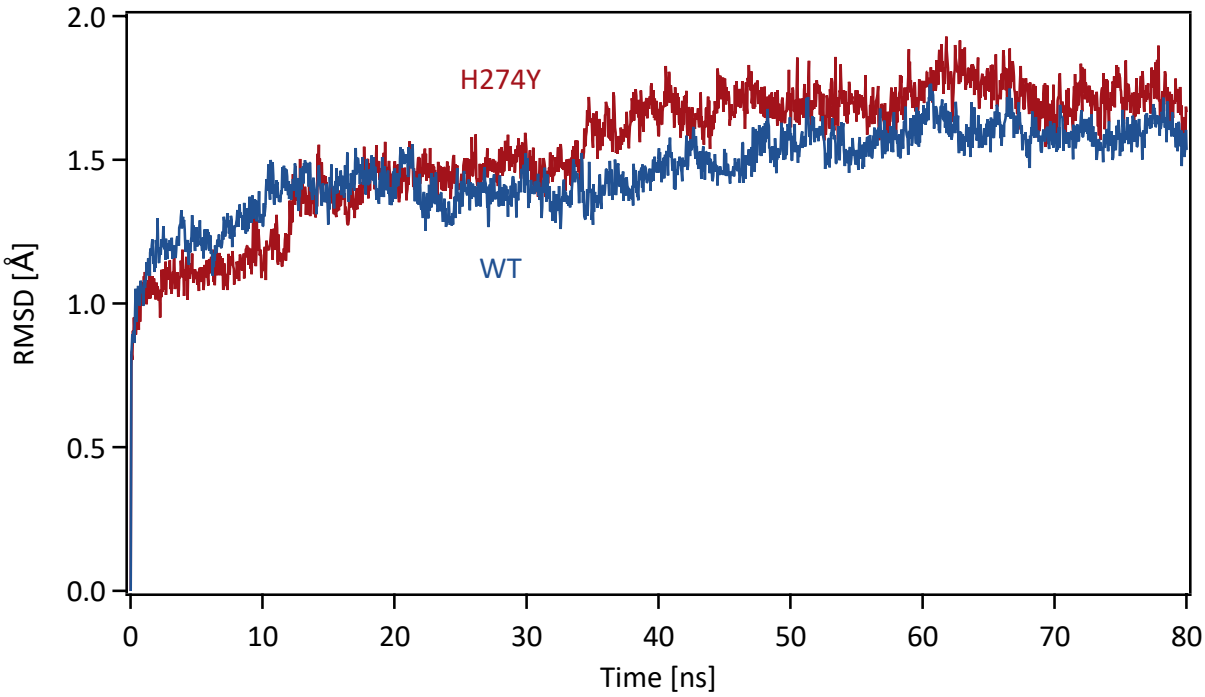

Figure 3.1: The time series of the root mean square displacement (RMSD) of wild type (WT) and H274Y mutant neuraminidase-oseltamivir complexes (from *Yadav et al., 2021a*). RMSDs for the protein backbone atoms in WT and H274Y mutant NA for 15th to 365th amino

acid residues, excluding both ends of NA, with respect to the initial structure along the simulation time. The production phase to be analyzed was the last 40 ns of MD simulations. Figure extracted directly from the original article by *Yadav et al.* (*2021a*), without modifications (CC BY 4.0 license, https://creativecommons.org/licenses/by/4.0).

3.3.3. Binding free energy calculations

The Molecular Mechanics Poisson Boltzmann Surface Area (MM-PBSA) method in Amber 20 package (MMPBSA.py) was used to estimate the binding free energies for OTV bound to WT and H274Y mutant NA (*Miller et al., 2012*). The adaptive Poisson Boltzmann (PB) solver was used to estimate the electrostatic contribution to the solvation free energy (*Baker et al., 2001*). The dielectric constant in the water was set to 80 and protein was set to 4. As the binding site of NA consists of many charged residues, a relatively large dielectric constant is desirable (*Hou et al., 2011*). The ionic strength was set at 150 mM. The ratio between the longest dimension of the rectangular finite-difference grid and that of the solute was set to four. The linear PB equation was solved using a maximum of 1,000 iterations. MM-PBSA calculations were performed over 2,000 frames extracted from the production phase in the last 40 ns of MD simulations.

The entropies due to the vibrational degrees of freedom were calculated for 100 configurations by normal mode analysis using the mmpbsa_py_nabnmode program in the Amber 20 package. Each configuration was energy minimized with a generalized Born solvent model, using a maximum of 10,000 steps with a target root-mean-square gradient of 10^{-3} kcal mol^{-1} $Å^{-1}$.

3.3.4. Dynamic Residue Interaction Network (dRIN) analysis

In the 40 ns production phase of the MD simulations, residue interactions were examined for 2,000 three-dimensional structures of the WT and H274Y mutant NA bound to OTV. In this study, residue-ligand interactions were included in the residue interactions. The residue-residue and residue-ligand interactions were classified into specific types, including hydrogen bond, disulfide bridge, salt bridge, van der Waals (vdW) interaction, π-π stacking interaction, and π-cation interaction, using the RING 2.0 software (*Piovesan et al., 2016*). The hydrogen bond between ligand and residues in the NA-OTV complexes was detected using the CPPTRAJ program (*Roe & Cheatham, 2013*) in the Amber 20 package, as the RING 2.0 software missed them. Even though the RING 2.0 software detected various types of interactions per residue

pair, only one interaction per interaction type was considered. We further examined the interactions between residues that were not included in the attractive interactions detected by the RING 2.0 software but were in close contact with one another. In this study, two residues were identified as being in close contact, if $d_{ij} - (\sigma_i + \sigma_j) < 0.4$ Å, where d_{ij} denotes the interatomic distance between the *i*- and *j*-th atoms in the two residues and σ_i is the vdW radius of the *i*-th atom. Several molecular structure visualization and analysis programs, including UCSF Chimera software (*Pettersen et al., 2004*), have adopted this definition of close contact. By repeating the above procedure, the dRINs were formed using the sets of residue interactions and close contacts obtained from the MD simulations for the WT and H274Y mutant NA-OTV complexes. The occupancy of residue interactions was calculated as the percentage of frames with interactions between residues in the MD simulation. The dRIN analysis is implemented using the ruby script (Appendix C.1). To graphically visualize the dRIN with residues represented by nodes and interactions between residues represented by edges, various software can be used such as the Cytoscape software (*Shannon et al., 2003*) and it can also be visualized using Matplotlib library for Python programming language (*Hunter, 2007*).

3.4. Results

3.4.1. Binding structures and energies

The snapshot images of the OTV binding site and the region adjacent to residue 274 obtained from the MD simulations of the WT and H274Y mutant NA-OTV complexes are shown in Figure 3.2. The estimated binding free energies (ΔG) of WT and H274Y mutant NA for OTV obtained from the MM-PBSA calculations, as well as the enthalpy (ΔH) and entropy ($T\Delta S$), are summarized in Table 3.1. The detailed results of the energetic components categorized by each intermolecular interaction are summarized in Table C.1. The binding free energies of OTV for the WT and H274Y mutant NA were estimated to be −11.54 and −4.34 kcal mol^{-1}, respectively. The H274Y mutation increases the binding free energy of OTV by 7.20 kcal mol^{-1}, which could significantly reduce the OTV susceptibility to NA. This is supported by the experimental fact that in H5N1 viruses, due to H274Y mutation in NA, the IC_{50} value of OTV increased by 300- to 1700-fold, indicating that in H274Y mutant NA the susceptibility to OTV was significantly reduced as compared to WT NA (*de Jong et al., 2005; Ives et al., 2002; Kiso et al., 2004; Mishin et al., 2005; Wang et al., 2002; Yen et al., 2007*). Several computational studies have been performed to estimate the effect of H274Y mutation on the OTV binding free energy (*Li et al., 2012; Malaisree et al., 2009; Nguyen et al., 2011; Park & Jo, 2009; Ripoll et*

al., 2012; Vergara-Jaque et al., 2012; Wang & Zheng, 2009; Woods et al., 2012; Woods et al., 2013; Yusuf et al., 2016). The current results are in qualitative agreement with previous experimental and computational studies, implying that the MD simulations, which are the basis of the subsequent analyses, were reliable.

The binding free energy estimated using the MM-PBSA method can be sensitive to various factors, including the dielectric constant (ε) value of the protein. In general, $\varepsilon = 1.0$ is used for proteins; however, in this study, $\varepsilon = 4.0$ was used for NA based on previous studies because the NA binding site consists of many charged residues (*Hou et al., 2011*). Table C.2 shows the results of binding free energies obtained from MM-PBSA calculations with $\varepsilon = 1.0$ to confirm the validity of this factor. The results estimated using $\varepsilon = 1.0$ showed a larger difference in binding free energies (10.48 kcal mol^{-1}) as compared to the results estimated using $\varepsilon = 4.0$ (7.20 kcal mol^{-1}), further reducing the OTV binding affinity to NA due to H274Y mutation. If experiments are performed under the same conditions, the relative binding free energy of $\Delta\Delta G = \Delta G^{(1)} - \Delta G^{(2)}$ can be approximated using $\Delta\Delta G \cong RT \ln (IC_{50}^{(1)} - IC_{50}^{(2)})$, where T is the temperature and R is the ideal gas constant. The difference in the binding free energy of the WT and H274Y mutant NA to OTV was estimated to be about 4.4 kcal mol^{-1}, based on the experimentally calculated IC_{50} value (*Yen et al., 2007*). This clearly shows that, as reported in the previous study (*Hou et al., 2011*), it is preferrable to use $\varepsilon = 4.0$ for NA in the MM-PBSA calculation.

Using the POVME 3.0 software (*Wagner et al., 2017*), the pocket cavity volume of the WT and H274Y mutant NA was calculated to further examine the structural changes caused by the H274Y mutation. The average pocket cavity volumes for the WT and H274Y mutant NA were estimated to be 394 and 853 $Å^3$, respectively, for the last 40 ns of MD simulations. As compared to WT NA, the pocket cavity volume of the H274Y mutant NA was increased by more than two-fold. In the following sections, such structural changes in the drug-binding site of NA have been examined in more detail with respect to the residue interactions.

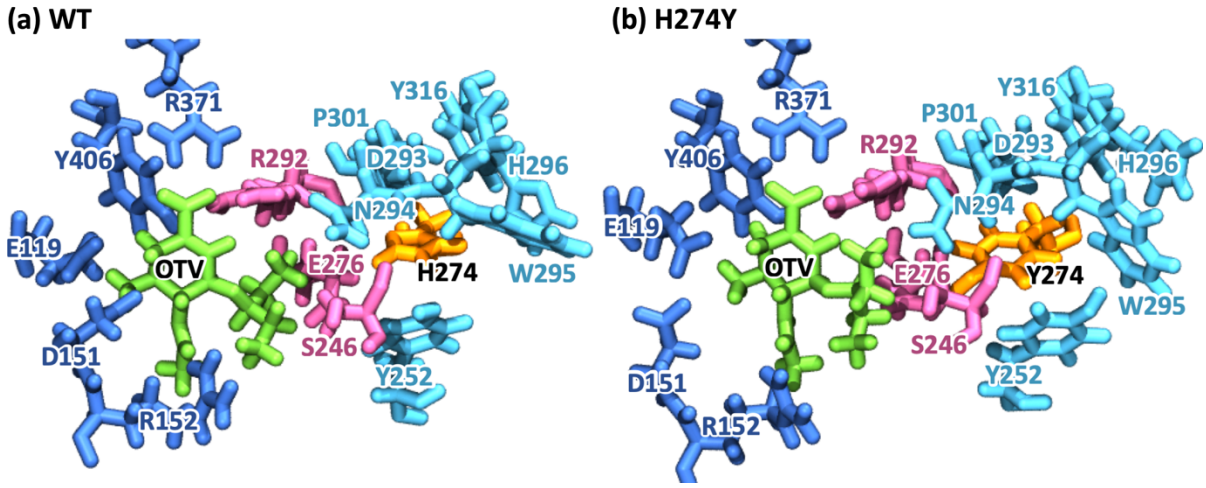

Figure 3.2: Snapshot images of (A) wild type (WT) and (B) H274Y mutant neuraminidase-oseltamivir complexes obtained from MD simulations, showing oseltamivir (OTV) binding site and H274Y mutation site (from *Yadav et al., 2021a*). OTV is shown in green, and residue 274 is shown in orange. The residues surrounding OTV and residue 274 can be categorized into 3 groups. The residues interacting directly with OTV alone are shown in blue, the residues interacting directly with residue 274 alone are shown in cyan and the residues interacting with both OTV and residue 274 are shown in purple. The snapshot images of WT and H274Y mutant NA-OTV complexes colored by atom are shown in Figure C.1. The superimposed snapshot image of WT and H274Y mutant NA-OTV complexes colored by atom is shown in Figure C.2. Figure extracted directly from the original article by *Yadav et al.* (*2021a*), without modifications (CC BY 4.0 license, https://creativecommons.org/licenses/by/4.0).

Table 3.1: Calculated binding free energies of wild type (WT) and H274Y mutant neuraminidase for oseltamivir obtained from MM-PBSA calculations.

	ΔH [kcal mol^{-1}]	$T\Delta S$ [kcal mol^{-1}]	ΔG [kcal mol^{-1}]	$\Delta\Delta G$ [kcal mol^{-1}]
WT	−35.19 ± 0.07	−23.65 ± 0.47	−11.54 ± 0.48	
H274Y	−27.28 ± 0.09	−22.94 ± 0.50	−4.34 ± 0.51	7.20

3.4.2. Dynamic Residue Interaction Network (dRIN) analysis

Figure 3.3 shows the dRIN graphs for the WT and H274Y mutant NA-OTV complexes as well as the difference between H274Y mutant and WT (H274Y-WT), showing any type of interactions (any), hydrogen bonds (hb), and van der Waals interaction (vdw). In H274Y-WT, the bonds lost are shown in red color and bonds gained are shown in blue color. In a dRIN graph, an amino acid residue or a ligand is represented by a node, and a residue-residue or a residue-ligand interaction is represented by an edge connecting two nodes. In most current methods, a single three-dimensional structure is used to model RIN (*Piovesan et al., 2016; Shcherbinin & Veselovsky, 2019*). dRIN is an extension of the original version as it models using multiple three-dimensional structures and provides statistical insights into residue interactions. The occupancy of interactions between residues is represented by the thickness of the edge.

As shown in dRIN graph of H274Y-WT in Figure 3.3, after the H274Y mutation, most changes in residue interactions occur near the OTV binding site and in the region adjacent to the residue 274, but changes in residue interactions at other sites also occurs. Generally, it is assumed that after the mutation, changes in residue interactions would occur only at the drug-binding site and the mutation site. However, as shown in dRIN graph of H274Y-WT in Figure 3.3, after the H274Y mutation, changes in residue interactions occurs not only at the OTV binding site and mutation site, but also at other sites. Hence, by using dRIN analysis, we could examine the changes in residue interactions caused by the mutation in the whole system, including the binding site, the mutation site, and the other sites.

To further examine the effect of H274Y mutation on the correlation between OTV binding site and mutation site of NA, the enlarged version of dRIN graphs focusing on OTV binding site and H274Y mutation site is constructed. Figure 3.4 shows the enlarged version of dRIN graphs for the WT and H274Y mutant NA-OTV complexes, showing the OTV binding site and H274Y mutation site; only residue interactions with total occupancy > 10% are shown.

The occupancies at which some residue interactions occur in WT and H274Y mutant NA-OTV complexes are shown in Figure 3.5a. Tables 3.2 and 3.3 summarizes the occupancies for each type of residue interaction. The changes in the occupancy of residue interactions after the H274Y mutation are shown in Figure 3.5b.

The per-residue decomposed binding free energies of the WT and H274Y mutant NA-OTV complexes estimated by using MM-PBSA calculations are shown in Figure 3.6a.

Tables 3.4 and 3.5 summarizes the detailed information on the protein-ligand interaction analysis, categorized by component per residue. The changes in the per-residue decomposed binding free energies after the H274Y mutation are shown in Figure 3.6b.

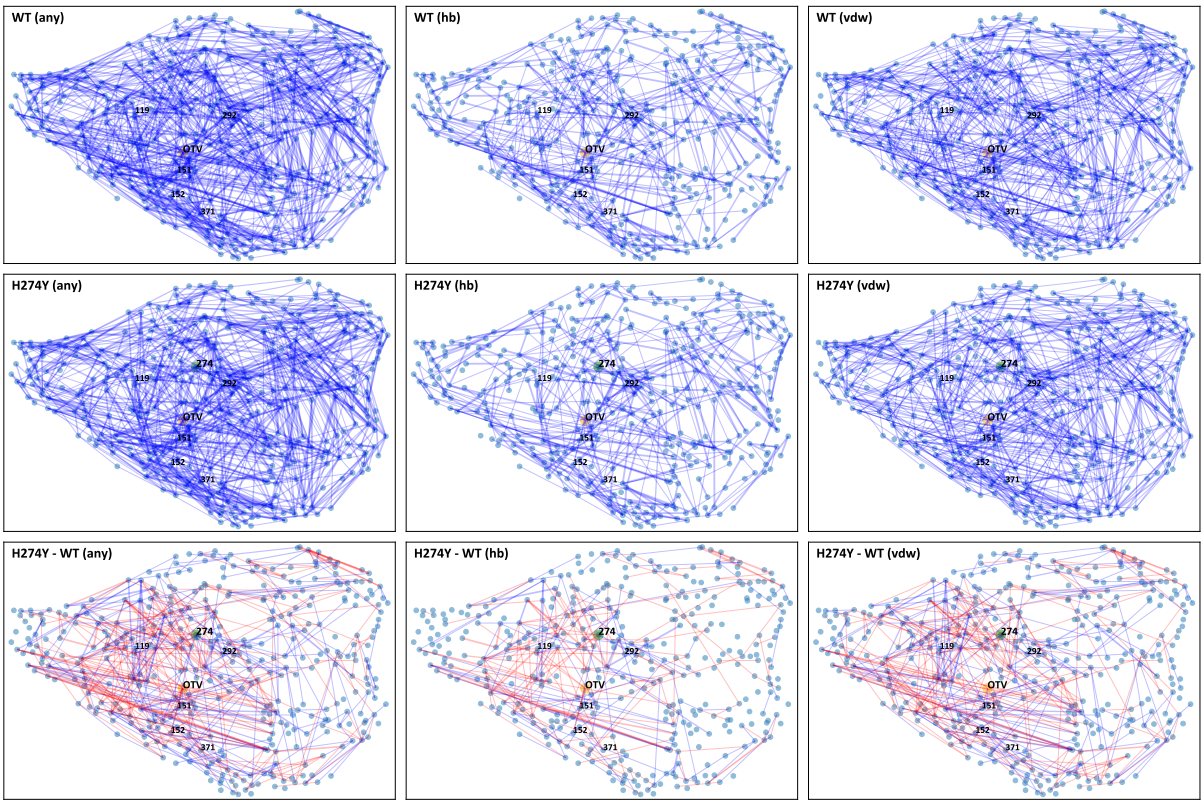

Figure 3.3: Dynamic residue interaction network (dRIN) graphs of neuraminidase-oseltamivir complexes. dRINs for wild type (WT), H274Y mutant (H274Y) and the difference between H274Y mutant and WT (H274Y-WT), showing any type of interactions (any), hydrogen bond interactions (hb), and van der Waals interaction (vdw). In H274Y-WT, the bonds lost are shown in red color and bonds gained are shown in blue color. The thickness of edge represents the occupancy of interactions.

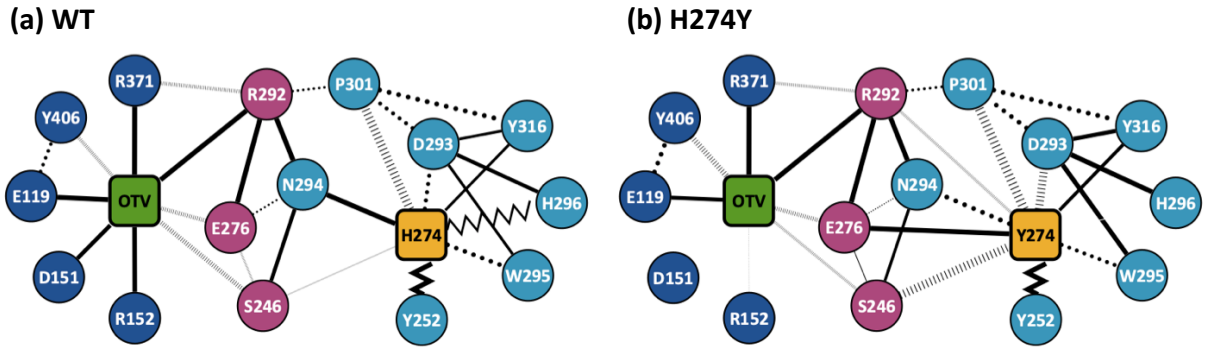

Figure 3.4: Enlarged version of dynamic residue interaction network (dRIN) graphs of (A) wild type (WT) and (B) H274Y mutant neuraminidase-oseltamivir complexes, showing oseltamivir (OTV) binding site and H274Y mutation site (from *Yadav et al., 2021a*). The OTV node is shown in green, and the residue 274 node is shown in orange. The type of residue interactions is represented by the type of edges. A hydrogen bond is represented by a solid edge, a vdW interaction is represented by a dotted edge, π-π stacking interaction is represented by a zigzag edge, and a close contact is represented by a dashed edge. The occupancy of residue interaction is represented by the thickness of the edge. The residues surrounding OTV and residue 274 can be categorized into 3 groups. The residues interacting directly with OTV alone are shown in blue, the residues interacting directly with residue 274 alone are shown in cyan and the residues interacting with both OTV and residue 274 are shown in purple. Figure extracted directly from the original article by *Yadav et al.* (*2021a*), without modifications (CC BY 4.0 license, https://creativecommons.org/licenses/by/4.0).

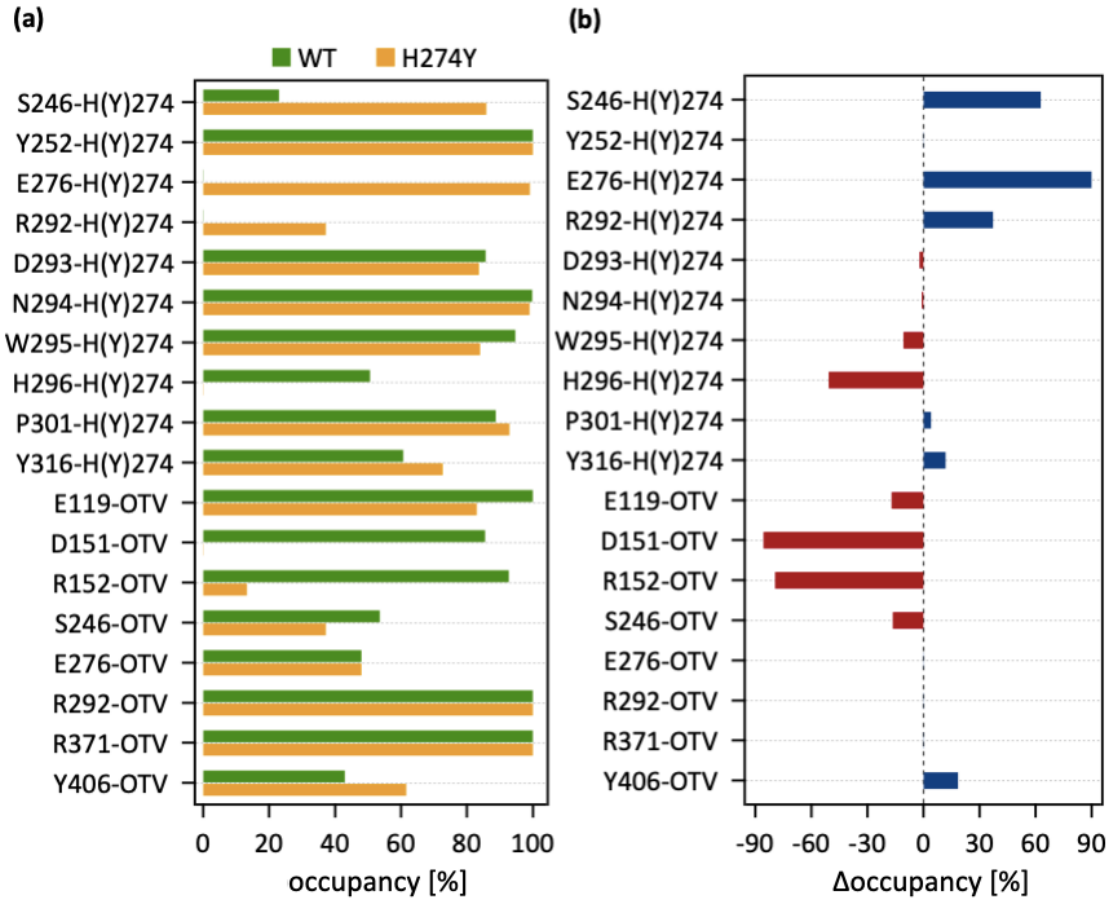

Figure 3.5: Occupancies at which some interactions are formed between residues (from *Yadav et al., 2021a*). (A) Occupancies of residue interactions for wild type (WT) and H274Y mutant within the oseltamivir (OTV) binding site and H274Y mutation site. (B) Changes in the occupancy of residue interactions after the H274Y mutation. Figure extracted directly from the original article by *Yadav et al.* (*2021a*), with modifications, label modified to (Δoccupancy [%]) in right panel (b) (CC BY 4.0 license, https://creativecommons.org/licenses/by/4.0).

Table 3.2: Occupancies at which some interactions are formed between residues in wild type (WT) neuraminidase bound to oseltamivir (OTV). Residue interaction includes hydrogen bond (HB), van der Waals interaction (vdW), π-π stacking interaction (π-π), and close contact (CC). "Any" represents the fraction of frames having any type of interaction between residues in the MD simulation.

Residue pair	HB [%]	vdW [%]	ππ [%]	CC [%]	Any [%]
S246-H274	5	8	0	12	23
Y252-H274	6	55	100	0	100
E276-H274	0	0	0	0	0
R292-H274	0	0	0	0	0
D293-H274	0	48	0	37	86
N294-H274	98	85	0	1	100
W295-H274	12	93	53	1	95
H296-H274	1	42	49	1	51
P301-H274	0	17	0	72	89
Y316-H274	55	0	0	6	61
E119-OTV	100	13	0	0	100
D151-OTV	85	15	0	1	86
R152-OTV	85	0	0	8	93
S246-OTV	0	0	0	54	54
E276-OTV	0	0	0	48	48
R292-OTV	100	0	0	0	100
R371-OTV	100	0	0	0	100
Y406-OTV	0	9	0	35	43

Table 3.3: Occupancies at which some interactions are formed between residues in H274Y mutant neuraminidase bound to oseltamivir (OTV). Residue interaction includes hydrogen bond (HB), van der Waals interaction (vdW), π-π stacking interaction (π-π), and close contact (CC). "Any" represents the fraction of frames having any type of interaction between residues in the MD simulation.

Residue pair	HB [%]	vdW [%]	ππ [%]	CC [%]	Any [%]
S246-Y274	3	6	0	77	86
Y252-Y274	0	63	100	0	100
E276-Y274	99	0	0	0	99
R292-Y274	0	0	0	37	37
D293-Y274	0	24	0	60	84
N294-Y274	57	98	0	1	99
W295-Y274	0	76	50	5	84
H296-Y274	0	0	0	0	0
P301-Y274	0	5	0	88	93
Y316-Y274	64	0	0	9	73
E119-OTV	81	7	0	2	83
D151-OTV	0	0	0	0	0
R152-OTV	6	0	0	7	13
S246-OTV	0	0	0	37	37
E276-OTV	0	0	0	48	48
R292-OTV	100	0	0	0	100
R371-OTV	100	0	0	0	100
Y406-OTV	1	18	0	42	62

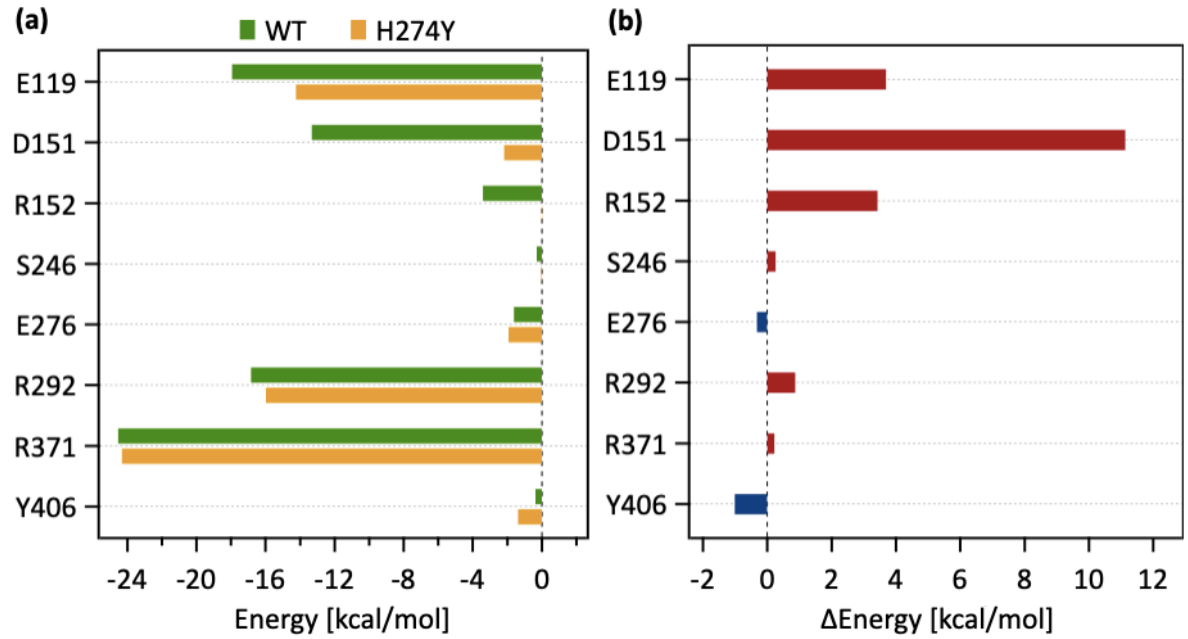

Figure 3.6: Per-residue decomposed binding free energies (from *Yadav et al., 2021a*). (A) Per-residue decomposed binding free energy of the ligand binding residues of wild type (WT) and H274Y mutant neuraminidase for oseltamivir (OTV) obtained from MM-PBSA calculations. (B) Changes in the per-residue decomposed binding free energy after the H274Y mutation. Figure extracted directly from the original article by *Yadav et al.* (*2021a*), with modifications, label modified to (ΔEnergy [kcal/mol]) in right panel (b) (CC BY 4.0 license, https://creativecommons.org/licenses/by/4.0).

Table 3.4: Per-residue decomposed binding free energy of wild type (WT) neuraminidase for oseltamivir (OTV) obtained from MM-PBSA calculations. Binding free energy is decomposed into contributions from amino acid residues around OTV and includes van der Waals (vdW), electrostatic (ES), polar solvation, and non-polar solvation components. "Total" is the sum of binding free energy components (vdW, ES, polar, and non-polar) of an amino acid residue and represents the binding free energy of an amino acid residue contributed towards the total binding free energy of NA-OTV complex.

Residue	vdW [kcal mol^{-1}]	ES [kcal mol^{-1}]	Polar [kcal mol^{-1}]	Non-polar [kcal mol^{-1}]	Total [kcal mol^{-1}]
E119	0.04	-23.90	5.92	0.00	-17.93
D151	-0.63	-16.37	3.69	0.00	-13.31
R152	-0.98	-3.25	0.81	0.00	-3.41
S246	-0.78	0.30	0.19	0.00	-0.29
E276	-0.98	-2.05	1.43	0.00	-1.61
R292	-0.60	-19.49	3.25	0.00	-16.83
R371	0.87	-30.45	5.06	0.00	-24.53
Y406	-1.40	1.41	-0.37	0.00	-0.37

Table 3.5: Per-residue decomposed binding free energy of H274Y mutant neuraminidase for oseltamivir (OTV) obtained from MM-PBSA calculations. Binding free energy is decomposed into contributions from amino acid residues around OTV and includes van der Waals (vdW), electrostatic (ES), polar solvation, and non-polar solvation components. "Total" is the sum of binding free energy components (vdW, ES, polar, and non-polar) of an amino acid residue and represents the binding free energy of an amino acid residue contributed towards the total binding free energy of NA-OTV complex.

Residue	vdW [kcal mol^{-1}]	ES [kcal mol^{-1}]	Polar [kcal mol^{-1}]	Non-polar [kcal mol^{-1}]	Total [kcal mol^{-1}]
E119	-0.13	-19.47	5.37	0.00	-14.24
D151	-0.29	-2.66	0.77	0.00	-2.18
R152	-0.63	0.30	0.35	0.00	0.02
S246	-0.59	0.43	0.12	0.00	-0.04
E276	-0.73	-3.12	1.93	0.00	-1.92
R292	-0.59	-18.61	3.24	0.00	-15.96
R371	0.89	-30.53	5.34	0.00	-24.30
Y406	-1.38	-0.03	0.04	0.00	-1.37

3.4.2.1. dRIN of WT NA

As shown in Figure 3.4a, in WT NA, OTV binding site contains five charged residues, E119, D151, R152, R292, and R371, forming strong hydrogen bond interactions with OTV. Among these, the three charged residues, E119, R292, and R371, formed very robust hydrogen bond interactions (100%); the remaining two charged residues, D151 and R152, have slightly lower hydrogen bond interaction occupancies (~90%) (Figure 3.5a and Table 3.2). The major contribution to the binding free energy of WT NA for OTV were made by E119, D151, R292, and R371, as shown in Figure 3.6a. The electrostatic interaction was the main component of contribution from these residues to the binding free energy of WT NA for OTV, as shown in Table 3.4. As shown in Table 3.2, the residues S246 and E276 formed close contact with OTV at approximately 50% occupancy, and these residues had no specific type of attractive interaction with OTV. As shown in Table 3.2, the main component of interaction between OTV

and Y406 was also close contact (35%) but formed small amount of vdW interaction (9%) as well. As shown in Figure 3.6a, the contribution from these three closely contacting residues, S246, E276, and Y406, to binding free energy of WT NA for OTV was very small.

As shown in Figure 3.4a, in the region adjacent to residue 274, H274 formed π-π stacking interactions with the aromatic residues, Y252 and H296, and vdW interaction with the aromatic residue W295. In Figure 3.4a, the edges corresponding to these residue-residue pairs only represented major interactions, but as shown in Table 3.2, the contributions of both π-π stacking and vdW interactions were significant in these aromatic residues. As shown in Table 3.2, the π-π stacking interaction between H274 and Y252 was very robust (100%), but the vdW interaction was also formed between these residues (~50%). As shown in Table 3.2, H274 and H296 formed both π-π stacking and vdW interactions, however, the π-π stacking interaction occupancy was 7% higher as compared to vdW interaction. As shown in Table 3.2, the main component of interaction between H274 and W295 was vdW interaction (~90%), however, the π-π stacking (~50%) and hydrogen bond (12%) interactions were also formed. As shown in Figure 3.4a, H274 formed hydrogen bond interactions with N294 and Y316. As shown in Table 3.2, the hydrogen bond interaction between H274 and N294 was very robust (~100%), but the vdW interactions (85%) were also formed frequently. As shown in Table 3.2, the hydrogen bond interaction occupancy between H274 and Y316 was approximately 50%. As shown in Table 3.2, the main component of interaction between H274 and P301 was close contact (72%), but a weak vdW interaction (17%) was also formed. As shown in Table 3.2, both the close contact and vdW interaction were formed between H274 and D293, however, the vdW interaction occupancy was approximately 10% higher as compared to close contact. As shown in Table 3.2, the interaction between H274 and S246 were formed in very small fractions.

The dRIN graph shows that there was no direct interaction between OTV and residue 274 (Figure 3.4a). Hence, the reduction in binding affinity between NA and OTV after the H274Y mutation can be due to the indirect effects of changes in the residue interaction network.

3.4.2.2. dRIN of H274Y mutant NA

Figure 3.4b shows that in comparison with the dRIN of WT NA, the dRIN characteristics of the H274Y mutant NA changed significantly. As shown in Figure 3.5b, due to H274Y mutation, the occupancy of residue-ligand interactions between OTV and the binding site residues, E119,

D151, R152, and S246 reduced, whereas the occupancy of interaction between OTV and the binding site residue Y406 increased. Particularly, the occupancies of interaction between OTV and the binding site residues D151 and R152 were highly reduced (> 80%) and could be expected to have significant contribution to the reduced binding affinity of H274Y mutant NA with OTV. Figure 3.6b shows that due to H274Y mutation, the decomposed binding free energy of residues E119, D151, and R152 increased significantly, leading to destabilization of interaction between H274Y mutant NA and OTV. The residues D151 and R152 are part of the 150-loop region of NA. According to previous studies, due to H274Y mutation, the conformation of the 150-loop region of NA can change from closed to open (*Kar & Knecht, 2012*). Hence, due to the H274Y mutation, the OTV binding affinity to NA reduced because of the cleavage of residue-ligand interaction.

As shown in Figure 3.4b, even after H274Y mutation, the structure of dRIN of the H274Y mutation site remained almost unchanged, except for the interface bordering the OTV and a few residue-residue pairs. Particularly, the π-π stacking and vdW interactions were formed between H274 and H296 in WT NA, however, no interaction was formed between them in H274Y mutant NA (Figure 3.4 and Tables 3.2 and 3.3). Notably, in WT NA, the high occupancies of both vdW and hydrogen bond interactions were observed between H274 and N294; however, after the H274Y mutation, the occupancy of hydrogen bond interaction decreased as compared to WT NA, resulting in vdW interaction becoming more prevalent (Tables 3.2 and 3.3). Similarly, in both WT and H274Y mutant NA, the overall occupancy of interaction between residue 274 and D293 was approximately 80%, but the major component of interaction was vdW interaction in WT NA, and close contact in H274Y mutant NA (Tables 3.2 and 3.3).

Figure 3.4b shows that three residues, S246, E276, and R292, were at the interface between H274Y mutation site and OTV binding site of NA and in H274Y mutant NA, these three interface residues were observed to have direct interaction with both residue 274 and OTV. H274Y mutation resulted in significant changes at the interface region in the dRIN. Figure 3.5b shows that due to H274Y mutation, the occupancies of interactions between the residue 274 and the three interface residues, S246, E276, and R292, increased, whereas the occupancies of interactions between OTV and the three interface residues, S246, E276, and R292, remained almost unchanged. Notably, in WT NA, there was no interaction observed between H274 and E276; however, a strong hydrogen bond interaction (~100%) was formed between Y274 and E276 in H274Y mutant NA (Figure 3.4 and Tables 3.2 and 3.3). In contrast, close contact with

an occupancy of about 50% were formed between OTV and E276 in WT NA, and even after the H274Y mutation, this occupancy remained unchanged (Figure 3.4 and Tables 3.2 and 3.3). In WT NA, weak interactions with an overall occupancy of about 23% were formed between S246 and residue 274, and due to H274Y mutation, the occupancy of close contact increased to about 80% and the overall occupancy increased to about 90% (Tables 3.2 and 3.3). On the contrary, in WT NA, the close contact occupancy between OTV and S246 was 54%, and after H274Y mutation, this occupancy decreased, but the difference was small, approximately 17% (Tables 3.2 and 3.3). In WT NA, no interaction was formed between H274 and R292; however, after H274Y mutation, close contact (~40%) was formed between Y274 and R292 (Tables 3.2 and 3.3). In contrast, in WT NA, a robust hydrogen bond interaction (100%) was formed between OTV and R292 and even after H274Y mutation, this occupancy remained unchanged (Tables 3.2 and 3.3).

3.5. Discussion

The results of dRIN analysis of WT and H274Y mutant NA clearly revealed that due to H274Y mutation, the residue interactions were partially altered at both H274Y mutation site and OTV binding site. Such changes in residue interactions can cause the reduction in OTV binding affinity to NA, resulting in drug resistance in influenza viruses. Based on the dRINs shown in Figure 3.4, the detailed molecular mechanism of OTV drug resistance caused by NA H274Y mutation can be explained as follows.

Due to the presence of bulky aromatic residues, Y252, W295, H296, and Y316, there is only a limited amount of free volume space accessible around residue 274. When histidine is mutated to the bulkier tyrosine at position 274 in NA, the phenyl and hydroxyl groups of Y274, which are the key contributors to the bulkiness, cannot be accommodated in such a limited amount of free volume space. After the H274Y mutation, the occupancy of interactions between residue 274 and its surrounding residues remained almost unchanged, except for S246, E276, R292, and H296. A strong hydrogen bond interaction is formed between interface residue E276 and the Y274 hydroxyl group facing the OTV binding site. Furthermore, more close contacts are formed between the Y274 phenyl group and the interface residues, S246 and R292. However, even after H274Y mutation, these interface residues remain in close contact with OTV. Overall, the orientation of OTV is slightly disrupted by these interface residues. Due to the change in orientation of OTV, the 150-loop region is pushed out of the binding site through D151 and R152. This results in the opening of 150-loop and the loss of interaction between

OTV and 150-loop residues, D151 and R152. Figure 3.6 shows that D151 significantly contributes to stabilize the binding between NA and OTV. Therefore, it results in the reduction in OTV binding affinity to H274Y mutant NA. Hence, the H274Y mutant NA becomes highly resistant to OTV.

Previous studies have shown that a large shift in the orientation of E276 occurs after the H274Y mutation in NA as compared to WT NA, causing a large shift in the OTV orientation (*Collins et al., 2008; Collins et al., 2009*). As mentioned earlier, after the H274Y mutation, the 150-loop of NA is reported to be in an open conformation (*Kar & Knecht, 2012*). *Kar & Knecht* (*2012*) showed that in the case of N8 NA, in both open and closed conformations of the 150-loop, the interaction between OTV and the binding site residues is mediated by the hydrogen bond bridges formed by water molecules; however, in the case of H5N1 NA, no water-mediated binding of OTV was observed. In this study, we investigated the OTV drug resistance mechanism of the H5N1 H274Y mutant NA, and similar to their study, no water-mediated binding of OTV was observed.

Furthermore, we investigated how the drug binding mechanism of NA is affected by the 150-loop dynamics. By superimposing 100 snapshot images obtained from MD simulations, the conformational changes of the 150-loop region (residues 147−152) in the WT and H274Y mutant NA-OTV complexes are shown in Figure 3.7. As shown in Figure 3.7a, the 150-loop region of WT NA tends to form closed conformations, thus the hydrogen bond interactions between OTV and 150-loop residues, D151 and R152, can be formed frequently. However, the 150-loop region of H274Y mutant NA is in the open conformation, thus the hydrogen bond interactions between OTV and 150-loop residues, D151 and R152, cannot be formed (Figure 3.7b). The structural fluctuations of each amino acid residue in the WT and H274Y mutant NA-OTV complexes are shown as B-factor values in Figure 3.8. The structural fluctuation of the 150-loop region of WT NA was significantly large (Figure 3.8). However, due to the H274Y mutation, the structural fluctuation of the 150-loop region significantly reduced (Figure 3.8). To summarize, Figures 3.7 and 3.8 shows that the 150-loop region of WT NA undergoes conformational changes with large fluctuations between the open and closed conformations, whereas the 150-loop region of H274Y mutant NA remains in open conformation. This behavior of the 150-loop region is consistent with that shown in the previous study (*Kar & Knecht, 2012*), and in this study, the dynamics of the 150-loop region was quantitatively clarified by combining it with the dRIN analysis.

The above discussion based on the dRIN analysis supports these previous studies and provides a new perspective for comprehensively understanding the molecular mechanism of OTV drug resistance in influenza viruses due to NA H274Y mutation.

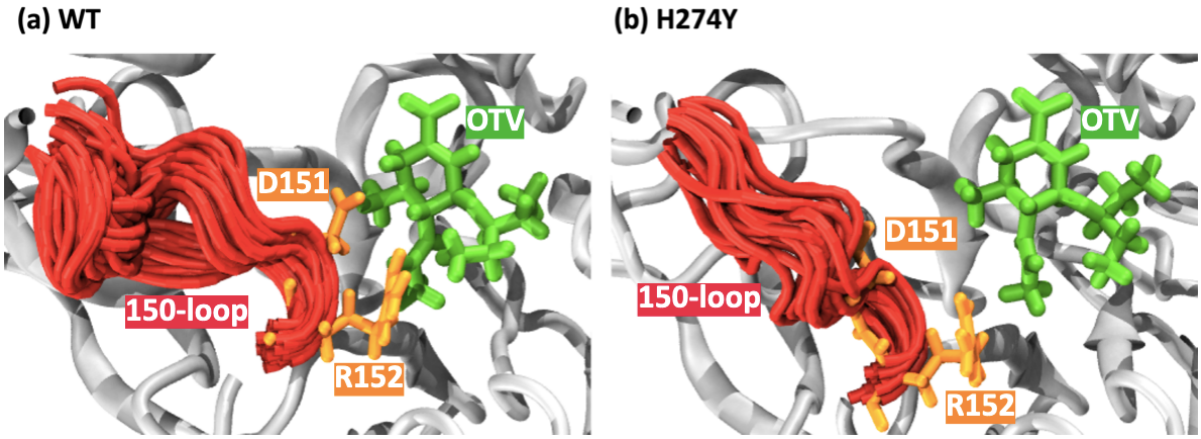

Figure 3.7: Snapshot images of the 150-loop region (residues 147-152) of (A) wild type (WT) and (B) H274Y mutant neuraminidase-oseltamivir complexes obtained from MD simulations (from *Yadav et al., 2021a*). The 150-loop region of NA is shown in red, and conformational changes are represented by superimposing 100 snapshot images obtained from MD simulation. Oseltamivir (OTV) is shown in green. Residues D151 and R152 are shown in orange. Figure extracted directly from the original article by *Yadav et al.* (*2021a*), with modifications, label added to both images (CC BY 4.0 license, https://creativecommons.org/licenses/by/4.0).

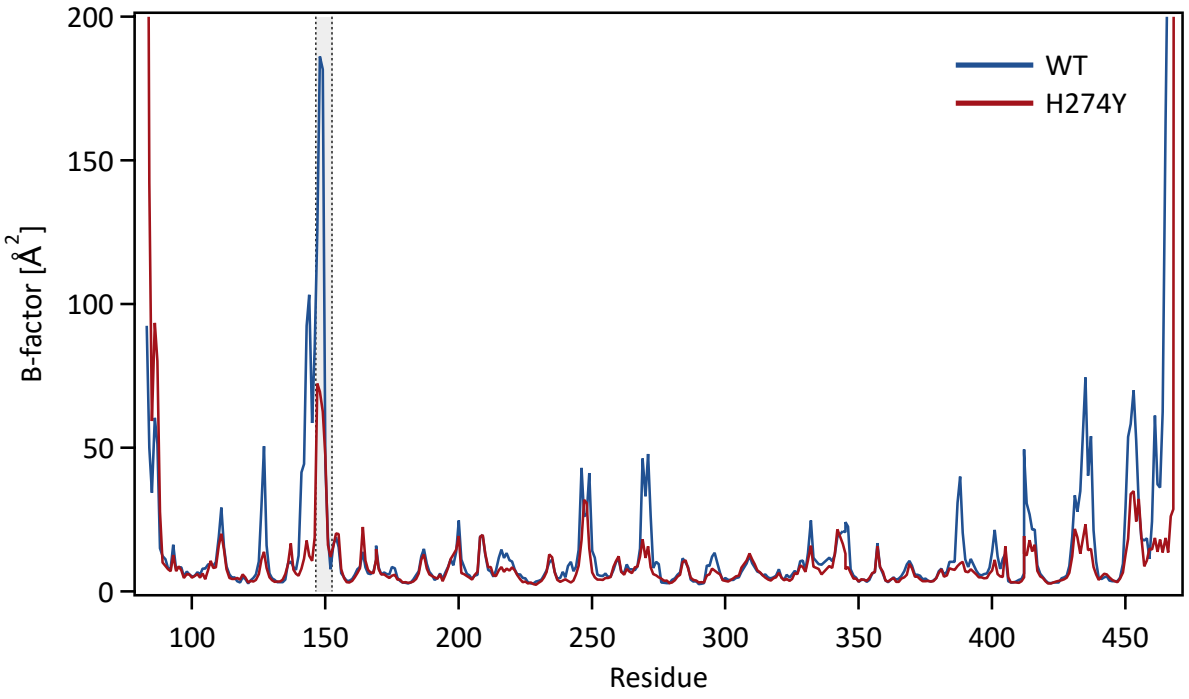

Figure 3.8: B-factor values for each residue (from *Yadav et al., 2021a*). The structural fluctuations of each amino acid residue in wild type (WT) and H274Y mutant neuraminidase bound to oseltamivir are shown as the B-factor values. The gray band represents the 150-loop region (residues 147-152). Figure extracted directly from the original article by *Yadav et al.* (*2021a*), without modifications (CC BY 4.0 license, https://creativecommons.org/licenses/by/4.0).

3.6. Conclusions

In this study, we used MD simulations to theoretically investigate the molecular mechanism of OTV drug resistance in influenza virus due to the H274Y mutation in N1 NA. The effect of H274Y mutation on the residue interactions in the OTV binding site and H274Y mutation site of NA is quantitatively shown using dRIN graphs. The results of dRIN analysis revealed that the interaction between OTV binding site and H274Y mutation site of NA is mediated by three interface residues connecting them. After the H274Y mutation, the interaction between residue 274 and the three interface residues in NA significantly enhanced, resulting in significant reduction in the interaction between OTV and its surrounding 150-loop residues. Such changes in residue interactions could lead to the reduction of OTV binding affinity to NA, resulting in drug resistance of OTV in influenza viruses. To conclude, using dRIN analysis, we succeeded in understanding the characteristic changes in residue interactions after the H274Y

mutation, which can elucidate the molecular mechanism of drug resistance of OTV in influenza viruses. Finally, the dRIN analysis used in this study can be applied to a wide range of systems, including individual proteins, protein-protein complexes, and protein-ligand complexes, to characterize the dynamic characteristics of the residue interactions.

4. "Theoretical insights into the molecular mechanism of I117V mutation in neuraminidase mediated reduction of oseltamivir drug susceptibility in A/H5N1 influenza virus"

4.1. Abstract

The mutation of Ile-to-Val at position 117 (I117V) in neuraminidase (NA) causes the reduction in the susceptibility of oseltamivir (OTV) to A/H5N1 influenza viruses. However, the molecular mechanism of the effect of I117V mutation on the intermolecular interactions of NA-OTV complex has not been fully elucidated yet. In this study, we analyzed the characteristic conformational changes associated with the I117V mutation that results in the reduction of the binding affinity of OTV to NA using molecular dynamics (MD) simulations. The results of MD simulations revealed that the secondary structure changes around the mutation site due to the NA I117V mutation, had a significant effect on the residue interactions within the OTV binding site. In WT NA-OTV complex, the positively charged side chain of R118 (part of the β-sheet region) and the negatively charged side chain of E119 (part of the OTV-binding site residues) interacted frequently. This can lead to the reduction in the electrostatic repulsion between the negatively charged side chains of E119 and D151, thus both E119 and D151 can simultaneously form the hydrogen bond interactions with OTV more frequently, hence greatly contributing towards the OTV binding affinity to NA. Due to NA I117V mutation, the β-sheet occupancy of R118 decreases, leading to the less frequent interaction between the positively charged side chain of R118 and the negatively charged side chain of E119; resulting in the increase in electrostatic repulsion between the negatively charged side chains of E119 and D151 as compared to the WT case, thus both E119 and D151 have difficulty in simultaneously forming hydrogen bond interactions with OTV, leading to the reduction in the OTV binding affinity to NA. Hence, the conformational changes in R118, E119, and D151 within the binding site and around the mutation site associated with the NA I117V mutation, results in the reduction of OTV susceptibility to influenza viruses.

4.2. Introduction

Influenza A virus is a zoonotic pathogen, that infects various birds and mammals, including human (*Webster et al., 1992*). Based on the antigenic variations in the surface glycoproteins, hemagglutinin (HA) and neuraminidase (NA), the influenza A viruses are categorized into various subtypes (*Gamblin & Skehel, 2010*). Till now, sixteen HA (H1-H16) and nine NA

(N1-N9) subtypes have been isolated from wild aquatic birds (*Fouchier et al., 2005*). HA binds to the terminal sialic acid of the surface receptor of the host cell and mediates entry of virus into the host cell via endocytosis. NA facilitates the exit of progeny viruses from the infected host cells by cleaving the bond between terminal sialic acid and cellular glycoconjugates. Currently, various anti-NA drugs are available for the influenza treatment, including oseltamivir (OTV), zanamivir, laninamivir, and peramivir (*McKimm-Breschkin, 2013c*). OTV is the most widely used anti-NA drug among them (*Kim et al., 1997*).

From avian and swine species as well as humans, OTV resistant H1N1 and H5N1 viruses have been isolated (*McKimm-Breschkin et al., 2007; Monto et al., 2006; Rameix-Welti et al., 2006*). This indicates that not only drug-selective pressure, but also natural genetic variation could cause the reduction of OTV sensitivity to influenza viruses. Several H5N1 viruses with an Ile-to-Val mutation at residue 117 (I117V) in NA were isolated from some avian species in the mid-2000s (*Chen et al., 2010; Creanga et al., 2017; Govorkova et al., 2009; Hurt et al., 2007; Ilyushina et al., 2010; Kode et al., 2019; Marinova-Petkova et al., 2014; McKimm-Breschkin et al., 2007; McKimm-Breschkin et al., 2013b; Takano et al., 2013*). *In vivo* and *in vitro* studies have shown that NA conferred reduced OTV susceptibility after the NA I117V mutation (*Chen et al., 2010; Creanga et al., 2017; Hurt et al., 2007; Ilyushina et al., 2010; Kode et al., 2019; McKimm-Breschkin et al., 2007; McKimm-Breschkin et al., 2013b; Takano et al., 2013*). The NA active site comprises of eight functional residues [R118, D151, R152, R224, E276, R292, R371, and Y406; N2 numbering] and eleven framework residues [E119, R156, W178, S179, D198, I222, E227, H274, E277, N294, and E425; N2 numbering], and surprisingly residue 117 is not included in the NA active site (*Colman et al., 1983; Colman et al., 1993*). The molecular mechanism behind how the mutation at residue 117, which is not included in the NA active site, impacts the molecular interaction between OTV and NA indirectly is still unclear.

Several computational studies have investigated the molecular mechanism of reduction in OTV susceptibility to I117V mutant NA using molecular dynamics (MD) simulations (*Mhlongo & Soliman, 2015; Takano et al., 2013*). *Takano et al.* (*2013*) investigated the effect of NA I117V mutation on susceptibility of OTV *in vivo*, *in vitro*, and *in silico*. According to their experimental results, due to NA I117V mutation, OTV susceptibility to NA reduced slightly *in vitro* and dramatically *in vivo*. Furthermore, they investigated the molecular mechanism of reduction in OTV susceptibility to I117V mutant NA using a single 2.5 ns trajectory obtained from MD simulations. According to their computational results, the

decrease in the OTV binding affinity to I117V mutant NA is due to the loss of hydrogen bond between the side chain of R118 of NA and the OTV carboxyl group. *Mhlongo & Soliman* (*2015*) investigated the molecular mechanism of reduction in OTV susceptibility to I117V mutant NA by analyzing four distinctive 25 ns trajectories obtained from MD simulations. According to their computational results, the OTV orientation in the drug binding site of NA is disrupted after the I117V mutation, due to the loss of hydrogen bond between the side chain of E119 of NA and the OTV amino group, causing the reduction in OTV binding affinity to NA. The production trajectory of the MD simulations was too short to reach reliable statistical result in these previous computational studies. Additionally, they only focused on analyzing the changes in the direct interactions between the NA active site residues and OTV. However, the molecular mechanism of how the NA II17V mutation, which is not contained in the NA active site, could affect the intermolecular interaction with OTV is still unclear.

In this study, we computed four distinctive 100 ns MD simulations for the WT and I117V mutant NA bound to OTV in the A/H5N1 influenza virus. We investigated the characteristic conformational changes around the I117V mutation site of NA that significantly affected the intermolecular interactions with OTV, based on the multiple production trajectories obtained from MD simulations. The results revealed that the conformational change of R118 near the I117V mutation site had significant effect on the interactions between OTV and active site residues, E119 and D151, resulting in the reduction of OTV binding affinity to NA after the I117V mutation. Hence, the present study succeeded in clarifying the molecular mechanism of how the I117V mutation reduces the OTV susceptibility to NA.

4.3. Methods

4.3.1. Initial structures

The Amber 20 package was used for structure preparation and MD simulations (*Case et al., 2020*). The crystal structure of WT NA-OTV complex in A/H5N1 avian influenza virus was obtained from the Protein Data Bank (PDB ID: 2HU4) (*Russell et al., 2006*) and a single monomer was used for modeling. The LEaP module in the Amber 20 package was used to generate the structure of I117V mutant NA-OTV complex by replacing isoleucine with valine at position 117 in the WT NA-OTV complex. One calcium ion is contained in H5N1 NA, which is required for structural stability (*Smith et al., 2006*). In the crystal structure of A/H5N1 NA registered as 2HU4, no calcium ion was found, therefore the coordinates of the calcium ion were determined from the related structure registered as 3CL0 (*Collins et al., 2008*). The

PDB2PQR server was used to determine the protonation state of histidine at pH 7 in the modeled complex (*Dolinsky et al., 2004*), and the other ionized residues (arginine, lysine, aspartic acid, and glutamic acid) were treated as charged entities. The missing hydrogen atoms of proteins and OTV were added using the LEaP module in the Amber 20 package. Eight disulfide bonds are present in H5N1 NA. The "bond" command was executed in the tLEaP program to form a covalent bond between the SG atoms of the proximate cysteine residues for each disulfide bond. For proteins, the FF14SB force field of AMBER was used (*Maier et al., 2015*). For OTV, the Generalized AMBER Force Field (GAFF) was used (*Wang et al., 2004*). The restrained electrostatic potential fitting procedure was used to determine the partial atomic charges of OTV (*Bayly et al., 1993*), based on HF/6-31G(d) level of quantum chemistry calculations using Gaussian 16 program (*Frisch et al., 2016*). The WT and I117V mutant NA-OTV complexes were dissolved in a truncated octahedral box of TIP3P water molecules with a distance of at least 10 Å around them. The total charge of the complexes was neutralized by adding sodium counter ions.

4.3.2. Molecular Dynamics (MD) simulations

The PMEMD module of Amber 20 package was used to perform all MD simulations (*Case et al., 2020*). The energy minimization of each system was performed using the steepest descent method for first 500 steps, followed by the conjugate gradient method for the next 4,500 steps. After energy minimization, each system was gradually heated to 300 K over a period of 200 ps in the *NVT* ensemble, with a harmonic restraint weight of 2 kcal mol^{-1} $Å^{-2}$ on the complexes, except for the hydrogen atoms. The weak-coupling algorithm was used to regulate the temperature (*Berendsen et al., 1984*). The SHAKE algorithm was used to constrain all bond lengths including hydrogen atoms (*Ryckaert et al., 1977*), allowing an MD time step of 2 fs to be used. Periodic boundary conditions were adopted. For the non-bonded interactions, a cut-off of 8 Å was used. The particle-mesh Ewald method was used to treat the long range electrostatics (*Darden et al., 1993*). After heating, the system was equilibrated by performing 10 ns of unrestrained MD simulations in the *NpT* ensemble at a pressure of 1.0 atm and a temperature of 300 K. The berendsen barostat was used to maintain the pressure. Finally, 100 ns of four distinctive MD simulations were performed starting with different coordinates and velocities in the *NpT* ensemble at a pressure of 1.0 atm and a temperature of 300 K, where the initial coordinates were randomly obtained from an additional 10 ns MD simulation trajectory after the equilibration phase and the initial velocities were randomly reassigned. The production

phase to be analyzed was the last 80 ns of MD simulations, which was determined based on the root mean square displacement (RMSD) of the protein backbone atoms with respect to the initial structure along the simulation time. Figure 4.1 shows the time series of RMSD of the WT and I117V mutant NA-OTV complexes. The time series of radius of gyration of the WT and I117V mutant NA-OTV complexes is shown in Figure D.1. After 20 ns, the changes in RMSD were almost constant, indicating that the MD simulations properly converged in the region of 20–100 ns.

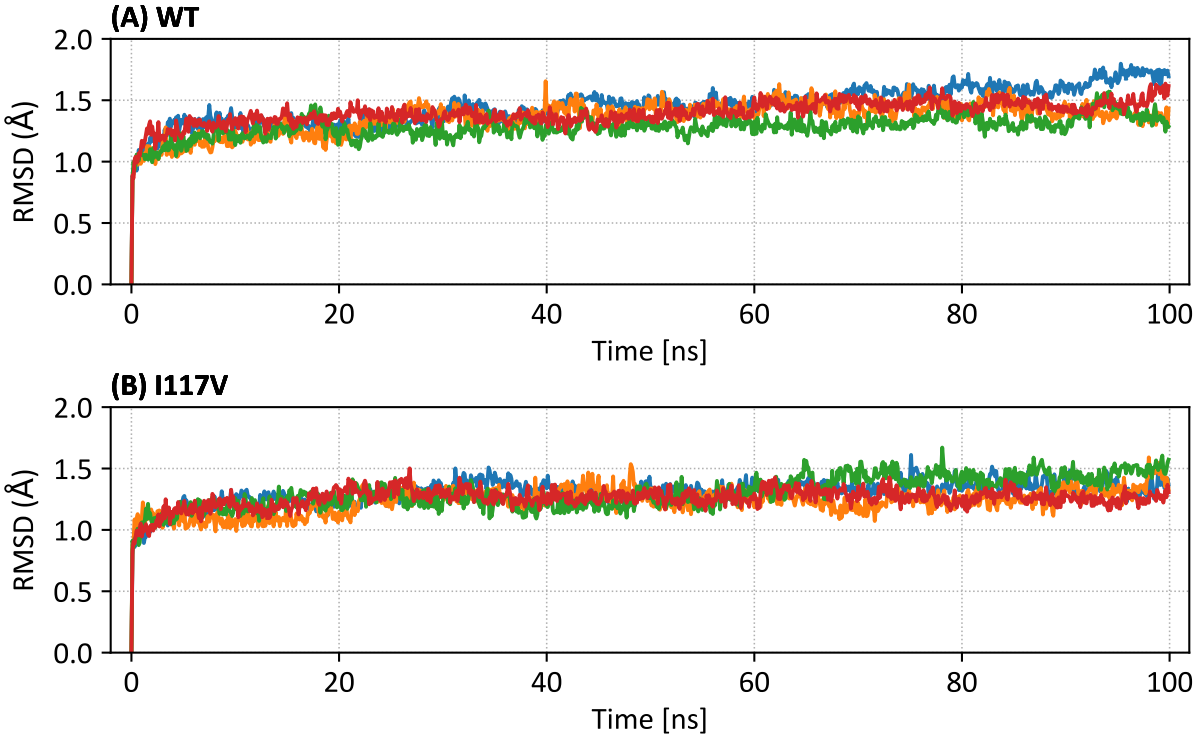

Figure 4.1: The time series of the root mean square displacement (RMSD) of four distinct MD trajectories of (A) wild type (WT) and (B) I117V mutant neuraminidase-oseltamivir complexes (from *Yadav et al., 2021b*). RMSDs for the protein backbone atoms in WT and I117V mutant NA for 15th to 365th amino acid residues, excluding both ends of NA, with respect to the initial structure along the simulation time. The production phase to be analyzed was the last 80 ns of MD simulations. Figure extracted directly from the original article by *Yadav et al.* (*2021b*), without modifications (CC BY 4.0 license, https://creativecommons.org/licenses/by/4.0).

4.3.3. Binding free energy calculations

The Molecular Mechanics Poisson Boltzmann Surface Area (MM-PBSA) continuum solvation method in the Amber 20 package (MMPBSA.py) was used to estimate the binding free energies

for OTV bound to WT and I117V mutant NA (*Miller et al., 2012*). The adaptive Poisson Boltzmann (PB) solver was used to estimate the electrostatic contribution to the solvation free energy (*Baker et al., 2001*). The dielectric properties of the protein interior and solvent phase are represented as dielectric constants in calculations using continuum methods. In the present study, the dielectric constant of the solvent phase was set to 80. As the NA active site consists of many charged residues, a relatively large dielectric constant is desirable for NA, hence, in the present study, the dielectric constant of the protein interior was set to 4 (*Hou et al., 2011*). The ionic strength was set at 150 mM. The ratio between the longest dimension of the rectangular finite-difference grid and that of the solute was set to four. The linear PB equation was solved using a maximum of 1,000 iterations. The Linear Combination of Pairwise Overlap (LCPO) algorithm was used to determine the surface area for the nonpolar solvation energy term (*Weiser et al., 1999*). MM-PBSA calculations were performed over 400 frames extracted from the four distinctive production phases of the MD simulations.

The entropy due to the vibrational degrees of freedom was calculated by normal mode analysis of 100 configurations using the NAB program in the Amber 20 package. Each configuration was energy minimized with a generalized Born solvent model, using a maximum of 10,000 steps with a target root-mean-square gradient of 10^{-3} kcal mol^{-1} $Å^{-1}$.

4.3.4. Dynamic Residue Interaction Network (dRIN) analysis

The dynamic residue interaction network (dRIN) analysis was performed over 400 frames extracted from the four distinctive production phases of the MD simulations of the WT and I117V mutant NA bound to OTV (*Yadav et al., 2021a*). In this study, residue-ligand interactions were included in the residue interactions. The residue-residue and residue-ligand interactions were classified into specific types, including hydrogen bond, disulfide bridge, salt bridge, van der Waals (vdW) interaction, π-π stacking interaction, and π-cation interaction, using the RING 2.0 software (*Piovesan et al., 2016*). The hydrogen bonds between ligand and residues in the NA-OTV complex were detected using the CPPTRAJ program (*Roe & Cheatham, 2013*) in the Amber 20 package, as the RING 2.0 software missed them. Even though the RING 2.0 software detected various types of interactions per residue pair, only one interaction per interaction type was considered. We further examined the interactions between residues that were not included in the attractive interactions detected by the RING 2.0 software but were in close contact with one another. In this study, two residues were identified as being in close contact, if $d_{ij} - (\sigma_i + \sigma_j) < 0.4$ Å, where d_{ij} denotes the interatomic distance between

the *i*- and *j*-th atoms in the two residues and σ_i is the vdW radius of the *i*-th atom. Several molecular structure visualization and analysis programs, including UCSF Chimera software (*Pettersen et al., 2004*), have adopted this definition of close contact. By repeating the above procedure, the dRINs were formed using the sets of residue interactions and close contacts obtained from the MD simulations for the WT and I117V mutant NA-OTV complexes. The occupancy of residue interactions was calculated as the percentage of frames with interactions between residues in the MD simulation. The dRIN analysis is implemented using the ruby script (Appendix C.1). To graphically visualize the dRIN, with residues represented by nodes and interactions between residues represented by edges, various software can be used such as the Cytoscape software (*Shannon et al., 2003*) and it can also be visualized using Matplotlib library for Python programming language (*Hunter, 2007*).

4.4. Results

4.4.1. Binding structures and energies

The snapshot images of the OTV binding site and the region around the I117V mutation site obtained from the MD simulations for the WT and I117V mutant NA bound to OTV is shown in Figure 4.2. As shown in Figure 4.2, in the WT and I117V mutant NA-OTV complexes, OTV forms hydrogen bond interactions with three positively charged residues, R152, R292, and R371, and two negatively charged residues, E119 and D151. No hydrogen bond interactions were observed between OTV and positively charged residue R118. This is supported by the co-crystal structure of WT A/H5N1 NA-OTV complex (PDB ID: 2HU4) (*Russell et al., 2006*) showing that R118 is not in a position to form hydrogen bond interactions with OTV.

The estimated binding free energies (ΔG) of the WT and I117V mutant NA for OTV obtained from the MM-PBSA calculations, as well as the enthalpy (ΔH) and entropy ($T\Delta S$), are summarized in Table 4.1. The estimated binding free energies of OTV for the WT and I117V mutant NA were −14.60 and −11.88 kcal mol^{-1}, respectively. The I117V mutation increases the binding free energy of OTV by 2.72 kcal mol^{-1}, which could slightly reduce the OTV susceptibility to NA. This is supported by the experimental fact that in H5N1 viruses, I117V mutant NA has a 3- to approximately 50-fold reduction in relative susceptibility to OTV as compared to WT NA (*Chen et al., 2010; Creanga et al., 2017; Hurt et al., 2007; Ilyushina et al., 2010; Kode et al., 2019; McKimm-Breschkin et al., 2007; McKimm-Breschkin et al., 2013b; Takano et al., 2013*). According to the antiviral working group criteria of World Health Organization (WHO), influenza A viruses with less than 10-fold change in the half maximal

inhibitory concentration (IC_{50}) value were characterized as exhibiting normal inhibition, while those with 10- to 100-fold and more than 100-fold changes exhibited reduced and highly reduced inhibition, respectively (*World Health Organization, 2012*). If experiments are performed under the same conditions, the relative binding free energy of $\Delta\Delta G = \Delta G^{(1)} - \Delta G^{(2)}$ can be approximated using $\Delta\Delta G \cong RT \ln (IC_{50}^{(1)} - IC_{50}^{(2)})$, where T is the temperature and R is the ideal gas constant. The experimentally observed 3- to 50-fold change in the IC_{50} value associated with the I117V mutation in NA, corresponds to a binding free energy difference of 0.7–2.3 kcal mol^{-1}. The current results are in qualitative agreement with the previous experimental studies, implying that the MD simulations, which are the basis of the subsequent analyses, are reliable.

In this study, we adopted the single-trajectory approach in MM-PBSA calculation because it assumes that no significant conformational changes occur upon ligand binding. The single-trajectory approach in MM-PBSA calculation has been widely used in previous studies, to compute the binding free energy differences as it has good balance between computational cost and reliability (*Wang et al., 2019*). In some cases, the single-trajectory approach in MM-PBSA calculation used in this study is less reliable for computing the binding free energies as compared to the multiple-trajectory approach in MM-PBSA calculation that considers the conformational changes upon ligand binding. However, we emphasize that the binding free energy difference of 2.72 kcal mol^{-1} between the WT and I117V mutant NA-OTV complexes observed in this study is in good agreement with the experimentally observed value of 0.7–2.3 kcal mol^{-1}, which shows that our MD simulations are sufficiently reliable for investigating changes in various intra-protein interactions, including hydrogen bond interactions, and secondary structures, which is the focus of this study.

As shown in Figure 4.2, in both WT and I117V mutant NA-OTV complex, there is no direct interaction between residue 117 of NA and OTV. Thus, after the I117V mutation, the reduction in OTV binding affinity to NA could be the result of indirect effects caused by changes in the interaction network of amino acid residues within the protein. As shown in Table 4.1, there is almost no change in the entropic component ($T\Delta S$) after the I117V mutation, indicating that the difference in the binding free energies ($\Delta\Delta G$) is mostly enthalpy driven rather than entropy driven. Based on this observation, subsequent analyses that focus on the factors responsible for changes in direct interactions between NA and OTV are expected to be reliable. To elucidate the molecular mechanism of how the II17V mutation of NA, which is not contained in the drug binding site of NA, could decrease the OTV susceptibility to NA, we performed the

following detailed analysis based on MD simulations.

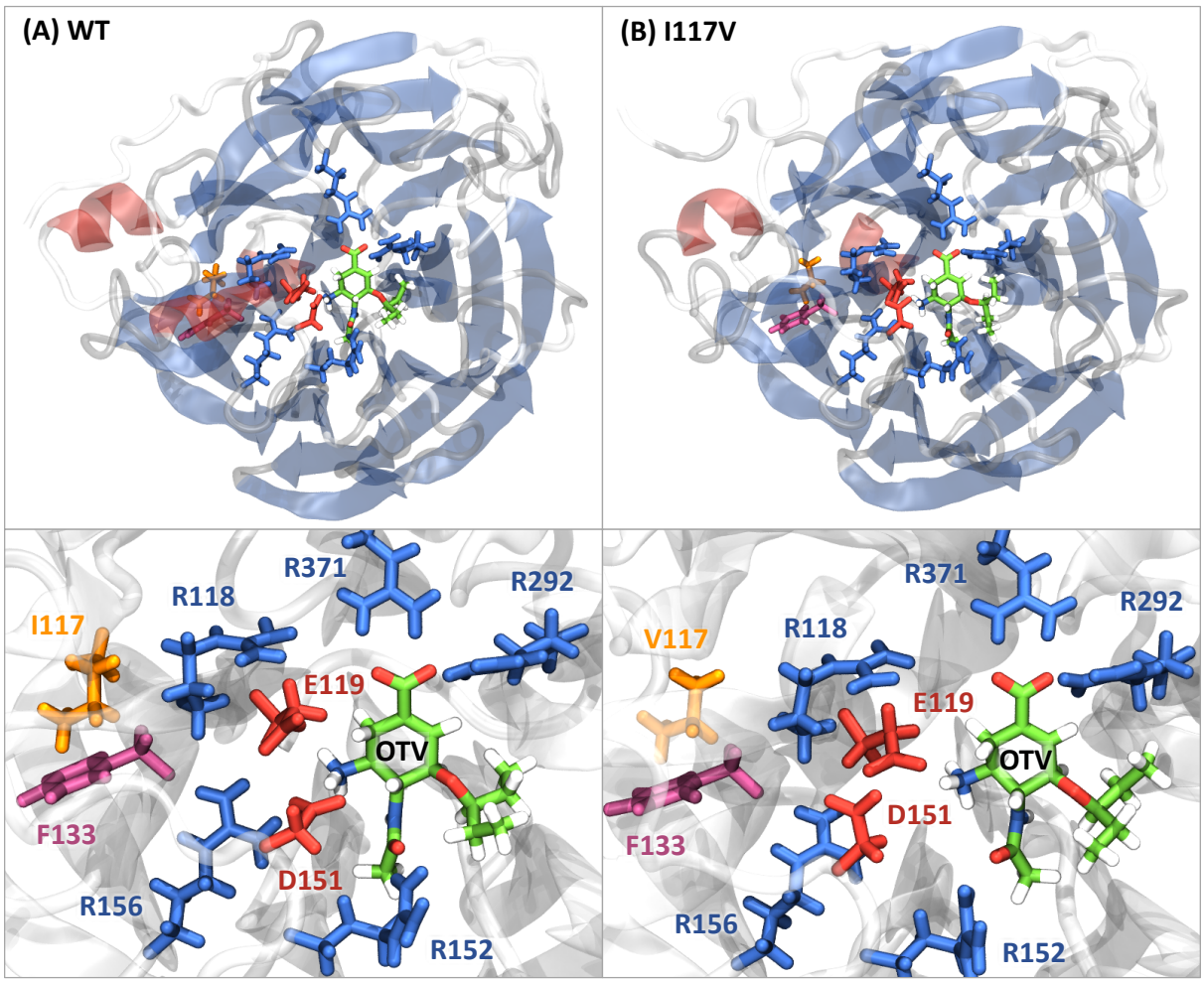

Figure 4.2: Snapshot images of (A) wild type (WT) and (B) I117V mutant neuraminidase-oseltamivir complexes (from *Yadav et al., 2021b*). In upper panels, the overall structure of the complex is shown in the cartoon representation, where the helix region is shown in red and the sheet region is shown in blue. In lower panels, the oseltamivir (OTV) binding site and the region around the I117V mutation site are shown. OTV is shown in green, residue 117 is shown in orange, and the residue adjacent to the residue 117 is shown in purple. In the OTV binding site, the positively charged residues (R118, R152, R156, R292, and R371) are shown in blue, whereas the negatively charged residues (E119 and D151) are shown in red. The snapshot images of WT and I117V mutant NA-OTV complexes colored by atom are shown in Figure D.3. The superimposed snapshot image of WT and I117V mutant NA-OTV complexes colored by atom is shown in Figure D.4. Figure extracted directly from the original article by *Yadav et al.* (*2021b*), without modifications (CC BY 4.0 license, https://creativecommons.org/licenses/by/4.0).

Table 4.1: Calculated binding free energies of wild type (WT) and I117V mutant neuraminidase for oseltamivir obtained from MM-PBSA calculations.

	ΔH [kcal mol^{-1}]	$T\Delta S$ [kcal mol^{-1}]	ΔG [kcal mol^{-1}]	$\Delta\Delta G$ [kcal mol^{-1}]
WT	−33.78 ± 0.08	−19.18 ± 1.15	−14.60 ± 1.23	
I117V	−31.06 ± 0.08	−19.18 ± 1.20	−11.88 ± 1.28	2.72

4.4.2. Dynamic Residue Interaction Network (dRIN) analysis

Figure 4.3 shows the dRIN graphs for the WT and I117V mutant NA-OTV complexes as well as the difference between I117V mutant and WT (I117V-WT), showing any type of interactions (any), hydrogen bonds (hb), and van der Waals interaction (vdw). In I117V-WT, the bonds lost are represented in red color and bonds gained are represented in blue color. In a dRIN graph, an amino acid residue or a ligand is shown by a node, and a residue-residue or a residue-ligand interaction is shown by an edge connecting the two nodes. In most current approaches, a single structure is used to model RIN (*Piovesan et al., 2016; Shcherbinin & Veselovsky, 2019*). dRIN is an extension of the original version as it models using multiple structures and provides statistical insights into residue interactions (*Yadav et al., 2021a*). The occupancy of interactions between residues is shown by the thickness of the edge.

As shown in dRIN graph of I117V-WT in Figure 4.3, after the I117V mutation, most changes in residue interactions are concentrated near the OTV binding site and in the region adjacent to the residue 117, but changes in residue interactions at other sites also occurs. In general, it is assumed that due to the mutation, changes in residue interactions would occur only at the drug-binding site and the mutation site. However, as shown in dRIN graph of I117V-WT in Figure 4.3, after the I117V mutation, changes in residue interactions occurs not only at the OTV binding site and mutation site, but also at other sites. Hence, by using dRIN analysis, we could observe the changes in residue interactions associated with the mutation in the whole system, including the binding site, the mutation site, and the other sites.

To further examine the effect of I117V mutation on the interaction between NA and OTV, we performed the following detailed analysis based on MD simulations.

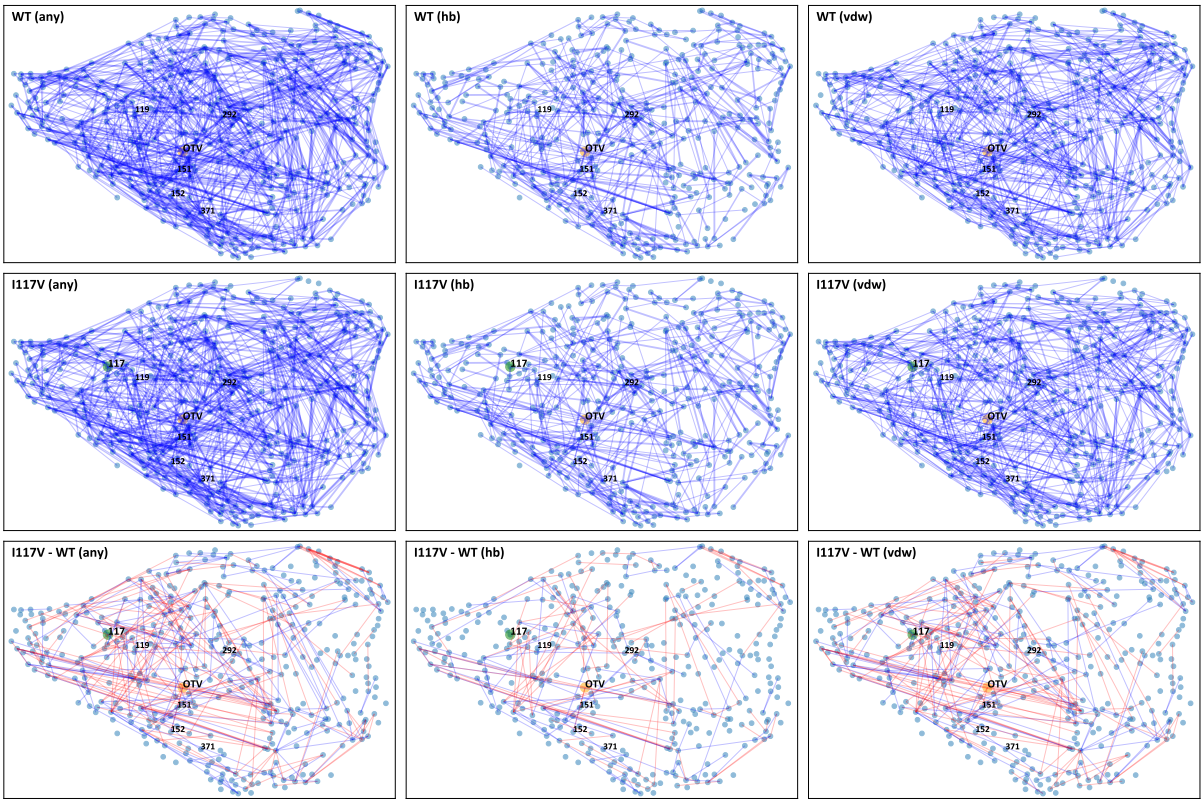

Figure 4.3: Dynamic residue interaction network (dRIN) graphs of neuraminidase-oseltamivir complexes. dRINs for wild type (WT), I117V mutant (I117V) and the difference between I117V mutant and WT (I117V-WT), showing any type of interactions (any), hydrogen bond interactions (hb), and van der Waals interaction (vdw). In I117V-WT, the bonds lost are shown in red color and the bonds gained are shown in blue color. The thickness of edge represents the occupancy of interactions.

4.4.3. Hydrogen bond analysis

Figure 4.4 shows the hydrogen bond occupancies of the WT and I117V mutant NA for OTV during the MD simulations. In hydrogen bond occupancies, the standard errors are small (< 1%); the 95% confidence intervals for hydrogen bond occupancies are represented as error bars in Figure 4.4. PYTRAJ (*Nguyen et al., 2016*), a Python front-end package of the CPPTRAJ program (*Roe & Cheatham, 2013*), was used to determine the hydrogen bond interactions. As shown in Figure 4.4, in NA-OTV complex, OTV forms hydrogen bond interactions with five charged amino acid residues, E119, D151, R152, R292, and R371. When forming hydrogen bond interactions with OTV, the side chains of R152, R292, and R371 acted as hydrogen donors, whereas the side chains of E119 and D151 acted as hydrogen acceptors. In both WT and I117V mutant NA-OTV complexes, the occupancies of the hydrogen bond interactions formed by

R292 and R371 with OTV were approximately 100%, showing that the interactions were extremely stable. The hydrogen bond interaction between R152 and OTV was observed to be relatively unstable, having an occupancy of about 60% in both WT and I117V mutant NA-OTV complexes. After NA I117V mutation, significant changes were observed in the hydrogen bond interactions formed by OTV with E119 and D151. Due to NA I117V mutation, the hydrogen bond occupancy between OTV and E119 enhanced by about 10%, while the hydrogen bond occupancy between OTV and D151 reduced by about 30%. When not bound to OTV, D151 formed hydrogen bond interaction with the adjacent positively charged amino acid residue R156. Hence, the instability of the hydrogen bond interaction between D151 and OTV caused by the I117V mutation might be the major reason for the reduction in OTV binding affinity to NA.

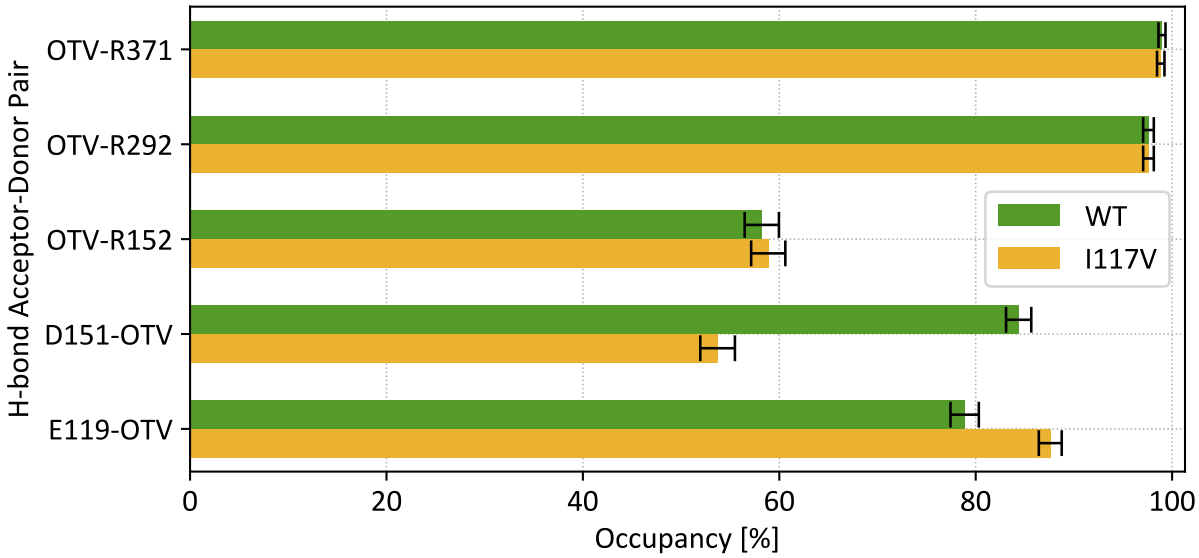

Figure 4.4: Hydrogen bond occupancies of oseltamivir (OTV) for wild type (WT) and I117V mutant neuraminidases (from *Yadav et al., 2021b*). When forming hydrogen bond interactions with OTV, the side chains of R152, R292, and R371 acted as hydrogen donors, whereas the side chains of E119 and D151 acted as hydrogen acceptors. Error bars represent 95% confidence intervals. Figure extracted directly from the original article by *Yadav et al.* (*2021b*), without modifications (CC BY 4.0 license, https://creativecommons.org/licenses/by/4.0).

4.4.4. Secondary structure analysis

Figures 4.5a and 4.5b show the secondary structure occupancies in the region between 100th and 150th residues of NA for the WT and I117V mutant NA-OTV complexes, respectively.

Figure 4.5c shows the changes in secondary structure occupancies caused by I117V mutation. The secondary structure occupancies of all NA residues in the WT and I117V mutant NA-OTV complexes are shown in Figure D.2. In secondary structure occupancies, the standard errors are small (< 1%); the 95% confidence intervals for secondary structure occupancies are represented as error bars in Figures 4.5a, 4.5b and 4.5c. PYTRAJ package (*Nguyen et al., 2016*) was used to classify secondary structures into 3 simplified categories (helix, sheet, and coil) based on the DSSP program (*Kabsch & Sander, 1983*). The secondary structure occupancies were computed using the assignment results for 3,200 three-dimensional structures extracted from four distinctive 80 ns trajectories in the production phase of MD simulations. The helix and sheet components are shown by red and blue bars, respectively, whereas the rest represents the coil in Figure 4.5.

As shown in Figure 4.2, NA has an overall β-sheet-rich structure with partial helices. As shown in Figure 4.5a, in WT NA, the helix components were found in the region between 105th and 111th residues and between 143rd and 149th residues of NA. The residue of interest of this study, 117th residue, was located in the β-sheet region formed between 115th and 124th residues. The secondary structure of NA was significantly changed due to the I117V mutation.

As shown in Figure 4.5c, after the I117V mutation, the occupancy of the helix component formed in the region between 147th and 149th residues was significantly decreased. Due to the I117V mutation, the secondary structure near the mutation site was also altered, showing that the β-sheet occupancy of R118 was decreased by about 12%. This may be because of a change in R118 orientation due to the mutation of the bulkier isoleucine to the smaller valine at 117th residue in NA, which causes the reduction in the hydrogen bond interaction with residue L134 located in the adjacent antiparallel β-sheet region. Such conformational changes of R118, which is a part of the drug binding site of NA, would cause the reduction in OTV binding affinity to I117V mutant NA, due to the indirect effect of the isoleucine to valine mutation at residue 117.

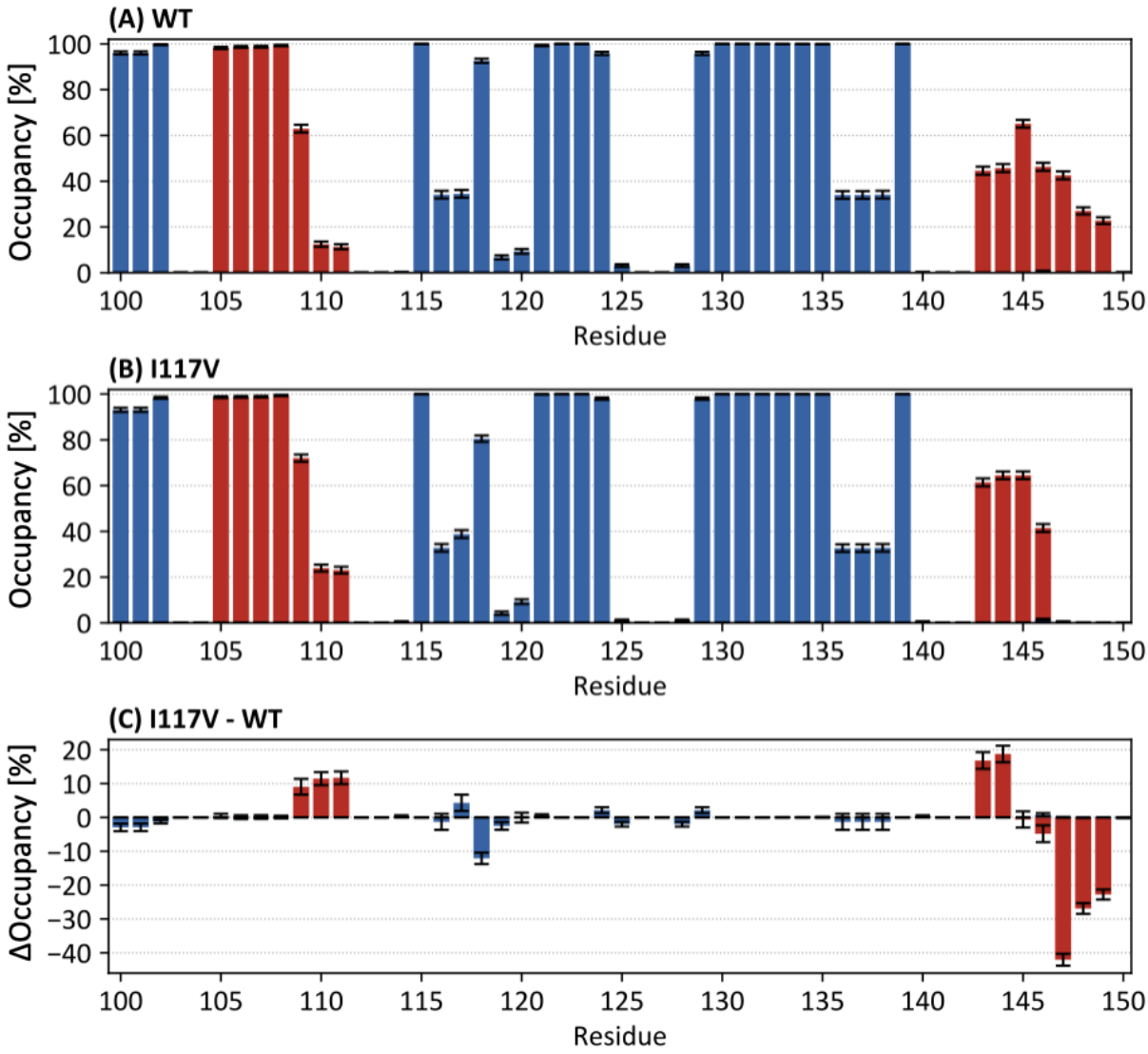

Figure 4.5: Secondary structure occupancies in the region between 100th and 150th residues for the neuraminidase-oseltamivir complexes (from *Yadav et al., 2021b*). (A) Wild type (WT) and (B) I117V mutant NA-OTV complexes. (C) Change in the secondary structure occupancies after the I117V mutation. Three categories (Helix, Sheet & Coil) were used to simplify the secondary structure classification. The helix component is shown by red bars and the sheet component is shown by blue bars, whereas the coil component is represented by the rest. Error bars represent 95% confidence intervals. Figure extracted directly from the original article by *Yadav et al.* (*2021b*), with modifications, label updated to (ΔOccupancy [%]) for the last panel (C) (CC BY 4.0 license, https://creativecommons.org/licenses/by/4.0).

4.4.5. Residue-residue and residue-drug interactions

Figure 4.6 shows the correlations between the distances of the R118-E119 pair ($R_{\text{R118-E119}}$) and the D151-OTV pair ($R_{\text{D151-OTV}}$) in the WT and I117V mutant NA-OTV complexes as scatter plots (shown in center panel) and probability densities (shown in upper and side panel); the WT NA-OTV complex data is shown in green color, whereas the I117V mutant NA-OTV complex data is shown in orange color. The interatomic distance between the carbon atom in the guanidino group of R118 and the carbon atom in the carboxyl group of E119 was measured to determine the value of $R_{\text{R118-E119}}$. The interatomic distance between the carbon atom in the carboxyl group of D151 and the nitrogen atom in the amino group of OTV was measured to determine the value of $R_{\text{D151-OTV.}}$ The conformational fluctuations of OTV binding site and adjacent I117V mutation site in the WT and I117V mutant NA bound to OTV are shown in Figure 4.7, by superimposing 100 snapshot images obtained from MD simulations. By superimposing 100 snapshot images obtained from MD simulations, the conformational changes of the 150-loop region (residues 147−152) in the WT and I117V mutant NA-OTV complexes are shown in Figure D.5.

As shown in Figure 4.6, in the WT NA-OTV complex, the distribution of $R_{\text{D151-OTV}}$ was monomodal and generally localized near 3.6 Å, implying that D151 tends to interact with OTV by forming hydrogen bond interactions. On the contrary, the distribution of $R_{\text{R118-E119}}$ was bimodal, with one strong distribution near 4.2 Å and another weak distribution near 6.0 Å, implying that the side chains of R118 and E119 tended to interact closely, but were sometimes too far apart to interact. In the superimposed snapshot images of the three-dimensional structure of WT NA-OTV complex shown in Figure 4.7a, these characteristic conformational fluctuations of R118, E119, and D151 can be seen.

As shown in Figure 4.6, in I117V mutant NA-OTV complex, the distribution of $R_{\text{D151-OTV}}$ was bimodal, with a peak localized near 3.6 Å, like the WT case and an additional peak localized near 6.2 Å, unlike the WT case; indicating that the frequency of hydrogen bond interaction between D151 and OTV was decreased due to the I117V mutation, which is also supported by the hydrogen bond occupancies results shown in Figure 4.4. The relatively large peak near 6.2 Å also indicates that due to the I117V mutation, the 150-loop of NA was frequently opened (Figure D.5), which is also supported by the observation in the NA mutants of various other drug-resistant strains (*Han et al., 2012; Kar & Knecht, 2012; Schaduangrat et al., 2016; Woods et al., 2012; Yadav et al., 2021a*). The distribution of $R_{\text{R118-E119}}$ was multimodal, with peaks around 4.2 Å and 6.0 Å, like the WT case, and an additional weak peak around

7.4 Å, unlike the WT case. Here, in comparison with the WT case, the probability density of the main distribution near 4.2 Å was reduced, whereas the other distributions near 6.0 Å and 7.4 Å enhanced; indicating that the side chains of R118 and E119 tended to separate frequently due to the I117V mutation, thus not interacting with each other, in comparison with the WT case.

In Figure 4.6, the center panel shows the scatter plot for the distance between R118 and E119 ($R_{\mathrm{R118\text{-}E119}}$) *versus* the distance between D151 and OTV ($R_{\mathrm{D151\text{-}OTV}}$) in WT and I117V mutant NA-OTV complexes. As shown in Figure 4.6, after the I117V mutation, the distance between R118 and E119 increased and the distance between D151 and OTV also increased. This indicates that there is a positive correlation between them; indicating that as the interaction between the side chains of R118 and E119 decreases after the I117V mutation, the interaction between the side chain of D151 and the OTV amino group also decreases.

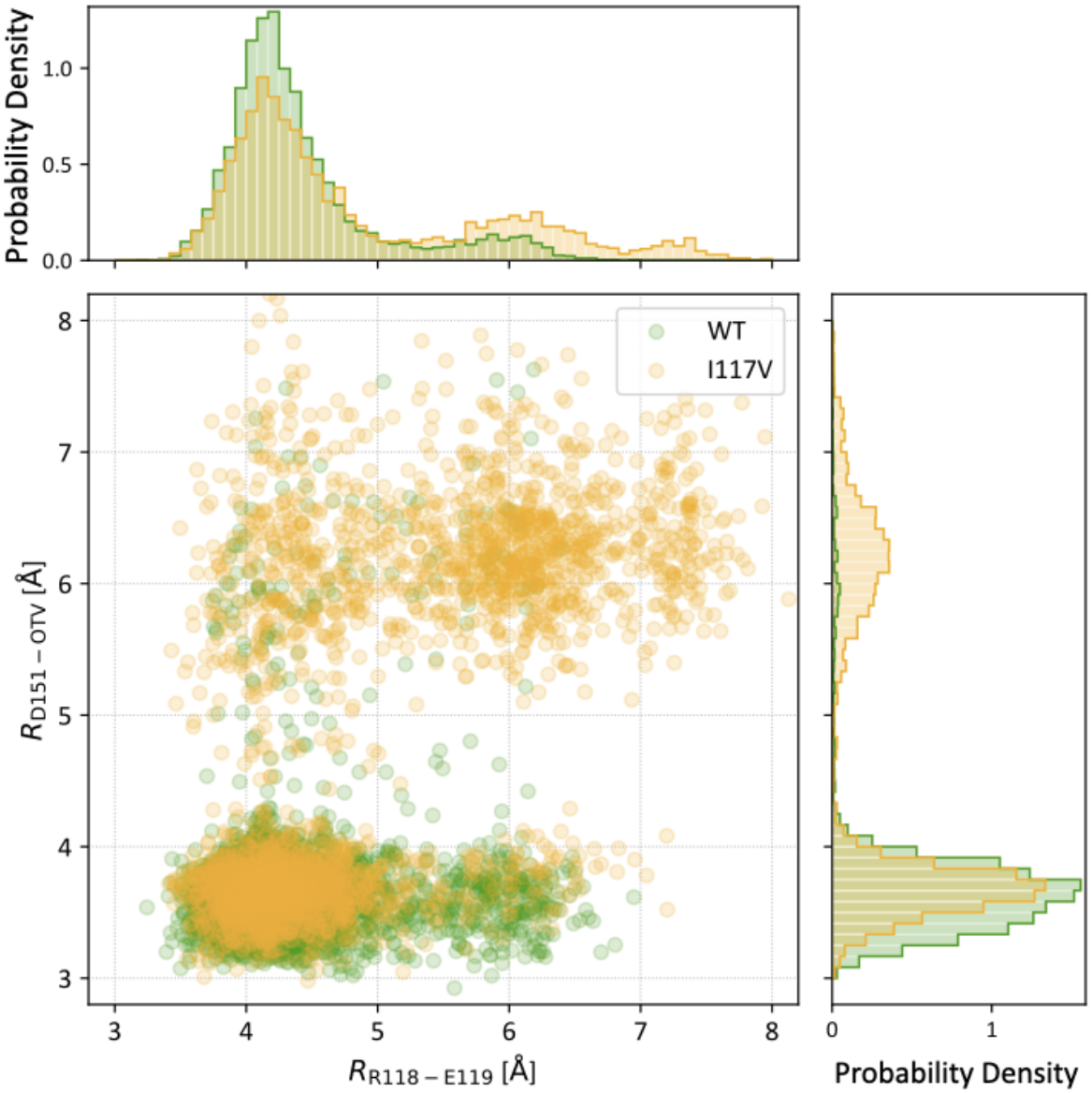

Figure 4.6: Correlations between residue-residue and residue-inhibitor interactions (from *Yadav et al., 2021b*). The center panel shows the scatter plot for the distance between R118 and E119 ($R_{R118\text{-}E119}$) *versus* the distance between D151 and OTV ($R_{D151\text{-}OTV}$) in wild type (WT) and I117V mutant NA-OTV complexes. The upper panel shows the probability density function distribution of the distance between R118 and E119 ($R_{R118\text{-}E119}$) in WT and I117V mutant NA-OTV complexes. The right panel shows the probability density function distribution of the distance between D151 and OTV ($R_{D151\text{-}OTV}$) in WT and I117V mutant NA-OTV complexes. In all three panels, the WT NA-OTV complex data is shown in green color, whereas the I117V mutant NA-OTV complex data is shown in orange color. Figure extracted directly from the original article by *Yadav et al.* (*2021b*), with modifications, label (Probability Density) is added to the upper and side panel (CC BY 4.0 license, https://creativecommons.org/licenses/by/4.0).

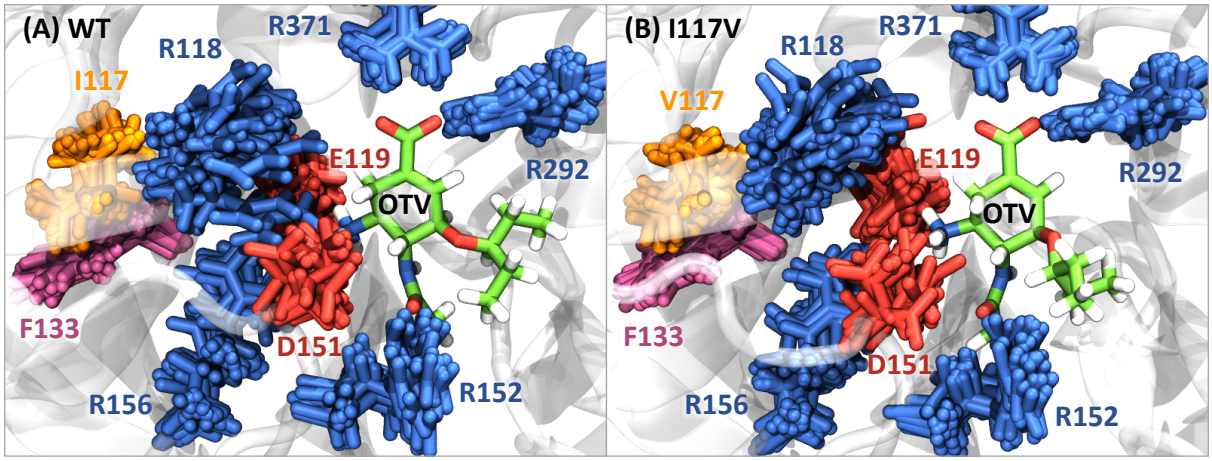

Figure 4.7: Superimposed snapshot images for the neuraminidase-oseltamivir complexes (from *Yadav et al., 2021b*). (A) Wild type (WT) and (B) I117V mutant NA-OTV complexes. OTV is shown in green, residue 117 is shown in orange, and the residue adjacent to the residue 117 is shown in purple. In the OTV binding site, the positively charged residues (R118, R152, R156, R292, and R371) are shown in blue, and the negatively charged residues (E119 and D151) are shown in red. Figure extracted directly from the original article by *Yadav et al.* (*2021b*), without modifications (CC BY 4.0 license, https://creativecommons.org/licenses/by/4.0).

4.5. Discussion

4.5.1. WT NA-OTV complex

In the WT NA-OTV complex, the residue-residue interaction between R118 and E119 may play a vital role in increasing the residue-inhibitor interaction between D151 and OTV to enhance the OTV binding affinity to WT NA. As shown in Figures 4.2a and 4.7a, the negatively charged side chains of E119 and D151 simultaneously interacts with the positively charged amino group of OTV. When E119 and D151 simultaneously interacts with OTV, they tend to approach each other, but the closer they get, the stronger the electrostatic repulsion between the negatively charged side chains. However, as shown in Figure 4.4, for both the E119-OTV and D151-OTV pairs, the hydrogen bond occupancy was about 80%, implying that the hydrogen bond interaction of E119 and D151 with OTV was relatively stable. As shown in Figure 4.5a, R118 is a part of the β-sheet region, implying that its side chain orientation can be rigid. Due to the strong directivity of R118, derived from its secondary structure formation, its positively charged side chain and the negatively charged side chain of the adjacent E119 can interact frequently. The positive and negative charges of the side chains of R118 and E119 neutralize each other

when they interact, resulting in the suppression of the electrostatic repulsion between the negatively charged side chains of E119 and D151. Hence, both E119 and D151 can form hydrogen bond interaction with OTV simultaneously, increasing OTV binding affinity to NA.

4.5.2. I117V mutant NA-OTV complex

In the I117V mutant NA-OTV complex, the reduction in OTV binding affinity to NA may be caused by the decrease in residue-inhibitor interaction between D151 and OTV, along with the decrease in residue-residue interaction between R118 and E119. As shown in Figure 4.5c, after the I117V mutation, the β-sheet occupancy of R118 reduced, implying that the directionality of its side chain was weakened. Due to the weakening of the directionality of the positively charged side chain of R118, its interaction with the negatively charged side chain of the adjacent E119 was reduced. Figure 4.6 shows the reduced interactions between the side chains of R118 and E119. As mentioned earlier, the interaction between R118 and E119 in the WT NA-OTV complex can contribute to the reduction of the electrostatic repulsion between E119 and D151. However, as the interaction between R118 and E119 is reduced in the I117V mutant NA-OTV complex, the electrostatic repulsion between E119 and D151 can be increased. This inhibits both E119 and D151 to simultaneously form the hydrogen bond interaction with the same positively charged amino group of OTV, causing the reduction in OTV binding affinity to NA. Hence, after the I117V mutation, the change in the interactions of these residues causes the slight reduction in the OTV binding affinity to NA, leading to the reduction in drug susceptibility of OTV to influenza viruses.

As mentioned in the Introduction, several computational studies have reported on the molecular mechanism underlying the reduction in OTV susceptibility to the I117V mutant NA using MD simulations (*Mhlongo & Soliman, 2015; Takano et al., 2013*). *Takano et al.* (*2013*) analyzed a single 2.5 ns trajectory obtained from MD simulations to show that the reduction in OTV susceptibility to NA after I117V mutation is due to the loss of hydrogen bond interaction between the side chain of R118 of NA and the carboxyl group of OTV. Previously, a study by *Takano et al.* (*2013*) showed that the hydrogen bond interactions are formed between the OTV and R118 of WT NA; however, this was not observed in the previous study by *Mhlongo & Soliman* (*2015*) as well as in the current study. We speculate that this discrepancy is because in the previous study by *Takano et al.* (*2013*) the MD trajectory used for analysis was too short to adequately sample the system's conformational space. *Mhlongo & Soliman* (*2015*) analyzed four distinctive 25 ns trajectories obtained from MD simulations to show that

the I117V mutation affects the residue-residue interactions in NA, causing the change in conformation of the drug binding site, leading to the change in the residue-inhibitor interaction between NA and OTV; however, the details were unclear. In the current study, we analyzed four distinctive 80 ns trajectories obtained from MD simulations to elucidate the correlation between the residue-residue interaction of the R118-E119 pair and the residue-inhibitor interaction of the D151-OTV pair in NA-OTV complexes, as shown in Figure 4.6. Hence, we clarified the detailed molecular mechanism of how the I117V mutation in NA causes the change in inter-residue interactions between R118, E119, and D151, and leads to the destabilization of the residue-inhibitor interaction between D151 and OTV, resulting in the reduction in OTV susceptibility to NA.

We speculate that the I117V mutation impacts not only the OTV susceptibility to NA but also viral fitness. Regarding viral fitness, we expect to extend the current study in the future to determine the impact of the I117V mutation on the binding affinity between NA and natural sialic acid substrate. However, according to *Adams et al.* (*2019*), viral fitness depends not only on the substrate-enzyme binding affinity, but also on the enzyme's catalytic efficiency. Hence, to study the effect of NA mutations on viral fitness, it is necessary to clarify the catalytic reaction mechanism of NA using expensive computational methods, such as the QM/MM method (*Sousa et al., 2017*). As the analysis of the catalytic reaction mechanism of NA is far beyond the scope of this study, we only mention it here as a future subject.

4.5.3. Designing a potential drug design against I117V mutant strains

As summarized in Table 4.1, due to the I117V mutation, the binding free energy of OTV to NA increased by 2.72 kcal mol^{-1}, corresponding to an approximately 100-fold reduction in the relative susceptibility of OTV to the I117V mutant NA as compared to the WT NA. Due to the I117V mutation in NA, the IC_{50} value of OTV has been experimentally observed to change by 3- to approximately 50-fold (*Chen et al., 2010; Creanga et al., 2017; Hurt et al., 2007; Ilyushina et al., 2010; Kode et al., 2019; McKimm-Breschkin et al., 2007; McKimm-Breschkin et al., 2013b; Takano et al., 2013*). As compared to the mutations that are selected under drug pressure and causes the increase in IC_{50} value by more that 600-fold, such as H274Y mutation in NA (*Hurt et al., 2012b*), the I117V mutation in NA does not dramatically affect the OTV susceptibility. Hence, OTV treatment may be effective against the influenza virus I117V mutant strain. However, in synergism with other mutations, the I117V mutation may cause the OTV resistance. For example, *Hurt et al.* (*2012b*) showed that after the dual

H274Y + I117V mutation in NA the OTV susceptibility reduced significantly (a 1896-fold increase in IC_{50}) as compared to the H274Y mutation alone (a 650-fold increase in IC_{50}). Hence, based on the new knowledge acquired in the present study, we propose drug design guidelines that avoid the loss of drug sensitivity caused by the I117V mutation in NA, to be prepared for the possible emergence of potent drug resistant strains.

Based on our study, we propose that an anti-NA inhibitor with a longer positively charged group is better than the one with a shorter positively charged group, such as the OTV amino group, to avoid resistance from the I117V mutation in NA that affects the interaction of drug binding site residues, E119 and D151, with the inhibitor. A longer positively charged group in the anti-NA inhibitor could help in the reduction of the electrostatic repulsion between the negatively charged side chains of E119 and D151. For example, to interact with the drug binding site residues, E119 and D151, OTV has a short positively charged amino group, whereas zanamivir has a long positively charged guanidino group. In fact, due to the I117V mutation in NA, the IC_{50} value of OTV changed significantly by 50-fold, whereas the IC_{50} value of zanamivir changed by only 1.6-fold, indicating that zanamivir is effective against the influenza virus I117V mutant strain (*McKimm-Breschkin et al., 2013b*). In this study, we analyzed the detailed molecular mechanism of OTV resistance caused by the I117V mutation in NA using molecular simulations, which helped in the establishment of new molecular design guidelines that effectively solve the problem of drug resistance.

4.6. Conclusions

In this study, we used MD simulations to theoretically investigate the detailed molecular mechanism of reduction in OTV drug susceptibility after the I117V mutation in NA in the A/H5N1 influenza virus.

In the WT NA-OTV complex, the interaction between R118 and E119 can play a significant role to increase the OTV binding affinity for NA. In this case, the positively charged side chain of R118, included in the β-sheet region, can interact with the negatively charged side chain of E119 frequently, to prevent the electrostatic repulsion between the negatively charged side chains of E119 and D151. This makes it possible for both the negatively charged side chains of E119 and D151 to simultaneously form hydrogen bond interactions with the same positively charged amino group of OTV, resulting in significant contribution towards the OTV binding affinity of NA.

In the I117V mutant NA-OTV complex, the OTV binding affinity to NA can be reduced by decreasing the frequency to form the interaction between R118 and E119. In this case, the I117V mutation in NA causes the reduction in the frequency of interaction between the positively charged side chain of R118 and the negatively charged side chain of E119 by reducing the β-sheet occupancy of R118. This results in the increase in the electrostatic repulsion between the negatively charged side chains of E119 and D151, thereby making it difficult for them to simultaneously form the hydrogen bond interaction with the same positively charged amino group of OTV, which in turn causes the reduction in the OTV binding affinity to NA. Hence, after the I117V mutation in NA, the influenza viruses become less susceptible to OTV due to the changes in the residue interactions between R118, E119, and D151.

The present study has succeeded in clarifying the molecular mechanism of how the I117V mutation in NA causes the reduction in OTV drug susceptibility to the A/H5N1 influenza virus.

5. Thesis summary

Influenza viruses are known to cause influenza, also known as flu, a highly contagious respiratory illness. Neuraminidase (NA), the influenza virus surface glycoprotein, plays a crucial role in replication and transmission of influenza virus. Thus, NA is used as a molecular drug target to develop anti-influenza drugs. Currently, four types of NA inhibitors, oseltamivir (OTV), zanamivir, peramivir, and laninamivir, are used for treatment and prevention of influenza in Japan. However, influenza virus drug resistant strains are emerging rapidly. Previously, several studies have reported on influenza virus drug resistance mechanism, but the detailed molecular mechanism of drug resistance in influenza virus is still not clear.

This study aimed to elucidate the detailed molecular mechanism of drug resistance in two mutant strains of A/H5N1 influenza virus, which reduces OTV sensitivity as compared to wild type (WT). Particularly, the H274Y mutant influenza virus strain in which histidine is mutated to bulkier tyrosine at residue 274 in NA, and the I117V mutant influenza virus strain in which bulkier isoleucine is mutated to smaller valine at residue 117 in NA, which reduces OTV binding affinity to NA as compared to WT, the detailed molecular mechanism of drug resistance of these mutant strains has been elucidated using molecular dynamics (MD) simulations.

In the study of H274Y mutant strain of influenza virus, a new method based on MD simulations, dynamic residue interaction network (dRIN) analysis, has been developed to quantitatively clarify the dynamic interaction network between amino acid residues in a protein. Using dRIN analysis, based on MD simulations, the correlation between OTV binding site and H274Y mutation site of NA was investigated. The results of dRIN analysis revealed that the OTV binding site and H274Y mutant site of NA interact indirectly via three interface residues, S246, E276, and R292, connecting the two sites. Due to the H274Y mutation, the interaction between residue 274 and the three interface residues, S246, E276, and R292, significantly increased, causing significant decrease in the interaction between OTV and its surrounding 150-loop residues, D151 and R152. To conclude, such changes in residue interactions after the H274Y mutation, causes the reduction in OTV binding affinity to NA, resulting in OTV drug resistance in influenza viruses. Hence, this study successfully clarified the molecular mechanism by which the H274Y mutation in NA caused OTV drug resistance to A/H5N1 influenza virus, using dRIN analysis based on MD simulations.

In the study of I117V mutant strain of influenza virus, the characteristics structural changes in NA due to I117V mutation was investigated based on MD simulations. The results

of MD simulations revealed that in the WT NA-OTV complex, the interaction between R118, a part of β-sheet region, and E119, a part of OTV binding site of NA, played a crucial role in increasing the OTV binding affinity to NA. In this case, the positively charged side chain of R118 and the negatively charged side chain of E119 interacted frequently, thereby preventing the electrostatic repulsion between the negatively charged side chains of E119 and D151. This made it possible for both E119 and D151 to simultaneously form the hydrogen bond interactions with the same positively charged amino group of OTV, thus contributing significantly towards the OTV binding affinity of NA. In the I117V mutant NA-OTV complex, the OTV binding affinity to NA reduced due to decreased frequency of interaction between R118 and E119. In this case, due to the I117V mutation, the β-sheet occupancy of R118 reduced, resulting in reduced frequency of interaction between the positively charged side chain of R118 and the negatively charged side chain of E119. This resulted in increase in the electrostatic repulsion between the negatively charged side chains of E119 and D151, thus making it difficult for both E119 and D151 to simultaneously form the hydrogen bond interactions with the same positively charged amino group of OTV, causing the reduction in OTV binding affinity to NA. Hence, due to the I117V mutation in NA, the influenza viruses became less susceptible to OTV because of the changes in the residue interactions among R118, E119, and D151. Hence, this study successfully clarified the molecular mechanism by which the I117V mutation of NA, which is not included in the OTV binding site of NA, caused the reduction in OTV drug susceptibility to the A/H5N1 influenza virus, using MD simulations.

To conclude, this study succeeded in clarifying the detailed molecular mechanism of drug resistance in two mutant strains, H274Y and I117V, of A/H5N1 influenza virus from a completely different perspective. The achievements of this study enable us to design effective novel anti-influenza drugs rationally avoiding drug resistance, which is expected to contribute significantly to the treatment against influenza. Finally, the dRIN analysis newly developed in this study can be applied to a wide variety of systems, including individual proteins, protein-protein complexes, and protein-ligand complexes, to characterize the dynamic aspects of the residue interactions.

References

Adams SE, Lee N, Lugovtsev VY, Kan A, Donnelly RP, Ilyushina NA. 2019. Effect of influenza H1N1 neuraminidase V116A and I117V mutations on NA activity and sensitivity to NA inhibitors. *Antiviral Research* **169:**104539 **DOI:**10.1016/j.antiviral.2019.104539

Air GM. 2012. Influenza neuraminidase. *Influenza and Other Respiratory Viruses* **6(4):**245–256 **DOI:**10.1111/j.1750-2659.2011.00304.x

Allen MP, Tildesley DJ. 1989. *Computer Simulation of Liquids*. Oxford: Oxford Science Publications, Clarendon Press.

Andersen HC. 1980. Molecular dynamics simulations at constant pressure and/or temperature. *Journal of Chemical Physics* **72(4):**2384-2393 **DOI:**10.1063/1.439486

Babcock HP, Chen C, Zhuang X. 2004. Using single-particle tracking to study nuclear trafficking of viral genes. *Biophysical Journal* **87(4):**2749–2758 **DOI:**10.1529/biophysj.104.042234

Babu YS, Chand P, Bantia S, Kotian P, Dehghani A, El-Kattan Y, Lin TH, Hutchison TL, Elliott AJ, Parker CD, Ananth SL, Horn LL, Laver GW, Montgomery JA. 2000. BCX-1812 (RWJ-270201): discovery of a novel, highly potent, orally active, and selective influenza neuraminidase inhibitor through structure-based drug design. *Journal of Medicinal Chemistry* **43(19):**3482-3486 **DOI:**10.1021/jm0002679

Baker NA, Sept D, Joseph S, Holst MJ, McCammon JA. 2001. Electrostatics of nanosystems: application to microtubules and the ribosome. *Proceedings of the National Academy of Sciences of the United States of America* **98(18):**10037-10041 **DOI:**10.1073/pnas.181342398

Bayly CI, Cieplak P, Cornell WD, Kollman PA. 1993. A well-behaved electrostatic potential based method using charge restraints for deriving atomic charges: the RESP model. *Journal of Physical Chemistry* **97(40):**10269-10280 **DOI:**10.1021/j100142a004

Berendsen HJC, Postma JPM, van Gunsteren WF, DiNola A, Haak JR. 1984. Molecular dynamics with coupling to an external bath. *Journal of Chemical Physics* **81(8):**3684-3690 **DOI:**10.1063/1.448118

Bhakat S, Martin AJM, Soliman MES. 2014. An integrated molecular dynamics, principal component analysis and residue interaction network approach reveals the impact of M184V mutation on HIV reverse transcriptase resistance to lamivudine. *Molecular BioSystems* **10:**2215–2228 **DOI:**10.1039/c4mb00253a

Bhattacharyya M, Bhat CR, Vishveshwara S. 2013. An automated approach to network features of protein structure ensembles. *Protein Science* **22(10):**1399–1416 **DOI:**10.1002/pro.2333

Blok J, Air GM. 1982. Variation in the membrane-insertion and "stalk" sequences in eight subtypes of influenza type A virus neuraminidase. *Biochemistry* **21(17):**4001-4007 **DOI:**10.1021/bi00260a015

Bloom JD, Gong LI, Baltimore D. 2010. Permissive secondary mutations enable the evolution of influenza oseltamivir resistance. *Science* **328(5983):**1272–1275 **DOI:**10.1126/science.1187816

Bos TJ, Davis AR, Nayak DP. 1984. NH2-terminal hydrophobic region of influenza virus neuraminidase provides the signal function in translocation. *Proceedings of the National Academy of Sciences of the United States of America* **81(8):**2327–2331 **DOI:**10.1073/pnas.81.8.2327

Boulo S, Akarsu H, Ruigrok RWH, Baudin F. 2007. Nuclear traffic of influenza virus proteins and ribonucleoprotein complexes. *Virus Reserach* **124(1-2):**12-21 **DOI:**10.1016/j.virusres.2006.09.013

Brandes U. 2008. On variants of shortest-path betweenness centrality and their generic computation. *Social Networks* **30(2):**136–145 **DOI:**10.1016/j.socnet.2007.11.001

Briedis DJ, Lamb RA. 1982. Influenza B virus genome: sequences and structural organization of RNA segment 8 and the mRNAs coding for the NS1 and NS2 proteins. *Journal of Virology* **42(1):**186-193 **DOI:**10.1128/jvi.42.1.186-193.1982

Brinda KV, Vishveshwara S. 2005. A network representation of protein structures: implications for protein stability. *Biophysical Journal* **89(6):**4159–4170 **DOI:**10.1529/biophysj.105.064485

Brown DK, Penkler DL, Amamuddy OS, Ross C, Atilgan AR, Atilgan C, Bishop ÖT. 2017. MD-TASK: a software suite for analyzing molecular dynamics trajectories. *Bioinformatics* **33(17):**2768–2771 **DOI:**10.1093/bioinformatics/btx349

Bui M, Whittaker G, Helenius A. 1996. Effect of M1 protein and low pH on nuclear transport of influenza virus ribonucleoproteins. *Journal of Virology* **70(12):**8391–8401 **DOI:**10.1128/jvi.70.12.8391-8401.1996

Buthelezi NM, Mhlongo NN, Amoako DG, Somboro AM, Sosibo SC, Shunmugam L, Machaba KE, Kumalo HM. 2020. Exploring the impact of H5N1 neuraminidase (H274Y) mutation on Peramivir: a bio-computational study from a molecular perspective. *Journal of Biomolecular Structure and Dynamics* **38(14):**4344–4352 **DOI:**10.1080/07391102.2019.1677501

Butler J, Hooper KA, Petrie S, Lee R, Maurer-Stroh S, Reh L, Guarnaccia T, Baas C, Xue L, Vitesnik S, Leang SK, McVernon J, Kelso A, Barr IG, McCaw JM, Bloom JD, Hurt AC. 2014. Estimating the fitness advantage conferred by permissive neuraminidase mutations in recent oseltamivir-resistant A(H1N1)pdm09 influenza viruses. *PLoS Pathogens* **10(4):**e1004065 **DOI:**10.1371/journal.ppat.1004065

Case DA, Belfon K, Ben-Shalom IY, Brozell SR, Cerutti DS, Cheatham TE III, Cruzeiro VWD, Darden TA, Duke RE, Giambasu G, Gilson MK, Gohlke H, Goetz AW, Harris R, Izadi S, Izmailov SA, Kasavajhala K, Kovalenko A, Krasny R, Kurtzman T, Lee TS, LeGrand S, Li P, Lin C, Liu J, Luchko T, Luo R, Man V, Merz KM, Miao Y, Mikhailovskii O, Monard G, Nguyen H, Onufriev A, Pan F, Pantano S, Qi R, Roe DR, Roitberg A, Sagui C, Schott-Verdugo S, Shen J, Simmerling CL, Skrynnikov NR, Smith J, Swails J, Walker RC, Wang J, Wilson L, Wolf RM, Wu X, Xiong Y, Xue Y, York DM, Kollman PA. 2020. In: *AMBER 2020.* San Francisco: University of California.

Chen C, Zhuang X. 2008. Epsin 1 is a cargo-specific adaptor for the clathrin-mediated endocytosis of the influenza virus. *Proceedings of the National Academy of Sciences of the United States of America* **105(33):**11790-11795 **DOI:**10.1073/pnas.0803711105

Chen W, Calvo PA, Malide D, Gibbs J, Schubert U, Bacik I, Basta S, O'Neill R, Schickli J, Palese P, Henklein P, Bennink JR, Yewdell JW. 2001. A novel influenza A virus mitochondrial protein that induces cell death. *Nature Medicine* **7:**1306-1312 **DOI:**10.1038/nm1201-1306

Chen Z, Zheng YH, Lin Y, Collins PJ, Hay AJ. 2010. Impact of avian influenza virus H5N1 neuraminidase mutations on the activity of neuraminidase and the sensibility to neuraminidase inhibitors. *National Medical Journal of China* **90(27):**1924-1928 **DOI:**10.3760/cma.j.issn.0376-2491.2010.27.014

Collins PJ, Haire LF, Lin YP, Liu J, Russell RJ, Walker PA, Martin SR, Daniels RS, Gregory V, Skehel JJ, Gamblin SJ, Hay AJ. 2009. Structural basis for oseltamivir resistance of influenza viruses. *Vaccine* **27(45):**6317–6323 **DOI:**10.1016/j.vaccine.2009.07.017

Collins PJ, Haire LF, Lin YP, Liu J, Russell RJ, Walker PA, Skehel JJ, Martin SR, Hay AJ, Gamblin SJ. 2008. Crystal structures of oseltamivir-resistant influenza virus neuraminidase mutants. *Nature* **453:**1258-1261 **DOI:**10.1038/nature06956

Colman PM, Hoyne PA, Lawrence MC. 1993. Sequence and structure alignment of paramyxovirus hemagglutinin-neuraminidase with influenza virus neuraminidase. *Journal of Virology* **67(6):**2972-2980 **DOI:**10.1128/jvi.67.6.2972-2980.1993

Colman PM, Varghese JN, Laver WG. 1983. Structure of the catalytic and antigenic sites in influenza virus neuraminidase. *Nature* **303:**41-44 **DOI:**10.1038/303041a0

Colman PM. 1989. Influenza virus neuraminidase: enzyme and antigen. In: Krug RM, ed. *The influenza viruses.* New York: Plenum Press, 175–218.

Contreras-Riquelme S, Garate J-A, Perez-Acle T, Martin AJM. 2018. RIP-MD: a tool to study residue interaction networks in protein molecular dynamics. *PeerJ* **6:**e5998 **DOI:**10.7717/peerj.5998

Cox NJ, Neumann G, Donis RO, Kawaoka Y. 2010. Orthomyxoviruses: Influenza. In: Mahy BWJ, ter Meulen V, eds. *Topley and Wilson's Microbiology and Microbial Infections.* New York: John Wiley & Sons, Ltd., 634-698.

Creanga A, Hang NLK, Cuong VD, Nguyen HT, Phuong HVM, Thanh LT, Thach NC, Hien PT, Tung N, Jang Y, Balish A, Dang NH, Duong MT, Huong NT, Hoa DN, Tho ND, Klimov A, Kapella BK, Gubareva L, Kile JC, Hien NT, Mai LQ, Davis CT. 2017. Highly pathogenic avian influenza A (H5N1) viruses at the animal–human interface in Vietnam, 2003–2010. *Journal of Infectious Diseases* **216(suppl_4):**S529–S538 **DOI:**10.1093/infdis/jix003

Csermely P, Korcsmáros T, Kiss HJM, London G, Nussinov R. 2013. Structure and dynamics of molecular networks: a novel paradigm of drug discovery: a comprehensive review. *Pharmacology & Therapeutics* **138(3):**333–408 **DOI:**10.1016/j.pharmthera.2013.01.016

da Silva DV, Nordholm J, Madjo U, Pfeiffer A, Daniels R. 2013. Assembly of subtype 1 influenza neuraminidase is driven by both the transmembrane and head domains. *Journal of Biological Chemistry* **288(1):**644-653 **DOI:**10.1074/jbc.M112.424150

Daggett V. 2000. Long Timescale Simulations. *Current Opinion in Structural Biology* **10(2):**160−164 **DOI:**10.1016/s0959-440x(00)00062-2

Darden T, York D, Pedersen L. 1993. Particle mesh Ewald: an $N\cdot\log(N)$ method for Ewald sums in large systems. *Journal of Chemical Physics* **98(12):**10089–10092 **DOI:**10.1063/1.464397

Dauber B, Heins G, Wolff T. 2004. The influenza B virus nonstructural NS1 protein is essential for efficient viral growth and antagonizes beta interferon induction. *Journal of virology* **78(4):**1865-1872 **DOI:**10.1128/jvi.78.4.1865-1872.2004

de Conto F, Covan S, Arcangeletti MC, Orlandini G, Gatti R, Dettori G, Chezzi C. 2011. Differential infectious entry of human influenza A/NWS/33 virus (H1N1) in mammalian kidney cells. *Virus Research* **155(1):**221–230 **DOI:**10.1016/j.virusres.2010.10.008

de Jong MD, Thanh TT, Khanh TH, Hien VM, Smith GJD, Chau NV, Cam BV, Qui PT, Ha DQ, Guan Y, Peiris JSM, Hien TT, Farrar J. 2005. Oseltamivir resistance during treatment of influenza A (H5N1) infection. *The New England Journal of Medicine* **353:**2667-2672 **DOI:**10.1056/nejmoa054512

de Vries E, Tscherne DM, Wienholts MJ, Cobos-Jiménez V, Scholte F, García-Sastre A, Rottier PJM, de Haan CAM. 2011. Dissection of the influenza A virus endocytic routes reveals macropinocytosis as an alternative entry pathway. *PLoS Pathogens* **7(3):**e1001329 **DOI:**10.1371/journal.ppat.1001329

Dharan NJ, Gubareva LV, Meyer JJ, Okomo-Adhiambo M, McClinton RC, Marshall SA, St George K, Epperson S, Brammer L, Klimov AI, Bresee JS, Fry AM, Oseltamivir-Resistance Working Group. 2009. Infections with oseltamivir-resistant influenza A(H1N1) virus in the United States. *JAMA* **301(10):**1034-1041 **DOI:**10.1001/jama.2009.294

di Paola L, de Ruvo M, Paci P, Santoni D, Giuliani A. 2013. Protein contact networks: an emerging paradigm in chemistry. *Chemical Reviews* **113(3):**1598–1613 **DOI:**10.1021/cr3002356

Dolinsky TJ, Nielsen JE, McCammon JA, Baker NA. 2004. PDB2PQR: an automated pipeline for the setup of Poisson-Boltzmann electrostatics calculations. *Nucleic Acids Research* **32(Web Server issue):**W665-W667 **DOI:**10.1093/nar/gkh381

Escuret V, Frobert E, Bouscambert-Duchamp M, Sabatier M, Grog I, Valette M, Lina B, Morfin F, Ferraris O. 2008. Detection of human influenza A (H1N1) and B strains with reduced sensitivity to neuraminidase inhibitors. *Journal of Clinical Virology* **41(1):**25–28 **DOI:**10.1016/j.jcv.2007.10.019

Fouchier RAM, Munster V, Wallensten A, Bestebroer TM, Herfst S, Smith D, Rimmelzwaan GF, Olsen B, Osterhaus AD. 2005. Characterization of a novel influenza A virus hemagglutinin subtype (H16) obtained from black-headed gulls. *Journal of Virology* **79(5):**2814-2822 **DOI:**10.1128/jvi.79.5.2814-2822.2005

Frisch MJ, Trucks GW, Schlegel HB, Scuseria GE, Robb MA, Cheeseman JR, Scalmani G, Barone V, Petersson GA, Nakatsuji H, Li X, Caricato M, Marenich AV, Bloino J, Janesko BG, Gomperts R, Mennucci B, Hratchian HP, Ortiz JV, Izmaylov AF, Sonnenberg JL, Williams-Young D, Ding F, Lipparini F, Egidi F, Goings J, Peng B, Petrone A, Henderson T, Ranasinghe D, Zakrzewski VG, Gao J, Rega N, Zheng G, Liang W, Hada M, Ehara M, Toyota K, Fukuda R, Hasegawa J, Ishida M, Nakajima T, Honda Y, Kitao O, Nakai H, Vreven T, Throssell K, Montgomery JA Jr, Peralta JE, Ogliaro F, Bearpark MJ, Heyd JJ, Brothers EN, Kudin KN, Staroverov VN, Keith TA, Kobayashi R, Normand J, Raghavachari K, Rendell AP, Burant JC, Iyengar SS, Tomasi J, Cossi M, Millam JM, Klene M, Adamo C, Cammi R, Ochterski JW, Martin RL, Morokuma K, Farkas O, Foresman JB, Fox DJ. 2016. *Gaussian 16, Revision C.01.* Wallingford CT: Gaussian, Inc.

Fujisaki S, Takashita E, Yokoyama M, Taniwaki T, Xu H, Kishida N, Sato H, Tashiro M, Imai M, Odagiri T. 2012. A single E105K mutation far from the active site of influenza B virus neuraminidase contributes to reduced susceptibility to multiple neuraminidase-inhibitor drugs. *Biochemical and Biophysical Research Communications* **429(1-2):**51-56 **DOI:**10.1016/j.bbrc.2012.10.095

Gamblin SJ, Skehel JJ. 2010. Influenza hemagglutinin and neuraminidase membrane glycoproteins. *Journal of Biological Chemistry* **285(37):**28403–28409 **DOI:**10.1074/jbc.r110.129809

García-Sastre A. 2001. Inhibition of interferon-mediated antiviral responses by influenza A viruses and other negative-strand RNA viruses. *Virology* **279(2):**375-384 **DOI:**10.1006/viro.2000.0756

Garman E, Laver G. 2005. The structure, function, and inhibition of influenza virus neuraminidase. In: Fischer W, ed. *Viral Membrane Proteins: Structure, Function, and Drug Design.* New York: Kluwer Academic/Plenum Publishers, 247-267.

Genheden S, Ryde U. 2015. The MM/PBSA and MM/GBSA methods to estimate ligand-binding affinities. *Expert Opinion on Drug Discovery* **10(5):**449-461 **DOI:**10.1517/17460441.2015.1032936

Gilson MK, Honig B. 1988. Calculation of the total electrostatic energy of a macromolecular system: solvation energies, binding energies, and conformational analysis. *Proteins* **4(1):**7-18 **DOI:**10.1002/prot.340040104

Giollo M, Martin AJM, Walsh I, Ferrari C, Tosatto SCE. 2014. NeEMO: a method using residue interaction networks to improve prediction of protein stability upon mutation. *BMC Genomics* **15:**S7 **DOI:**10.1186/1471-2164-15-s4-s7

Govorkova EA, Ilyushina NA, McClaren JL, Naipospos TSP, Douangngeun B, Webster RG. 2009. Susceptibility of highly pathogenic H5N1 influenza viruses to the neuraminidase inhibitor oseltamivir differs in vitro and in a mouse model. *Antimicrobial Agents and Chemotherapy* **53(7):**3088-3096 **DOI:**10.1128/AAC.01667-08

Gubareva LV, Besselaar TG, Daniels RS, Fry A, Gregory V, Huang W, Hurt AC, Jorquera PA, Lackenby A, Leang SK, Lo J, Pereyaslov D, Rebelo-de-Andrade H, Siqueira MM, Takashita E, Odagiri T, Wang D, Zhang W, Meijer A. 2017. Global update on the susceptibility of human influenza viruses to neuraminidase inhibitors, 2015-2016. *Antiviral Research* **146:**12-20 **DOI:**10.1016/j.antiviral.2017.08.004

Gubareva LV, Kaiser L, Matrosovich MN, Soo-Hoo Y, Hayden FG. 2001. Selection of influenza virus mutants in experimentally infected volunteers treated with oseltamivir. *The Journal of Infectious Diseases* **183(4):**523–531 **DOI:**10.1086/318537

Han N, Liu X, Mu Y. 2012. Exploring the mechanism of zanamivir resistance in a neuraminidase mutant: a molecular dynamics study. *PLoS ONE* **7(9):**e44057 **DOI:**10.1371/journal.pone.0044057

Harris A, Cardone G, Winkler DC, Heymann JB, Brecher M, White JM, Steven AC. 2006. Influenza virus pleiomorphy characterized by cryoelectron tomography. *Proceedings of the National Academy of Sciences of the United States of America* **103(50):**19123-19127 **DOI:**10.1073/pnas.0607614103

Hause BM, Collin EA, Liu R, Huang B, Sheng Z, Lu W, Wang D, Nelson EA, Li F. 2014. Characterization of a novel influenza virus in cattle and swine: proposal for a new genus in the *Orthomyxoviridae* family. *mBio* **5(2):**e00031-14 **DOI:**10.1128/mBio.00031-14

Hause BM, Ducatez M, Collin EA, Ran Z, Liu R, Sheng Z, Armien A, Kaplan B, Chakravarty S, Hoppe AD, Webby RJ, Simonson RR, Li F. 2013. Isolation of a novel swine influenza virus from Oklahoma in 2011 which is distantly related to human influenza C viruses. *PLoS Pathogens* **9(2):**e1003176 **DOI:**10.1371/journal.ppat.1003176

Hooper KA, Bloom JD. 2013. A mutant influenza virus that uses an N1 neuraminidase as the receptor-binding protein. *Journal of Virology* **87(23):**12531-12540 **DOI:**10.1128/jvi.01889-13

Hou T, Wang J, Li Y, Wang W. 2011. Assessing the performance of the MM/PBSA and MM/GBSA Methods. 1. The accuracy of binding free energy calculations based on molecular dynamics simulations. *Journal of Chemical Information and Modeling* **51(1):**69-82 **DOI:**10.1021/ci100275a

Hunter JD. 2007. Matplotlib: a 2D graphics environment. *Computing in Science & Engineering* **9(3):**90-95 **DOI:**10.1109/MCSE.2007.55

Hurt AC, Barr IG, Hartel G, Hampson AW. 2004. Susceptibility of human influenza viruses from Australasia and South East Asia to the neuraminidase inhibitors zanamivir and oseltamivir. *Antiviral Research* **62(1):**37–45 **DOI:**10.1016/j.antiviral.2003.11.008

Hurt AC, Chotpitayasunondh T, Cox NJ, Daniels R, Fry AM, Gubareva LV, Hayden FG, Hui DS, Hungnes O, Lackenby A, Lim W, Meijer A, Penn C, Tashiro M, Uyeki TM, Zambon M. 2012a. Antiviral resistance during the 2009 influenza A H1N1 pandemic: public health, laboratory, and clinical perspectives. *The Lancet Infectious Diseases* **12(3):**240-248 **DOI:**10.1016/S1473-3099(11)70318-8

Hurt AC, Ernest J, Deng Y-M, Iannello P, Besselaar TG, Birch C, Buchy P, Chittaganpitch M, Chiu S-C, Dwyer D, Guigon A, Harrower B, Kei IP, Kok T, Lin C, McPhie K, Mohd A, Olveda R, Panayotou T, Rawlinson W, Scott L, Smith D, D'Souza H, Komadina N, Shaw R, Kelso A, Barr IG. 2009. Emergence and spread of oseltamivir-resistant A(H1N1) influenza viruses in Oceania, South East Asia and South Africa. *Antiviral Research* **83(1):**90–93 **DOI:**10.1016/j.antiviral.2009.03.003

Hurt AC, Leang SK, Speers DJ, Barr IG, Maurer-Stroh S. 2012b. Mutations I117V and I117M and oseltamivir sensitivity of pandemic (H1N1) 2009 viruses. *Emerging Infectious Diseases* **18(1):**109-112 **DOI:**10.3201/eid1801.111079

Hurt AC, Selleck P, Komadina N, Shaw R, Brown L, Barr IG. 2007. Susceptibility of highly pathogenic A(H5N1) avian influenza viruses to the neuraminidase inhibitors and adamantanes. *Antiviral Research* **73(3):**228-231 **DOI:**10.1016/j.antiviral.2006.10.004

Ilyushina NA, Seiler JP, Rehg JE, Webster RG, Govorkova EA. 2010. Effect of neuraminidase inhibitor-resistant mutations on pathogenicity of clade 2.2 A/Turkey/15/06 (H5N1) influenza virus in ferrets. *PLoS Pathogens* **6(5):**e1000933 **DOI:**10.1371/journal.ppat.1000933

Ives JAL, Carr JA, Mendel DB, Tai CY, Lambkin R, Kelly L, Oxford JS, Hayden FG, Roberts NA. 2002. The H274Y mutation in the influenza A/H1N1 neuraminidase active site following oseltamivir phosphate treatment leave virus severely compromised both in vitro and in vivo. *Antiviral Research* **55(2):**307–317 **DOI:**10.1016/s0166-3542(02)00053-0

Jackson D, Elderfield RA, Barclay WS. 2011. Molecular studies of influenza B virus in the reverse genetics era. *Journal of General Virology* **92(Pt 1):**1-17 **DOI:**10.1099/vir.0.026187-0

Jagger BW, Wise HM, Kash JC, Walters KA, Wills NM, Xiao YL, Dunfee RL, Schwartzman LM, Ozinsky A, Bell GL, Dalton RM, Lo A, Efstathiou S, Atkins JF, Firth AE, Taubenberger JK, Digard P. 2012. An overlapping protein-coding region in influenza A virus segment 3 modulates the host response. *Science* **337(6091):**199-204 **DOI:**10.1126/science.1222213

Jensen F. 2007. *Introduction to computational chemistry. 2nd edition.* West Sussex: John Wiley & Sons Ltd. ISBN-13 978-0-470-01187-4

Jung HE, Lee HK. 2020. Host protective immune responses against influenza A virus infection. *Viruses* **12(5):**504 **DOI:**10.3390/v12050504

Kabsch W, Sander C. 1983. Dictionary of protein secondary structure: pattern recognition of hydrogen-bonded and geometrical features. *Biopolymers* **22(12):**2577-2637 **DOI:**10.1002/bip.360221211

Kar P, Knecht V. 2012. Mutation-induced loop opening and energetics for binding of tamiflu to influenza N8 neuraminidase. *The Journal of Physical Chemistry B* **116(21):**6137-6149 **DOI:**10.1021/jp3022612

Kemler I, Whittaker G, Helenius A. 1994. Nuclear import of microinjected influenza virus ribonucleoproteins. *Virology* **202(2):**1028–1033 **DOI:**10.1006/viro.1994.1432

Kim CU, Lew W, Williams MA, Liu H, Zhang L, Swaminathan S, Bischofberger N, Chen MS, Mendel DB, Tai CY, Laver WG, Stevens RC. 1997. Influenza neuraminidase inhibitors possessing a novel hydrophobic interaction in the enzyme active site: design, synthesis, and structural analysis of carbocyclic sialic acid analogues with potent anti-influenza activity. *Journal of the American Chemical Society* **119(4):**681-690 **DOI:**10.1021/ja963036t

Kiso M, Mitamura K, Sakai-Tagawa Y, Shiraishi K, Kawakami C, Kimura K, Hayden FG, Sugaya N, Kawaoka Y. 2004. Resistant influenza A viruses in children treated with oseltamivir: descriptive study. *Lancet* **364:**759–765 **DOI:**10.1016/s0140-6736(04)16934-1

Kochs G, García-Sastre A, Martínez-Sobrido L. 2007. Multiple anti-interferon actions of the influenza A virus NS1 protein. *Journal of Virology* **81(13):**7011-7021 **DOI:**10.1128/JVI.02581-06

Kode SS, Pawar SD, Tare DS, Keng SS, Hurt AC, Mullick J. 2019. A novel I117T substitution in neuraminidase of highly pathogenic avian influenza H5N1 virus conferring reduced susceptibility to oseltamivir and zanamivir. *Veterinary Microbiology* **235:**21–24 **DOI:**10.1016/j.vetmic.2019.06.005

Koyama K, Takahashi M, Nakai N, Takakusa H, Murai T, Hoshi M, Yamamura N, Kobayashi N, Okazaki O. 2010. Pharmacokinetics and disposition of CS-8958, a long-acting prodrug of the novel neuraminidase inhibitor laninamivir in rats. *Xenobiotica* **40(3):**207-216 **DOI:**10.3109/00498250903447691

Krug RM, Fodor E. 2013. The virus genome and its replication. In: Webster RG, Monto AS, Braciale TJ, Lamb RA, eds. *Textbook of Influenza, 2nd edition.* West Sussex: John Wiley & Sons, Ltd., 57-66.

Lakadamyali M, Rust MJ, Zhuang X. 2004. Endocytosis of influenza viruses. *Microbes and Infection* **6(10):**929–936 **DOI:**10.1016/j.micinf.2004.05.002

Lakadamyali M, Rust MJ, Zhuang X. 2006. Ligands for clathrin-mediated endocytosis are differentially sorted into distinct populations of early endosomes. *Cell* **124(5):**997–1009 **DOI:**10.1016/j.cell.2005.12.038

Lamb RA, Choppin PW, Chanock RM, Lai CJ. 1980. Mapping of the two overlapping genes for polypeptides NS1 and NS2 on RNA segment 8 of influenza virus genome. *Proceedings of the National Academy of Sciences of the United States of America* **77(4):**1857-1861 **DOI:**10.1073/pnas.77.4.1857

Lee MS, Olson MA. 2006. Calculation of absolute protein−ligand binding affinity using path and endpoint approaches. *Biophysical Journal* **90(3):**864-877 **DOI:**10.1529/biophysj.105.071589

Lepsik M, Kriz Z, Havlas Z. 2004. Efficiency of a second-generation HIV-1 protease inhibitor studied by molecular dynamics and absolute binding free energy calculations. *Proteins* **57(2):**279-293 **DOI:**10.1002/prot.20192

Li L, Li Y, Zhang L, Hou T. 2012. Theoretical studies on the susceptibility of oseltamivir against variants of 2009 A/H1N1 influenza neuraminidase. *Journal of Chemical Information and Modeling* **52(10):**2715–2729 **DOI:**10.1021/ci300375k

Li Q, Qi J, Zhang W, Vavricka CJ, Shi Y, Wei J, Feng E, Shen J, Chen J, Liu D, He J, Yan J, Liu H, Jiang H, Teng M, Li X, Gao GF. 2010. The 2009 pandemic H1N1 neuraminidase N1 lacks the 150-cavity in its active site. *Nature Structural & Molecular Biology* **17:**1266-1268 **DOI:**10.1038/nsmb.1909

Li TCM, Chan MCW, Lee N. 2015. Clinical implications of antiviral resistance in influenza. *Viruses* **7(9):**4929–4944 **DOI:**10.3390/v7092850

Lin YP, Gregory V, Collins P, Kloess J, Wharton S, Cattle N, Lackenby A, Daniels R, Hay A. 2010. Neuraminidase receptor binding variants of human influenza A(H3N2) viruses resulting from substitution of aspartic acid 151 in the catalytic site: a role in virus attachment? *Journal of Virology* **84(13):**6769-6781 **DOI:**10.1128/JVI.00458-10

Lina B, Boucher C, Osterhaus A, Monto AS, Schutten M, Whitley RJ, Nguyen-Van-Tam JS. 2018. Five years of monitoring for the emergence of oseltamivir resistance in patients with influenza A infections in the Influenza Resistance Information Study. *Influenza and Other Respiratory Viruses* **12(2):**267–278 **DOI:**10.1111/irv.12534

Maier JA, Martinez C, Kasavajhala K, Wickstrom L, Hauser KE, Simmerling C. 2015. ff14SB: improving the accuracy of protein side chain and backbone parameters from ff99SB. *Journal of Chemical Theory and Computation* **11(8):**3696-3713 **DOI:**10.1021/acs.jctc.5b00255

Malaisree M, Rungrotmongkol T, Nunthaboot N, Aruksakunwong O, Intharathep P, Decha P, Sompornpisut P, Hannongbua S. 2009. Source of oseltamivir resistance in avian influenza H5N1 virus with the H274Y mutation. *Amino Acids* **37:**725–732 **DOI:**10.1007/s00726-008-0201-z

Marinova-Petkova A, Feeroz MM, Rabiul Alam SM, Kamrul Hasan M, Akhtar S, Jones-Engel L, Walker D, McClenaghan L, Rubrum A, Franks J, Seiler P, Jeevan T, McKenzie P, Krauss S, Webby RJ, Webster RG. 2014. Multiple introductions of highly pathogenic avian influenza H5N1 viruses into Bangladesh. *Emerging Microbes & Infections* **3:**e11 **DOI:**10.1038/emi.2014.11

Martin AJM, Vidotto M, Boscariol F, Di Domenico T, Walsh I, Tosatto SCE. 2011. RING: networking interacting residues, evolutionary information and energetics in protein structures. *Bioinformatics* **27(14):**2003–2005 **DOI:**10.1093/bioinformatics/btr191

Matrosovich M, Tuzikov A, Bovin N, Gambaryan A, Klimov A, Castrucci MR, Donatelli I, Kawaoka Y. 2000. Early alterations of the receptor-binding properties of H1, H2, and H3 avian influenza virus hemagglutinins after their introduction into mammals. *Journal of Virology* **74(18):**8502-8512 **DOI:**10.1128/jvi.74.18.8502-8512.2000

Matrosovich MN, Matrosovich TY, Gray T, Roberts NA, Klenk HD. 2004. Neuraminidase is important for the initiation of influenza virus infection in human airway epithelium. *Journal of Virology* **78(22):**12665–12667 **DOI:**10.1128/JVI.78.22.12665-12667.2004

Matsuoka Y, Swayne DE, Thomas C, Rameix-Welti MA, Naffakh N, Warnes C, Altholtz M, Donis R, Subbarao K. 2009. Neuraminidase stalk length and additional glycosylation of the hemagglutinin influence the virulence of influenza H5N1 viruses for mice. *Journal of Virology* **83(9):**4704-4708 **DOI:**10.1128/JVI.01987-08

McAuley JL, Gilbertson BP, Trifkovic S, Brown LE, McKimm-Breschkin JL. 2019. Influenza virus neuraminidase structure and functions. *Frontiers in Microbiology* **10:**39 **DOI:**10.3389/fmicb.2019.00039

McKimm-Breschkin JL, Barrett S, Pudjiatmoko, Azhar M, Wong FYK, Selleck P, Mohr PG, McGrane J, Kim M. 2013b. I222 neuraminidase mutations further reduce oseltamivir susceptibility of Indonesian clade 2.1 highly pathogenic avian influenza A (H5N1) viruses. *PLoS ONE* **8(6):**e66105 **DOI:**10.1371/journal.pone.0066105

McKimm-Breschkin JL, McDonald M, Blick TJ, Colman PM. 1996. Mutation in the influenza virus neuraminidase gene resulting in decreased sensitivity to the neuraminidase inhibitor 4-Guanidino-Neu5Ac2en leads to instability of the enzyme. *Virology* **225(1):**240–242 **DOI:**10.1006/viro.1996.0595

McKimm-Breschkin JL, Selleck PW, Usman TB, Johnson MA. 2007. Reduced sensitivity of influenza A (H5N1) to oseltamivir. *Emerging Infectious Diseases* **13(9):**1354-1357 **DOI:**10.3201/eid1309.070164

McKimm-Breschkin JL, Williams J, Barrett S, Jachno K, McDonald M, Mohr PG, Saito T, Tashiro M. 2013a. Reduced susceptibility to all neuraminidase inhibitors of influenza H1N1 viruses with haemagglutinin mutations and mutations in non-conserved residues of the neuraminidase. *Journal of Antimicrobial Chemotherapy* **68(10):**2210-2221 **DOI:**10.1093/jac/dkt205

McKimm-Breschkin JL. 2013c. Influenza neuraminidase inhibitors: antiviral action and mechanisms of resistance. *Influenza and Other Respiratory Viruses* **7(suppl_1):**25–36 **DOI:**10.1111/irv.12047

Mhlongo NN, Soliman MES. 2015. Single H5N1 influenza A neuraminidase mutation develops resistance to oseltamivir due to distorted conformational and drug binding landscape: multiple molecular dynamics analyses. *RSC Advances* **5(14):**10849–10861 **DOI:**10.1039/C4RA13494J

Miller BR III, McGee TD Jr, Swails JM, Homeyer N, Gohlke H, Roitberg AE. 2012. MMPBSA.py: an efficient program for end-state free energy calculations. *Journal of Chemical Theory and Computation* **8(9):**3314-3321 **DOI:**10.1021/ct300418h

Mishin VP, Hayden FG, Gubareva LV. 2005. Susceptibilities of antiviral-resistant influenza viruses to novel neuraminidase inhibitors. *Antimicrobial Agents and Chemotherapy* **49(11):**4515–4520 **DOI:**10.1128/AAC.49.11.4515-4520.2005

Mohr PG, Deng YM, McKimm-Breschkin JL. 2015. The neuraminidases of MDCK grown human influenza A(H3N2) viruses isolated since 1994 can demonstrate receptor binding. *Virology Journal* **12:**67 **DOI:**10.1186/s12985-015-0295-3

Monto AS, McKimm-Breschkin JL, Macken C, Hampson AW, Hay A, Klimov A, Tashiro M, Webster RG, Aymard M, Hayden FG, Zambon M. 2006. Detection of influenza viruses resistant to neuraminidase inhibitors in global surveillance during the first 3 years of their use. *Antimicrobial Agents and Chemotherapy* **50(7):**2395–2402 **DOI:**10.1128/AAC.01339-05

Moscona A. 2005. Neuraminidase inhibitors for influenza. *The New England Journal of Medicine* **353:**1363-1373 **DOI:**10.1056/NEJMra050740

Moscona A. 2009. Global transmission of oseltamivir-resistant influenza. *The New England Journal of Medicine* **360:**953–956 **DOI:**10.1056/NEJMp0900648

Moules V, Ferraris O, Terrier O, Giudice E, Yver M, Rolland JP, Bouscambert-Duchamp M, Bergeron C, Ottmann M, Fournier E, Traversier A, Boule C, Rivoire A, Lin Y, Hay A, Valette M, Marquet R, Rosa-Calatrava M, Naffakh N, Schoehn G, Thomas D, Lina B. 2010. In vitro characterization of naturally occurring influenza H3NA- viruses lacking the NA gene segment: toward a new mechanism of viral resistance? *Virology* **404(2):**215-224 **DOI:**10.1016/j.virol.2010.04.030

Muramoto Y, Noda T, Kawakami E, Akkina R, Kawaoka Y. 2013. Identification of novel influenza A virus proteins translated from PA mRNA. *Journal of Virology* **87(5):**2455-2462 **DOI:**10.1128/JVI.02656-12

Murti KG, Webster RG. 1986. Distribution of hemagglutinin and neuraminidase on influenza virions as revealed by immunoelectron microscopy. *Virology* **149(1):**36-43 **DOI:**10.1016/0042-6822(86)90084-X

Nayak DP, Hui EK, Barman S. 2004. Assembly and budding of influenza virus. *Virus Research* **106(2):**147-165 **DOI:**10.1016/j.virusres.2004.08.012

Nayak DP, Shivakoti S, Balogun RA, Lee G, Zhou ZH. 2013. Structure, disassembly, assembly, and budding of influenza viruses. In: Webster RG, Monto AS, Braciale TJ, Lamb RA, eds. *Textbook of Influenza, 2nd edition.* West Sussex: John Wiley & Sons, Ltd., 37-56.

Nguyen H, Roe DR, Swails J, Case DA. 2016. PYTRAJ: interactive data analysis for molecular dynamics simulations. *Available at https://github.com/Amber-MD/pytraj*

Nguyen TT, Mai BK, Li MS. 2011. Study of tamiflu sensitivity to variants of A/H5N1 virus using different force fields. *Journal of Chemical Information and Modeling* **51(9):**2266–2276 **DOI:**10.1021/ci2000743

Nivitchanyong T, Yongkiettrakul S, Kramyu J, Pannengpetch S, Wanasen N. 2011. Enhanced expression of secretable influenza virus neuraminidase in suspension mammalian cells by influenza virus nonstructural protein 1. *Journal of Virological Methods* **178(1-2):**44–51 **DOI:**10.1016/j.jviromet.2011.08.010

Palese P, Shaw ML. 2007. *Orthomyxoviridae*: the viruses and their replication. In: Knipe DM, Howley PM, Griffin DE, Lamb RA, Martin MA, Roizman B, Straus SE, eds. *Fields Virology. 5th edition, volume 2.* Philadelphia: Wolters Kluwer/Lippincott Williams & Wilkins, 1647–1689.

Palese P. 2004. Influenza: old and new threats. *Nature Medicine* **10:**S82–S87 **DOI:**10.1038/nm1141

Park JW, Jo WH. 2009. Infiltration of water molecules into the oseltamivir-binding site of H274Y neuraminidase mutant causes resistance to oseltamivir. *Journal of Chemical Information and Modeling* **49(12):**2735–2741 **DOI:**10.1021/ci900348n

Parrish CR, Murcia PR, Holmes EC. 2015. Influenza virus reservoirs and intermediate hosts: dogs, horses, and new possibilities for influenza virus exposure of humans. *Journal of Virology* **89(6):**2990-2994 **DOI:**10.1128/JVI.03146-14

Pasi M, Tiberti M, Arrigoni A, Papaleo E. 2012. xPyder: A PyMOL plugin to analyze coupled residues and their networks in protein structures. *Journal of Chemical Information and Modeling* **52(7):**1865–1874 **DOI:**10.1021/ci300213c

Paterson D, Fodor E. 2012. Emerging roles for the influenza A virus nuclear export protein (NEP). *PLoS Pathogens* **8(12):**e1003019 **DOI:**10.1371/journal.ppat.1003019

Perez JT, Varble A, Sachidanandam R, Zlatev I, Manoharan M, García-Sastre A, tenOever BR. 2010. Influenza A virus-generated small RNAs regulate the switch from transcription to replication. *Proceedings of the National Academy of Sciences of the United States of America* **107(25):**11525-11530 **DOI:**10.1073/pnas.1001984107

Pettersen EF, Goddard TD, Huang CC, Couch GS, Greenblatt DM, Meng EC, Ferrin TE. 2004. UCSF Chimera - a visualization system for exploratory research and analysis. *Journal of Computational Chemistry* **25(13):**1605-1612 **DOI:**10.1002/jcc.20084

Pinto LH, Holsinger LJ, Lamb RA. 1992. Influenza virus M2 protein has ion channel activity. *Cell* **69(3):**517-528 **DOI:**10.1016/0092-8674(92)90452-i

Piovesan D, Minervini G, Tosatto SCE. 2016. The RING 2.0 web server for high quality residue interaction networks. *Nucleic Acids Research* **44(W1):**W367–W374 **DOI:**10.1093/nar/gkw315

Rameix-Welti MA, Agou F, Buchy P, Mardy S, Aubin JT, Véron M, van der Werf S, Naffakh N. 2006. Natural variation can significantly alter the sensitivity of influenza A (H5N1) viruses to oseltamivir. *Antimicrobial Agents and Chemotherapy* **50(11):**3809-3815 **DOI:**10.1128/AAC.00645-06

Ran Z, Shen H, Lang Y, Kolb EA, Turan N, Zhu L, Ma J, Bawa B, Liu Q, Liu H, Quast M, Sexton G, Krammer F, Hause BM, Christopher-Hennings J, Nelson EA, Richt J, Li F, Ma W. 2015. Domestic pigs are susceptible to infection with influenza B viruses. *Journal of Virology* **89(9):**4818-4826 **DOI:**10.1128/JVI.00059-15

Ripoll DR, Khavrutskii IV, Chaudhury S, Liu J, Kuschner RA, Wallqvist A, Reifman J. 2012. Quantitative predictions of binding free energy changes in drug-resistant influenza neuraminidase. *PLoS Computational Biology* **8(8):**e1002665 **DOI:**10.1371/journal.pcbi.1002665

Ritchey MB, Palese P, Kilbourne ED. 1976. RNAs of influenza A, B, and C viruses. *Journal of Virology* **18(2):**738–744 **DOI:**10.1128/JVI.18.2.738-744.1976

Roe DR, Cheatham TE III. 2013. PTRAJ and CPPTRAJ: software for processing and analysis of molecular dynamics trajectory data. *Journal of Chemical Theory and Computation* **9(7):**3084-3095 **DOI:**10.1021/ct400341p

Russell RJ, Gamblin SJ, Skehel JJ. 2013. Influenza glycoproteins: hemagglutinin and neuraminidase. In: Webster RG, Monto AS, Braciale TJ, Lamb RA, eds. *Textbook of Influenza, 2nd edition.* West Sussex: John Wiley & Sons, Ltd., 67-100.

Russell RJ, Haire LF, Stevens DJ, Collins PJ, Lin YP, Blackburn GM, Hay AJ, Gamblin SJ, Skehel JJ. 2006. The structure of H5N1 avian influenza neuraminidase suggests new opportunities for drug design. *Nature* **443:**45-49 **DOI:**10.1038/nature05114

Ryckaert JP, Ciccotti G, Berendsen HJC. 1977. Numerical integration of the cartesian equations of motion of a system with constraints: molecular dynamics of *n*-alkanes. *Journal of Computational Physics* **23(3):**327-341 **DOI:**10.1016/0021-9991(77)90098-5

Schaduangrat N, Phanich J, Rungrotmongkol T, Lerdsamran H, Puthavathana P, Ubol S. 2016. The significance of naturally occurring neuraminidase quasispecies of H5N1 avian influenza virus on resistance to oseltamivir: a point of concern. *Journal of General Virology* **97(6):**1311-1323 **DOI:**10.1099/jgv.0.000444

Schrauwen EJ, Fouchier RA. 2014. Host adaptation and transmission of influenza A viruses in mammals. *Emerging Microbes & Infections* **3:**e9 **DOI:**10.1038/emi.2014.9

Serçinoğlu O, Ozbek P. 2018. gRINN: a tool for calculation of residue interaction energies and protein energy network analysis of molecular dynamics simulations. *Nucleic Acids Research* **46(W1):**W554-W562 **DOI:**10.1093/nar/gky381

Sethi A, Eargle J, Black AA, Luthey-Schulten Z. 2009. Dynamical networks in tRNA:protein complexes. *Proceedings of the National Academy of Sciences of the United States of America* **106:**6620–6625 **DOI:**10.1073/pnas.0810961106

Shannon P, Markiel A, Ozier O, Baliga NS, Wang JT, Ramage D, Amin N, Schwikowski B, Ideker T. 2003. Cytoscape: a software environment for integrated models of biomolecular interaction networks. *Genome Research* **13:**2498–2504 **DOI:**10.1101/gr.1239303

Shaw ML, Palese P. 2013. *Orthomyxoviridae.* In: Knipe DM, Howley PM, eds. *Fields Virology. 6th edition, volume 1.* Philadelphia: Lippincott Williams & Wilkins, 1151-1185.

Shcherbinin D, Veselovsky A. 2019. Analysis of protein structures using residue interaction networks. In: Mohan CG ed. *Structural Bioinformatics: Applications in Preclinical Drug Discovery Process. Challenges and Advances in Computational Chemistry and Physics.* Cham: Springer, 55–69 **DOI:**10.1007/978-3-030-05282-9_3

Sieczkarski SB, Whittaker GR. 2002. Influenza virus can enter and infect cells in the absence of clathrin-mediated endocytosis. *Journal of Virology* **76(20):**10455–10464 **DOI:**10.1128/JVI.76.20.10455-10464.2002

Skehel JJ, Wiley DC. 2000. Receptor binding and membrane fusion in virus entry: the influenza hemagglutinin. *Annual Review of Biochemistry* **69:**531-569 **DOI:**10.1146/annurev.biochem.69.1.531

Smith BJ, Huyton T, Joosten RP, McKimm-Breschkin JL, Zhang JG, Luo CS, Lou MZ, Labrou NE, Garrett TPJ. 2006. Structure of a calcium-deficient form of influenza virus neuraminidase: implications for substrate binding. *Acta Crystallographica Section D Structural Biology* **62:**947-952 **DOI:**10.1107/S0907444906020063

Sousa SF, Ribeiro AJM, Neves RPP, Brás NF, Cerqueira NMFSA, Fernandes PA, Ramos MJ. 2017. Application of quantum mechanics/molecular mechanics methods in the study of enzymatic reaction mechanisms. *Wiley Interdisciplinary Reviews: Computational Molecular Science* **7(2):**e1281 **DOI:**10.1002/wcms.1281

Spacková N, Cheatham TE III, Ryjácek F, Lankas F, van Meervelt L, Hobza P, Sponer J. 2003. Molecular dynamics simulations and thermodynamics analysis of DNA-drug complexes. Minor groove binding between 4',6-diamidino-2-phenylindole and DNA duplexes in solution. *Journal of the American Chemical Society* **125(7):**1759-1769 **DOI:**10.1021/ja025660d

Srinivasan J, Cheatham TE III, Cieplak P, Kollman PA, Case DA. 1998. Continuum solvent studies of the stability of DNA, RNA, and phosphoramidate−DNA Helices. *Journal of the American Chemical Society* **120(37):**9401−9409 **DOI:**10.1021/ja981844+

Steinhauer DA, Wharton SA. 1998. Structure and function of the haemagglutinin. In: Nicholson KG, Webster RG, Hay AJ, eds. *Textbook of Influenza.* London: Blackwell Science Oxford Ltd., 54-64.

Stevens J, Blixt O, Tumpey TM, Taubenberger JK, Paulson JC, Wilson IA. 2006. Structure and receptor specificity of the hemagglutinin from an H5N1 influenza virus. *Science* **312(5772):**404-410 **DOI:**10.1126/science.1124513

Suzuki Y, Ito T, Suzuki T, Holland RE Jr, Chambers TM, Kiso M, Ishida H, Kawaoka Y. 2000. Sialic acid species as a determinant of the host range of influenza A viruses. *Journal of Virology* **74(24):**11825-11831 **DOI:**10.1128/jvi.74.24.11825-11831.2000

Swanson JMJ, Henchman RH, McCammon JA. 2004. Revisiting free energy calculations: a theoretical connection to MM/PBSA and direct calculation of the association free energy. *Biophysical Journal* **86(1):**67-74 **DOI:**10.1016/S0006-3495(04)74084-9

Sylte MJ, Suarez DL. 2009. Influenza neuraminidase as a vaccine antigen. In: Compans R, Orenstein W, eds. *Vaccines for Pandemic Influenza. Current Topics in Microbiology and Immunology.* Berlin, Heidelberg: Springer, **333:**227-241 **DOI:**10.1007/978-3-540-92165-3_12

Takano R, Kiso M, Igarashi M, Le QM, Sekijima M, Ito K, Takada A, Kawaoka Y. 2013. Molecular mechanisms underlying oseltamivir resistance mediated by an I117V substitution in the neuraminidase of subtype H5N1 avian influenza A viruses. *The Journal of Infectious Diseases* **207(1):**89-97 **DOI:**10.1093/infdis/jis633

Takashita E, Fujisaki S, Shirakura M, Nakamura K, Kishida N, Kuwahara T, Shimazu Y, Shimomura T, Watanabe S, Odagiri T, The Influenza Virus Surveillance Group of Japan. 2016. Influenza A(H1N1)pdm09 virus exhibiting enhanced cross-resistance to oseltamivir and peramivir due to a dual H275Y/G147R substitution, Japan, March 2016. *Eurosurveillance* **21(24):**30258 **DOI**:10.2807/1560-7917.ES.2016.21.24.30258

Takashita E, Fujisaki S, Yokoyama M, Shirakura M, Morita H, Nakamura K, Kishida N, Kuwahara T, Sato H, Doi I, Sato Y, Takao S, Shimazu Y, Shimomura T, Ito T, Watanabe S, Odagiri T, The Influenza Virus Surveillance Group of Japan. 2020. In vitro characterization of multidrug-resistant influenza A(H1N1)pdm09 viruses carrying a dual neuraminidase mutation isolated from immunocompromised patients. *Pathogens* **9(9):**725 **DOI:**10.3390/pathogens9090725

Theodorou DN, Suter UW. 1985. Geometrical considerations in model systems with periodic boundaries. *Journal of Chemical Physics* **82(2):**955–966 **DOI:**10.1063/1.448472

Tiberti M, Invernizzi G, Lambrughi M, Inbar Y, Schreiber G, Papaleo E. 2014. PyInteraph: a framework for the analysis of interaction networks in structural ensembles of proteins. *Journal of Chemical Information and Modeling* **54(5):**1537–1551 **DOI:**10.1021/ci400639r

Tong S, Zhu X, Li Y, Shi M, Zhang J, Bourgeois M, Yang H, Chen X, Recuenco S, Gomez J, Chen LM, Johnson A, Tao Y, Dreyfus C, Yu W, McBride R, Carney PJ, Gilbert AT, Chang J, Guo Z, Davis CT, Paulson JC, Stevens J, Rupprecht CE, Holmes EC, Wilson IA, Donis RO. 2013. New world bats harbor diverse influenza A viruses. *PLoS Pathogens* **9(10):**e1003657 **DOI:**10.1371/journal.ppat.1003657

Toxvaerd S. 1993. Molecular dynamics at constant temperature and pressure. *Physical Review E* **47:**343 **DOI:**10.1103/PhysRevE.47.343

Umbach JL, Yen HL, Poon LLM, Cullen BR. 2010. Influenza A virus expresses high levels of an unusual class of small viral leader RNAs in infected cells. *mBio* **1(4):**e00204-10 **DOI:**10.1128/mBio.00204-10

Varghese JN, Laver WG, Colman PM. 1983. Structure of the influenza virus glycoprotein antigen neuraminidase at 2.9 Å resolution. *Nature* **303:**35–40 **DOI:**10.1038/303035a0

Vergara-Jaque A, Poblete H, Lee EH, Schulten K, González-Nilo F, Chipot C. 2012. Molecular basis of drug resistance in A/H1N1 virus. *Journal of Chemical Information and Modeling* **52(10):**2650–2656 **DOI:**10.1021/ci300343w

Verlet L. 1967. Computer "experiments" on classical fluids. I. Thermodynamical properties of Lennard-Jones molecules**.** *Physical Review Journals* **159(1):**98-103 **DOI:**10.1103/PhysRev.159.98

von Itzstein M, Wu WY, Kok GB, Pegg MS, Dyason JC, Jin B, Van Phan T, Smythe ML, White HF, Oliver SW, Colman PM, Varghese JN, Ryan DM, Woods JM, Bethell RC, Hotham VJ, Cameron JM, Penn CR. 1993. Rational design of potent sialidase-based inhibitors of influenza virus replication. *Nature* **363:**418-423 **DOI:**10.1038/363418a0

Wagner JR, Sørensen J, Hensley N, Wong C, Zhu C, Perison T, Amaro RE. 2017. POVME 3.0: software for mapping binding pocket flexibility. *Journal of Chemical Theory and Computation* **13(9):**4584–4592 **DOI:**10.1021/acs.jctc.7b00500

Wagner R, Matrosovich M, Klenk HD. 2002. Functional balance between haemagglutinin and neuraminidase in influenza virus infections. *Reviews in Medical Virology* **12(3):**159-166 **DOI:**10.1002/rmv.352

Wang E, Sun H, Wang J, Wang Z, Liu H, Zhang JZH, Hou T. 2019. End-point binding free energy calculation with MM/PBSA and MM/GBSA: strategies and applications in drug design. *Chemical Reviews* **119(16):**9478-9508 **DOI:**10.1021/acs.chemrev.9b00055

Wang J, Wolf RM, Caldwell JW, Kollman PA, Case DA. 2004. Development and testing of a general amber force field. *Journal of Computational Chemistry* **25(9):**1157-1174 **DOI:**10.1002/jcc.20035

Wang J, Hou T, Xu X. 2006. Recent advances in free energy calculations with a combination of molecular mechanics and continuum models. *Current Computer-Aided Drug Design* **2(3):**287-306 **DOI:**10.2174/157340906778226454

Wang MZ, Tai CY, Mendel DB. 2002. Mechanism by which mutations at His274 alter sensitivity of influenza A virus N1 neuraminidase to oseltamivir carboxylate and zanamivir. *Antimicrobial Agents and Chemotherapy* **46(12):**3809–3816 **DOI:**10.1128/aac.46.12.3809-3816.2002

Wang NX, Zheng JJ. 2009. Computational studies of H5N1 influenza virus resistance to oseltamivir. *Protein Science* **18(4):**707–715 **DOI:**10.1002/pro.77

Ward CW, Colman PM, Laver WG. 1983. The disulphide bonds of an Asian influenza virus neuraminidase. *FEBS Letters* **153(1):**29–33 **DOI:**10.1016/0014-5793(83)80113-6

Webster RG, Bean WJ, Gorman OT, Chambers TM, Kawaoka Y. 1992. Evolution and ecology of influenza A viruses. *Microbiological Reviews* **56(1):**152-179 **DOI:**10.1128/mr.56.1.152-179.1992

Weiser J, Shenkin PS, Still WC. 1999. Approximate atomic surfaces from linear combinations of pairwise overlaps (LCPO). *Journal of Computational Chemistry* **20(2):**217-230 **DOI:**10.1002/(SICI)1096-987X(19990130)20:2<217::AID-JCC4>3.0.CO;2-A

Wiley DC, Skehel JJ. 1987. The structure and function of the hemagglutinin membrane glycoprotein of influenza virus. *Annual Review of Biochemistry* **56:**365–394 **DOI:**10.1146/annurev.bi.56.070187.002053

Wise HM, Foeglein A, Sun J, Dalton RM, Patel S, Howard W, Anderson EC, Barclay WS, Digard P. 2009. A complicated message: identification of a novel PB1-related protein translated from influenza A virus segment 2 mRNA. *Journal of Virology* **83(16):**8021-8031 **DOI:**10.1128/JVI.00826-09

Wolek K, Gómez-Sicilia Á, Cieplak M. 2015. Determination of contact maps in proteins: a combination of structural and chemical approaches. *Journal of Chemical Physics* **143(24):**243105 **DOI:**10.1063/1.4929599

Woods CJ, Malaisree M, Long B, McIntosh-Smith S, Mulholland AJ. 2013. Analysis and assay of oseltamivir-resistant mutants of influenza neuraminidase via direct observation of drug unbinding and rebinding in simulation. *Biochemistry* **52(45):**8150–8164 **DOI:**10.1021/bi400754t

Woods CJ, Malaisree M, Pattarapongdilok N, Sompornpisut P, Hannongbua S, Mulholland AJ. 2012. Long time scale GPU dynamics reveal the mechanism of drug resistance of the dual mutant I223R/H275Y neuraminidase from H1N1-2009 influenza virus. *Biochemistry* **51(21):**4364-4375 **DOI:**10.1021/bi300561n

World Health Organization. 1980. A revision of the system of nomenclature for influenza viruses: a WHO memorandum. *Bulletin of the World Health Organization* **58(4):**585–591 *Available at* https://apps.who.int/iris/handle/10665/262025

World Health Organization. 2012. Meetings of the WHO working group on surveillance of influenza antiviral susceptibility – Geneva November 2011 and June 2012. *Weekly Epidemiological Record* **87(39):**369–374 *Available at https://apps.who.int/iris/handle/10665/241965*

Wrigley NG. 1979. Electron microscopy of influenza virus. *British Medical Bulletin* **35(1):**35-38 **DOI:**10.1093/oxfordjournals.bmb.a071539

Wu Y, Wu Y, Tefsen B, Shi Y, Gao GF. 2014. Bat-derived influenza-like viruses H17N10 and H18N11. *Trends in Microbiology* **22(4):**183-191 **DOI:**10.1016/j.tim.2014.01.010

Xue W, Ban Y, Liu H, Yao X. 2014. Computational study on the drug resistance mechanism against HCV NS3/4A protease inhibitors vaniprevir and MK-5172 by the combination use of molecular dynamics simulation, residue interaction network, and substrate envelope analysis. *Journal of Chemical Information and Modeling* **54(2):**621–633 **DOI:**10.1021/ci400060j

Xue W, Jin X, Ning L, Wang M, Liu H, Yao X. 2013. Exploring the molecular mechanism of cross-resistance to HIV-1 integrase strand transfer inhibitors by molecular dynamics simulation and residue interaction network analysis. *Journal of Chemical Information and Modeling* **53(1):**210–222 **DOI:**10.1021/ci300541c

Yadav M, Igarashi M, Yamamoto N. 2021a. Dynamic residue interaction network analysis of the oseltamivir binding site of N1 neuraminidase and its H274Y mutation site conferring drug resistance in influenza A virus. *PeerJ* **9:**e11552 **DOI:**10.7717/peerj.11552

Yadav M, Igarashi M, Yamamoto N. 2021b. Theoretical insights into the molecular mechanism of I117V mutation in neuraminidase mediated reduction of oseltamivir drug susceptibility in A/H5N1 influenza virus. *PeerJ Physical Chemistry* **3:**e19 **DOI:**10.7717/peerj-pchem.19

Yan W, Zhou J, Sun M, Chen J, Hu G, Shen B. 2014. The construction of an amino acid network for understanding protein structure and function. *Amino Acids* **46:**1419–1439 **DOI:**10.1007/s00726-014-1710-6

Yang X, Steukers L, Forier K, Xiong R, Braeckmans K, Van Reeth K, Nauwynck H. 2014. A beneficiary role for neuraminidase in influenza virus penetration through the respiratory mucus. *PloS ONE* **9(10):**e110026 **DOI:**10.1371/journal.pone.0110026

Yen HL, Ilyushina NA, Salomon R, Hoffmann E, Webster RG, Govorkova EA. 2007. Neuraminidase inhibitor-resistant recombinant A/Vietnam/1203/04 (H5N1) influenza viruses retain their replication efficiency and pathogenicity in vitro and in vivo. *Journal of Virology* **81(22):**12418-12426 **DOI:**10.1128/JVI.01067-07

Yongkiettrakul S, Boonyapakron K, Jongkaewwattana A, Wanitchang A, Leartsakulpanich U, Chitnumsub P, Eurwilaichitr L, Yuthavong Y. 2009. Avian influenza A/H5N1 neuraminidase expressed in yeast with a functional head domain. *Journal of Virological Methods* **156(1-2):**44–51 **DOI:**10.1016/j.jviromet.2008.10.025

Yusuf M, Mohamed N, Mohamad S, Janezic D, Damodaran KV, Wahab HA. 2016. H274Y's effect on oseltamivir resistance: What happens before the drug enters the binding site. *Journal of Chemical Information and Modeling* **56(1):**82–100 **DOI:**10.1021/acs.jcim.5b00331

Zhang Q, An X, Liu H, Wang S, Xiao T, Liu H. 2019. Uncovering the resistance mechanism of *Mycobacterium tuberculosis* to rifampicin due to RNA polymerase H451D/Y/R mutations from computational perspective. *Frontiers in Chemistry* **7:**819 **DOI:**10.3389/fchem.2019.00819

Zhu X, Yang H, Guo Z, Yu W, Carney PJ, Li Y, Chen LM, Paulson JC, Donis RO, Tong S, Stevens J, Wilson IA. 2012. Crystal structures of two subtype N10 neuraminidase-like proteins from bat influenza A viruses reveal a diverged putative active site. *Proceedings of the National Academy of Sciences of the United States of America* **109(46):**18903-18908 **DOI:**10.1073/pnas.1212579109

Appendix A: Introduction to Molecular Dynamics (MD) simulations

Molecular dynamics (MD) simulations are an important tool for gaining atomic-level insights into the structural, dynamic, and thermodynamic properties of a molecular system. Newton's second equation can be solved to stimulate the dynamics of nuclei approximately behaving like classical particle.

$$\begin{aligned} \mathrm{F} &= ma \\ -\frac{dV}{dr} &= m\frac{d^2r}{dt^2} \end{aligned} \tag{1}$$

Here, for particle at position *r*, the force (F) on particle is in the negative direction of the gradient of potential energy (*V*).

A.1. Integration algorithms

Integration algorithms are the numerical method to solve Newton's second equation.

A.1.1. Verlet algorithm

For particle at position (r_i), Taylor expansion can be used to derive position (r_{i+1}) at later time step (Δt):

$$\begin{aligned} r_{i+1} &= r_i + \frac{\partial r}{\partial t}(\Delta t) + \frac{1}{2}\frac{\partial^2 r}{\partial t^2}(\Delta t)^2 + \frac{1}{6}\frac{\partial^3 r}{\partial t^3}(\Delta t)^3 + \cdots \\ r_{i+1} &= r_i + v_i(\Delta t) + \frac{1}{2}a_i(\Delta t)^2 + \frac{1}{6}b_i(\Delta t)^3 + \cdots \end{aligned} \tag{2}$$

where, velocity (v_i) is the first derivative, acceleration (a_i) is the second derivative and hyperacceleration (b_i) is the third derivative of position with respect to time. In equation (2), by replacing (Δt) with ($-\Delta t$), position (r_{i-1}) at previous time step (Δt) can be derived:

$$r_{i-1} = r_i - v_i(\Delta t) + \frac{1}{2}a_i(\Delta t)^2 - \frac{1}{6}b_i(\Delta t)^3 + \cdots \tag{3}$$

By adding equations (2) and (3), an equation to predict the position (r_{i+1}) at later time step (Δt) using previous position (r_{i-1}) and current position (r_i) and acceleration (a_i) can be derived:

$$\begin{aligned} r_{i+1} &= (2r_i - r_{i-1}) + a_i(\Delta t)^2 + \cdots \\ a_i &= \frac{\mathrm{F}_i}{m_i} = -\frac{1}{m_i}\frac{dV}{dr_i} \end{aligned} \tag{4}$$

Equation (4) is the Verlet algorithm (*Verlet, 1967*) to numerically solve Newton's second equation. The numerical disadvantage of this algorithm is that to obtain the new

positions, two terms are added, the position difference ($2r_i - r_{i\text{-}1}$) and the time step $(\Delta t)^2$. Truncation errors because of finite precision may occur as the difference between two large numbers ($2r_i - r_{i\text{-}1}$) is added to a small number $(\Delta t)^2$. Another disadvantage of this algorithm is that the velocity is not calculated explicitly.

A.1.2. Leap-Frog algorithm

The leap-frog algorithm (*Allen & Tildesley, 1989*) can be used to resolve the problem related to the Verlet algorithm. Equation (5) is derived by doing Taylor expansions similar to equations (2) and (3) using half a time step, then doing subtraction:

$$r_{i+1} = r_i + v_{i+\frac{1}{2}}\Delta t \tag{5}$$

To derive equation (6), using similar expansions, the velocity is calculated:

$$v_{i+\frac{1}{2}} = v_{i-\frac{1}{2}} + a_i\Delta t \tag{6}$$

The leap-frog algorithm is defined by equations (5) and (6). The advantage of this algorithm is that the velocity is calculated explicitly. The disadvantage of this algorithm is that the position and velocity are not updated simultaneously and are always out of phase by half a time step.

A.1.3. Velocity Verlet algorithm

The velocity Verlet algorithm (*Andersen, 1980*) can be used to resolve the problem related to the leap-frog algorithm. The velocity Verlet algorithm is defined by equation (7):

$$\begin{aligned} r_{i+1} &= r_i + v_i\Delta t + \frac{1}{2}a_i\Delta t^2 \\ v_{i+1} &= v_i + \frac{1}{2}\{a_i + a_{i+1}\}\Delta t \end{aligned} \tag{7}$$

The advantage of this algorithm is that the velocity is calculated explicitly as well as the position and velocity are updated simultaneously.

In MD simulations, the time-reversible algorithms, such as Verlet and leap-frog algorithms are preferred because it tend to improve the conservation of energy over long period of simulation (*Toxvaerd, 1993*).

A.2. Thermodynamic ensembles

The simulation of a molecular system can be distinguished by various quantities, including temperature (T), volume (V), pressure (P), number of particles (N), total energy (E), and chemical potential (μ). The thermodynamic ensemble of a molecular system is labelled based on the constant/fixed quantities, with the simulation data being used to derive the remaining quantities and thus showing a statistical fluctuation.

Table A.1: Various thermodynamic ensembles of a molecular system.

Name	Acronym	Constant quantities
Micro-canonical	NVE	Number of particles (N), Volume (V), Total energy (E)
Canonical	NVT	Number of particles (N), Volume (V), Temperature (T)
Isothermal-isobaric	NPT	Number of particles (N), Pressure (P), Temperature (T)
Grand canonical	μVT	Chemical potential (μ), Volume (V), Temperature (T)
Isoenthalpic-isobaric	NPH	Number of particles (N), Pressure (P), Enthalpy (H)

A.3. Force field

In MD simulation, a potential energy function is used to derive the force acting on an atom for describing the interatomic interactions. This potential energy function is also known as force field. By adding different energy terms, the energy of force field (E_{FF}) is calculated; each term corresponds to the energy needed to distort a molecule in a certain way (*Jensen, 2007*):

$$E_{\mathrm{FF}} = E_{\mathrm{str}} + E_{\mathrm{bend}} + E_{\mathrm{tors}} + E_{\mathrm{vdw}} + E_{\mathrm{el}} + E_{\mathrm{cross}}$$

where E_{str}, E_{bend}, E_{tors}, and E_{cross} describes the bonded interatomic interactions, whereas E_{vdw} and E_{el} describes the non-bonded interatomic interactions. E_{str} is *stretch energy* needed to stretch a bond between a pair of atoms, E_{bend} is *bending energy* needed to bend an angle, E_{tors} is *torsional energy* needed to rotate around a bond, and E_{cross} represents the *cross terms* describing the coupling between E_{str}, E_{bend}, and E_{tors}. E_{el} is *electrostatic energy* and E_{vdw} is *van der Waals energy*.

The minima on optimized (energy minimized) E_{FF} surface corresponds to stable molecules. To analyze conformational transitions of a molecule, different conformations of a molecule can be located on the optimized (energy minimized) E_{FF} surface.

A.4. Periodic boundary conditions

In MD simulation, the size of a molecular system (number of atoms) that can be simulated is always limited for reducing the computational cost. To study the characteristics of a real macroscopic system (for instance, ~10^{23} atoms), a smaller molecular system containing hundreds or thousands of atoms can be simulated using periodic boundary conditions (PBCs) (*Theodorou & Suter, 1985*). PBCs is used to minimize surface effects and to prevent boiling off the solvent molecules on the outer surface. Under PBCs, the modeled molecular system is assumed to be a unit cell in an ideal crystal and is surrounded by infinite number of duplicate images in all directions of the unit cell. Minimum image convention is often used along with PBCs. If an atom exits the unit cell from one side, its periodic image will simultaneously enter the unit cell through the opposite site from the neighboring unit cell with the same velocity, thus the total number of atoms in the unit cell remains constant (Figure A.1). An atom in the simulation unit cell forms interatomic interactions with other atoms in this unit cell as well as with its images in the surrounding unit cells. In this case, the surface effects are minimized as the atoms will not feel the surface forces.

Under PBCs, the size of the simulation unit cell must be at least as large as the largest cut-off length used in the simulation; or else some interatomic interactions would be counted at least twice (once within the unit cell and once with an image in the neighboring unit cell). For van der Waals interactions, if the cut-offs are reasonably large (~8-10 Å), the interactions are not affected significantly. For electrostatic interactions, due to the long range nature of interactions, Ewald sums are generally preferred over cut-offs.

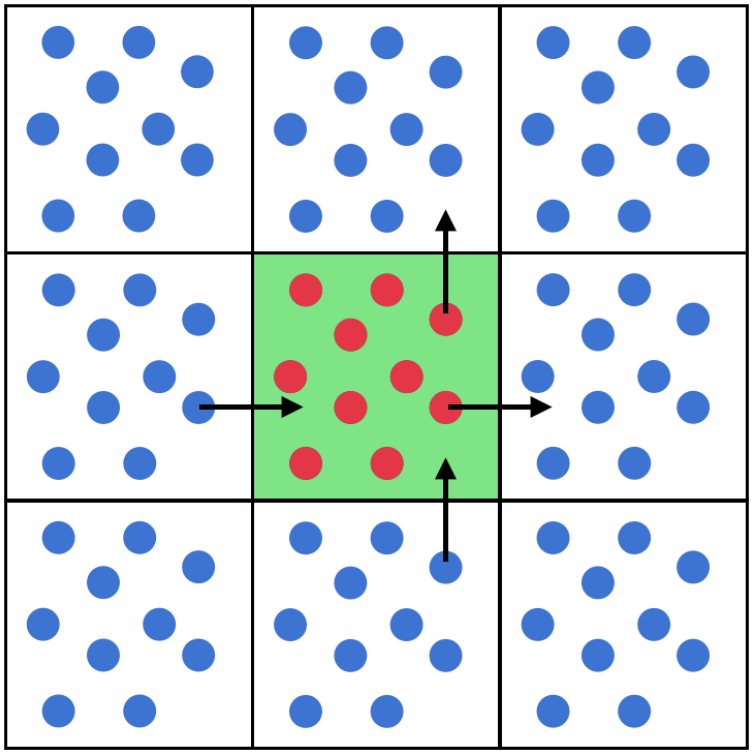

Figure A.1: Periodic boundary condition represented in two-dimension. The simulation box is shown by central unit cell (in green). The simulation box particles are shown by red circles and their periodic image in surrounding unit cells are shown by blue circles. The two particles movement near the boundary is shown by arrows; when a particle exits from the simulation box simultaneously its periodic image enters the simulation box through the opposite site from the neighboring unit cell with the same velocity.

A.5. Thermostat

To perform MD simulation in NVT or NPT ensemble, the temperature of the molecular system is controlled by coupling it to a heat bath or thermostat with a fixed temperature. One of the widely used thermostat is the Berendsen thermostat, also known as the weak-coupling thermostat (*Berendsen et al., 1984*).

In the Berendsen thermostat, the temperature of the molecular system is controlled by scaling the velocities by a factor λ:

$$\lambda = \sqrt{1 + \frac{\Delta t}{\tau_T}\left(\frac{T_0}{T} - 1\right)}$$

where λ is the velocity scale factor, T_0 is the reference temperature, T is the actual temperature, Δt is the time-step, and τ_T is the coupling time constant.

In the Berendsen thermostat, the velocities are scaled by a factor λ at each time-step such that it is quite efficient in pushing the instantaneous temperature towards the desired temperature for molecular systems that are far from equilibrium. The drawback of the Berendsen thermostat is that the fluctuations of the kinetic energy of the molecular system are suppressed and are not consistent with the thermodynamic ensemble.

A.6. Barostat

To perform MD simulation in NPT ensemble, the pressure of the molecular system is controlled by coupling it to a pressure bath or barostat with a fixed pressure. One of the widely used barostat is the Berendsen barostat (*Berendsen et al., 1984*).

In the Berendsen barostat, the pressure of the molecular system is controlled by scaling the volume of the molecular system (all coordinates of the simulation box) by a factor μ:

$$\mu = \sqrt[3]{1 - \beta \frac{\Delta t}{\tau_P}(P_0 - P)}$$

where μ is the coordinate scale factor, P_0 is the reference pressure, P is the actual pressure, Δt is the time-step, τ_P is the coupling time constant, and β is the isothermal compressibility.

In the Berendsen barostat, the size of the simulation box is scaled by a factor μ at each time-step, but the shape of the simulation box remains invariant. This method is found to be highly efficient for a molecular system to reach a desired pressure, but it does not produce correct thermodynamic ensemble.

A.7. Energy minimization

Energy minimization of a molecular system is performed to find a local minimum on its potential energy surface in order to eliminate the net force imposed on each atom. To optimize the initial structure of a molecular system with bad contacts (for example, two non-bonded atoms are extremely close to each other), the energy minimization is performed before MD simulation so that the resulting minimized structure is appropriate for subsequent equilibration and production runs. Two of the most widely used energy minimization algorithms are steepest descent and conjugate gradient algorithms.

In the steepest descent algorithm, the molecular system is pushed in the direction of the negative gradient of the potential energy function to find a local minimum state. To remove bad contacts from an unreasonably high energy structure of a molecular system, steepest

descent algorithm is quite efficient. However, the steepest descent algorithm is inefficient in reaching a local minimum and can lead the search towards a local minimum near the initial state.

In the conjugate gradient algorithm, previous gradient information is used to update the coordinates and thus the potential energy function. During the minimization process, the conjugate gradient algorithm is observed to converge fast for a molecular system that is close to the minimum.

In many cases, a combination of energy minimization algorithms is preferrable. For example, first the steepest descent algorithm is used to remove bad contacts from an unreasonably high energy structure of a molecular system, followed by the conjugate gradient algorithm to make the structure of a molecular system reach a local minimum on its potential energy surface.

Appendix B: Introduction to binding free energy calculations

One of the methods to estimate the binding free energy is Molecular Mechanics Poisson Boltzmann Surface Area (MM-PBSA) method. MM-PBSA method is based on end-state free energy method and implicit solvent model (*Miller et al., 2012*). In MM-PBSA method, the binding free energy (ΔG_{bind}) to from complex (RL) by binding ligand (L) to receptor (R):

$$\Delta G_{bind} = G_{RL} - G_R - G_L \quad (1)$$

can be decomposed into different interactions contributions and described as (*Srinivasan et al., 1998*):

$$\Delta G_{bind} = \Delta H - T\Delta S = \Delta E_{MM} + \Delta G_{sol} - T\Delta S \quad (2)$$

in which:

$$\Delta E_{MM} = \Delta E_{int} + \Delta E_{ele} + \Delta E_{vdw} \quad (3)$$

$$\Delta G_{sol} = \Delta G_{PB/GB} + \Delta G_{SA} \quad (4)$$

$$\Delta G_{SA} = \gamma \cdot \mathrm{SASA} + \mathrm{b} \quad (5)$$

where the changes in enthalpy (ΔH) includes the changes in molecular mechanics (MM) energy in gas phase (ΔE_{MM}) and the changes in solvation free energy (ΔG_{sol}) upon ligand binding. ΔE_{MM} consists of ΔE_{int}, ΔE_{ele}, and ΔE_{vdw}, where ΔE_{int} is the changes in internal (bond, angle & dihedral) energy, ΔE_{ele} is the changes in electrostatic energy, and ΔE_{vdw} is the changes in van der Waals energy upon ligand binding. ΔG_{sol} consists of the changes in non-polar solvation energy (ΔG_{SA}) and the changes in polar (electrostatic) solvation energy ($\Delta G_{PB/GB}$) between the continuum solvent and the solute upon ligand binding. Solvent-accessible surface area (SASA) is usually used to estimate ΔG_{SA}, whereas either Generalized Born (GB) or Poisson-Boltzmann (PB) model is used to estimate $\Delta G_{PB/GB}$ (*Gilson & Honig, 1988; Wang et al., 2006*). However, the GB method is faster than the PB method because it provides an analytical expression of $\Delta G_{PB/GB}$. T is temperature. Normal mode analysis is usually used to estimate the change in conformational entropy (ΔS) upon ligand binding by analyzing a group of conformational snapshots obtained from MD simulations (*Srinivasan et al., 1998*). When the ligands are similar and only relative binding free energies are required, usually the changes in conformational entropy are neglected due to high cost of computation.

There are two protocols to generate the required ensembles for the bound and unbound state of binding free energy calculations: single trajectory protocol (STP) in which all ensembles are extracted from a single MD trajectory and multiple trajectory protocol (MTP) in which all ensembles are generated using separate MD simulations (*Lee & Olson, 2006; Wang et al., 2006*). Both protocols have distinct advantages and disadvantages.

In practice, STP is more widely used and preferrable because it provides more accurate results with lower standard errors (*Spacková et al., 2003; Lepsik et al., 2004; Genheden & Ryde, 2015*). The computational cost of STP is less than MTP, because all ensembles are generated from a single MD trajectory. However, STP assumes that the structures obtained from unbound ensembles (the isolated ligand and the apo protein) are sufficiently similar to the structures obtained from the bound ensemble (protein-ligand complex). This assumption is valid for most cases but could be invalid for some cases where large conformational changes occur upon protein-ligand binding (*Swanson et al., 2004*). The main advantage of STP is that the difference in energy between the unbound ensembles (isolated ligand and apo protein) and the bound ensemble (protein-ligand complex) is calculated using exactly identical configurations, hence the errors in internal energy of the systems can be cancelled. However, in MTP, the difference in energy between the unbound ensembles (isolated ligand and apo protein) and the bound ensemble (protein-ligand complex) is calculated using averages obtained from separate unbound (isolated ligand and apo protein) and bound (protein-ligand complex) MD trajectories, hence due to large errors in internal energy of different conformations, MTP may cause additional noise/errors and by just doing longer MD simulations, it is difficult to remove these errors. Generally, in MTP, to correctly determine if the simulation has properly converged is challenging (*Daggett, 2000*). However, in STP, due to cancellation of errors in internal energy, the fluctuation in components of energy is small, but in STP, sampling of unbound ensembles (isolated ligand and apo protein) may be inadequate.

Appendix C: Supplementary information of "Dynamic residue interaction network analysis of the oseltamivir binding site of N1 neuraminidase and its H274Y mutation site conferring drug resistance in influenza A virus"

C.1. Dynamic residue interaction network (dRIN) analysis ruby script

GitHub link: https://github.com/yamnor/dRIN

```
#!/usr/local/bin/ruby

dir = "drin"

def cpptraj(cmd)
  File.open("cpp.cmd", "w"){|fw| fw.puts cmd}
  system("module load amber/20/update0; cpptraj < cpp.cmd > cpp.log; rm cpp.cmd
cpp.log")
end

def s2n(str)
  return str.split("_").at(1).delete(":").to_i
end

def s2s(str)
  return str.split(":").at(0).downcase.intern
end

def modpdb(pdb_inp, pdb_out)
  pdb = File.open(pdb_inp).readlines
  pdb.map!{|x| x.gsub("CYX", "CYS")}
  pdb.map!{|x| x =~ /OTV/ ? x.gsub("ATOM  ", "HETATM") : x}
  File.open(pdb_out, "w"){|fw| fw.puts pdb.join}
end
```

```
def exec_ring(dir, nsamples)
  [*1..nsamples].each do |m|
    if File.size("#{dir}/rin_#{m}.pdb") > 100
      modpdb("#{dir}/rin_#{m}.pdb", "#{dir}/rin_#{m}_mod.pdb")
      system("export VICTOR_ROOT=~/apl/ring/; ~/apl/ring/bin/Ring -i
#{dir}/rin_#{m}_mod.pdb --no_energy -E #{dir}/rin_#{m}.edge -N #{dir}/rin_#{m}.node
>& #{dir}/rin_#{m}.log")
      system("export VICTOR_ROOT=~/apl/ring/; ~/apl/ring/bin/Ring -i
#{dir}/rin_#{m}_mod.pdb --no_energy --get_iac -t 4.0 -E #{dir}/rin_#{m}.edge_iac -N
#{dir}/rin_#{m}.node_iac >& #{dir}/rin_#{m}.log_iac")
    end
  end
end

def read_hbond(filename, nsamples)
  resid, *hbond = File.open(filename).readlines
  resid = resid.split.drop(1).map{|a| x = a.gsub("@", "_").split("_"); *x = [x[1].to_i,
x[3].to_i].sort}
  hbond = hbond.map{|a| a.split.drop(1).map(&:to_i)}.transpose
  dat = Array.new(nsamples).map{Array.new}
  nsamples.times do |t|
    resid.zip(hbond).each do |id, hb|
      dat[t] << id if hb[t] > 0
    end
  end
  return dat
end

def read_rin(dir, nsamples)
  vdwrad = {"H": 1.0000, "C": 1.700, "N": 1.625, "O": 1.480, "S": 1.782}
  ritype = {hbond: :hb, vdw: :vdw, ssbond: :ss, ionic: :ion, pipistack: :pp, pication: :pc,
iac: :iac}
  dat = Hash.new
```

```
    ritype.each_value{|v| dat[v] = Array.new(nsamples).map{Array.new}}
    nsamples.times do |t|
      flg = Array.new(400).map{Array.new(400, true)}
      tmp = File.open("#{dir}/rin_#{t+1}.edge").readlines.drop(1).map{|x|
x.split("\t")}.map{|id_1, int, id_2, dist, angle, ene, atom_1, atom_2| [[s2n(id_1),
s2n(id_2)].sort, s2s(int), [atom_1[0].intern, atom_2[0].intern], dist.to_f]}
      tmp.each do |id, int, atom, dist|
        if int != :iac
          dat[ritype[int]][t] << id if ritype.has_key?(int)
          flg[id[0]][id[1]] = false
        end
      end
      tmp = File.open("#{dir}/rin_#{t+1}.edge_iac").readlines.drop(1).map{|x|
x.split("\t")}.map{|id_1, int, id_2, dist, angle, ene, atom_1, atom_2| [[s2n(id_1),
s2n(id_2)].sort, s2s(int), [atom_1[0].intern, atom_2[0].intern], dist.to_f]}
      tmp.each do |id, int, atom, dist|
        if dist - (vdwrad[atom[0]] + vdwrad[atom[1]]) < 0.4
          if flg[id[0]][id[1]]
            dat[ritype[int]][t] << id
          end
        end
      end
    end
    return dat
end

def remove_duplicates(rin, nsamples)
    key = rin.keys
    key.delete(:iac)
    nsamples.times do |t|
      key.each do |k|
        rin[k][t].each do |id|
          rin[:iac][t].delete(id)
```

```
          end
        end
    end
    return rin
end

def write_series(filename, rin)
    key, val = rin.to_a.transpose
    val = val.transpose
    nsamples = val.size
    File.open(filename, "w") do |fw|
        nsamples.times do |t|
            str = [(t+1).to_s]
            key.each_with_index do |k, i|
                val[t][i].each do |id|
                    str << k
                    str << id.map(&:to_s).join("\t")
                end
            end
            fw.puts str.join("\t")
        end
    end
end

def calc_fraction(rin)
    key = rin.keys + [:any]
    dim = 400
    num = rin[:hb].size
    tmp = Hash.new
    key.each{|k| tmp[k] = Array.new(num).map{Array.new(dim).map{Array.new(dim,
false)}}}
    rin.each do |k, vk|
        vk.each_with_index do |vt, t|
```

```
            vt.each do |i, j|
              tmp[k][t][i][j]      = true
              tmp[:any][t][i][j] = true
            end
          end
        end
        dat = Hash.new
        key.each do |k|
          dat[k] = Array.new(dim).map{Array.new(dim, 0.0)}
          for i in 0..(dim-1)
            for j in (i+1)..(dim-1)
              cnt = 0.0
              tmp[k].each do |vt|
                dat[k][i][j] += 1.0 if vt[i][j]
                cnt += 1.0
              end
              dat[k][i][j] /= cnt
            end
          end
        end
        return dat
    end

    def write_fraction(filename, rin, threshold: 0.05)
        dat = calc_fraction(rin)
        key = dat.keys
        dim = dat[:hb].size
        File.open(filename, "w") do |fw|
          fw.puts ([:i, :j] + key).map(&:to_s).join("\t")
          for i in 0..(dim-1)
            for j in (i+1)..(dim-1)
              if dat[:any][i][j] > threshold
                val = Array.new
```

```
                key.each do |k|
                   val << dat[k][i][j]
                end
                fw.puts ([i, j] + val.map{|x| "%6.4f"%[x]}).join("\t")
             end
          end
       end
   end
end

cmd = Hash.new

cmd[:hbond] = <<TEXT
parm     com.top
trajin     5_pro/amb.trj
hbond    :1-387 angle 117 dist 3.5 avgout #{dir}/hbn.edge series uuseries #{dir}/hbn.series
TEXT

cmd[:pdb] = <<TEXT
parm     com.top
trajin     5_pro/amb.trj
TEXT

nsamples = 2000

[*1..nsamples].each do |n|
   cmd[:pdb] += "trajout #{dir}/rin_#{n}.pdb pdb nobox onlyframes #{n}\n"
end

cpptraj(cmd[:hbond])
cpptraj(cmd[:pdb])
exec_ring(dir, nsamples)
```

```
rin = read_rin(dir, nsamples)
rin[:hb] = read_hbond("#{dir}/hbn.series", nsamples)

rin = remove_duplicates(rin, nsamples)

write_series("#{dir}/rin.series", rin)
write_fraction("#{dir}/rin.occupancy", rin)
```

C.2. Difference between van der Waals interaction and close contact

In dynamic residue interaction network (dRIN) analysis, the interaction between residues is calculated using RING 2.0 software (*Piovesan et al., 2016*). In RING 2.0 software, the van der Waals (vdW) interaction is defined as:

$$d_{ij} - \left(\sigma_i + \sigma_j\right) < 0.5 \text{ Å}$$

where d_{ij} is interatomic distance between *i*- and *j*-th atoms, σ_i is the vdW radius of the *i*-th atom and σ_j is the vdW radius of the *j*-th atom. Furthermore, in RING 2.0 software, the atoms considered valid for the van der Waals interactions are limited:

All residues: Any C, Any S

Glutamine: NE2, OE1

Asparagine: ND2, OD1

Hence, in dRIN analysis, to investigate the interaction between residues that are not considered valid by the RING 2.0 software but are in close contact with each other, the close contact between residues is calculated. In dRIN analysis, the close contact between residues is calculated for all atoms (except the atoms considered valid for van der Waals interaction in RING 2.0 software). In dRIN analysis, the close contact is defined as:

$$d_{ij} - \left(\sigma_i + \sigma_j\right) < 0.4 \text{ Å}$$

where d_{ij} is interatomic distance between *i*- and *j*-th atoms, σ_i is the vdW radius of the *i*-th atom and σ_j is the vdW radius of the *j*-th atom.

From the physiochemical point of view, the van der Waals interaction are attraction or repulsion between non-bonded atoms, depending on the distance. At large interatomic distances, there is no van der Waals interaction between atoms. At intermediate distances, due to electron correlation, the two electron clouds form induced dipole-dipole interactions, which creates a weak attraction between atoms; the force associated with this interaction is called “London” or

"dispersion" force. At short distances, the negatively charged electrons repel each other as the two electron clouds overlap and thus there is repulsion between two atoms; this is defined by Pauli exclusion principle.

From the physiochemical point of view, when the atoms are in close contact, the negatively charged electrons repel each other as the two electron clouds overlap and thus there is repulsion between atoms; this is defined by Pauli exclusion principle.

C.3. Supplementary figures

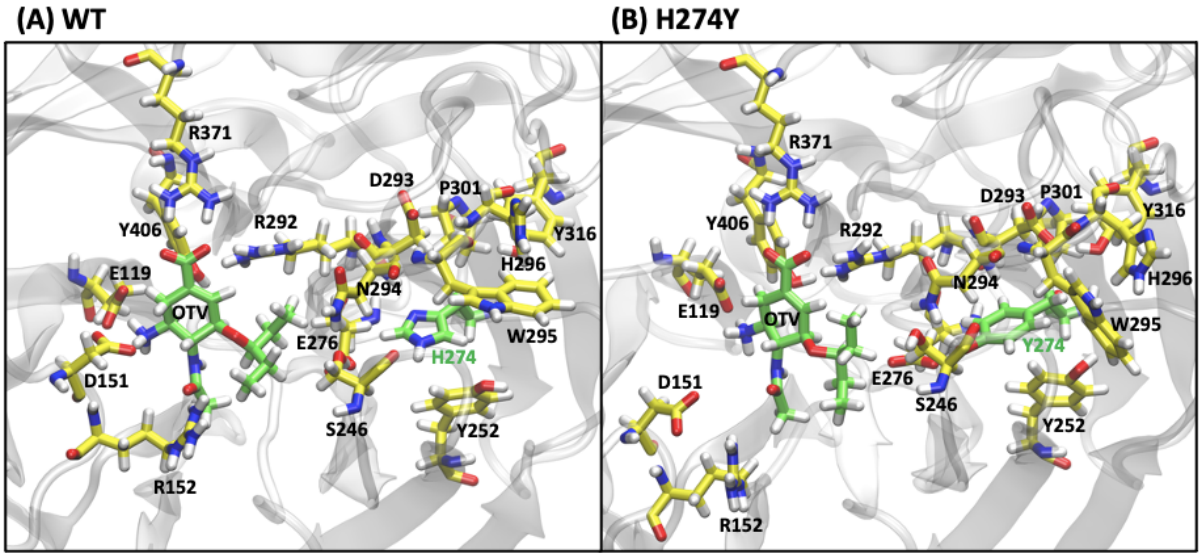

Figure C.1: Snapshot images of (A) wild type (WT) and (B) H274Y mutant neuraminidase-oseltamivir complexes obtained from MD simulations, showing oseltamivir (OTV) binding site and H274Y mutation site. OTV and residue 274 are shown in green, and the rest of the residues are shown in yellow.

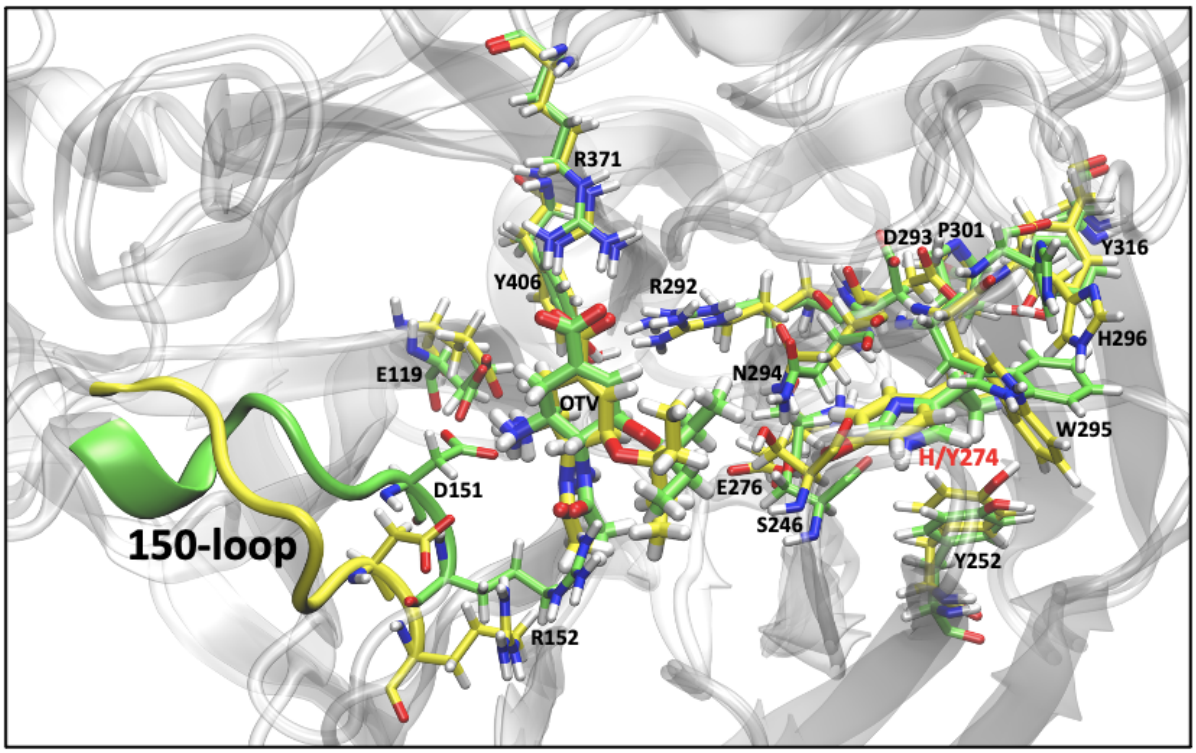

Figure C.2: Superimposed snapshot image of wild type (WT) and H274Y mutant neuraminidase-oseltamivir complexes obtained from MD simulations, showing oseltamivir (OTV) binding site and H274Y mutation site. WT NA-OTV complex is shown in green and H274Y mutant NA-OTV complex is shown in yellow. The 150-loop region is formed by residues 147-152.

C.4. Supplementary tables

Table C.1: Calculated binding free energy components of wild type (WT) and H274Y mutant neuraminidase for oseltamivir obtained from MM-PBSA calculations. Binding free energy includes van der Waals (vdW), electrostatic (ES), polar solvation, and non-polar solvation components.

	vdW [kcal mol^{-1}]	ES [kcal mol^{-1}]	Polar [kcal mol^{-1}]	Non-polar [kcal mol^{-1}]	Total [kcal mol^{-1}]
WT	−28.19 ± 0.08	−46.96 ± 0.08	43.51 ± 0.06	−3.54 ± 0.00	−35.19 ± 0.07
H274Y	−22.50 ± 0.09	−40.82 ± 0.10	39.35 ± 0.08	−3.31 ± 0.00	−27.28 ± 0.09

Table C.2: Calculated binding free energies of wild type (WT) and H274Y mutant neuraminidase for oseltamivir obtained from MM-PBSA calculations with the dielectric constant (ε) value set to 1.0.

	ΔH [kcal mol^{-1}]	$T\Delta S$ [kcal mol^{-1}]	ΔG [kcal mol^{-1}]	$\Delta\Delta G$ [kcal mol^{-1}]
WT	−32.84 ± 0.13	−23.65 ± 0.47	−9.19 ± 0.49	
H274Y	−21.65 ± 0.19	−22.94 ± 0.50	1.29 ± 0.53	10.48

Appendix D: Supplementary information of "Theoretical insights into the molecular mechanism of I117V mutation in neuraminidase mediated reduction of oseltamivir drug susceptibility in A/H5N1 influenza virus"

D.1. Error bar calculation

In Figures 4.4 and 4.5, the error bars represent 95% confidence intervals. The standard error of the mean (SE) is used to construct confidence intervals. Error bars equivalent to 2 X SE graphically represents 95% confidence interval.

$$\mathrm{SE} = \frac{s}{\sqrt{N}}$$

$$s = \sqrt{\frac{1}{N-1}\sum_{i=1}^{N}(x_i - \bar{x})^2}$$

where s is the standard deviation, N is the size of the sample, x_i is the observed value of sample i, $\bar{x}$ is the mean value of samples.

D.2. Supplementary figures

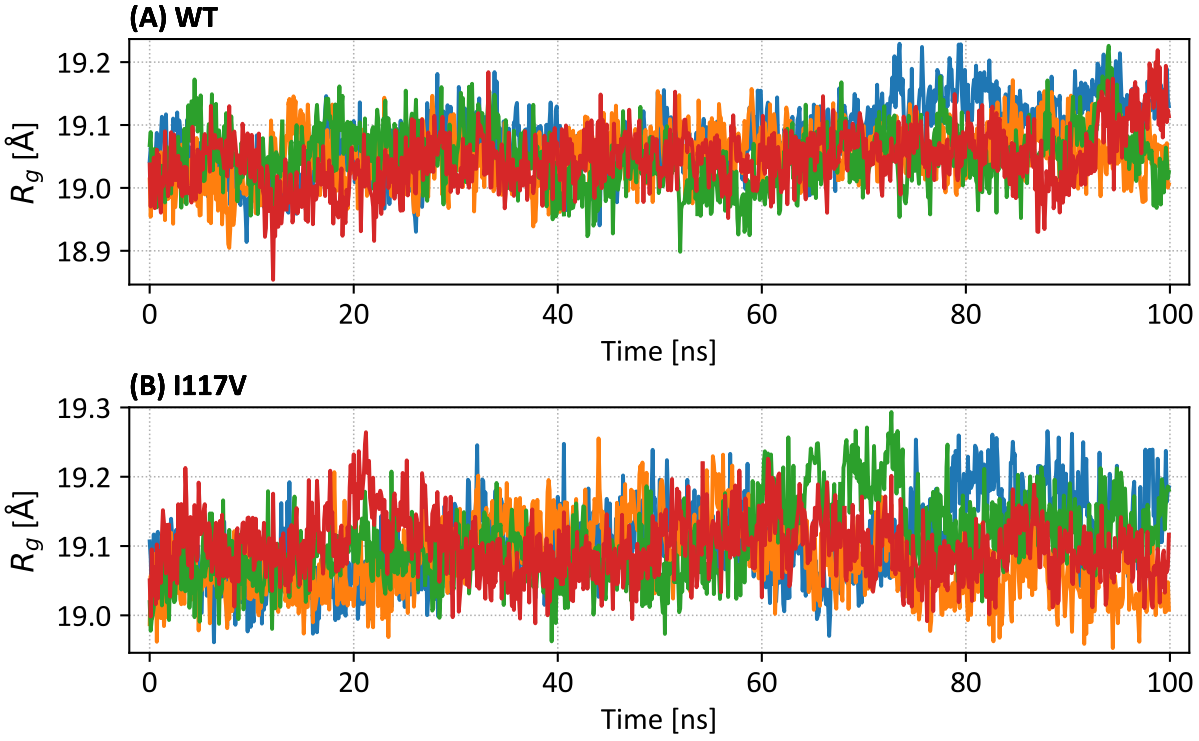

Figure D.1: The time series of radius of gyration (R_g) of four distinct MD trajectories of (A) wild type (WT) and (B) I117V mutant neuraminidase-oseltamivir complexes (from

***Yadav et al., 2021b*).** The R_g values were calculated for the protein backbone atoms in WT and I117V mutant NA for 15th to 365th amino acid residues, excluding both ends of NA, with respect to the initial structure along the simulation time. Figure extracted directly from the original article by *Yadav et al.* (*2021b*), without modifications (CC BY 4.0 license, https://creativecommons.org/licenses/by/4.0).

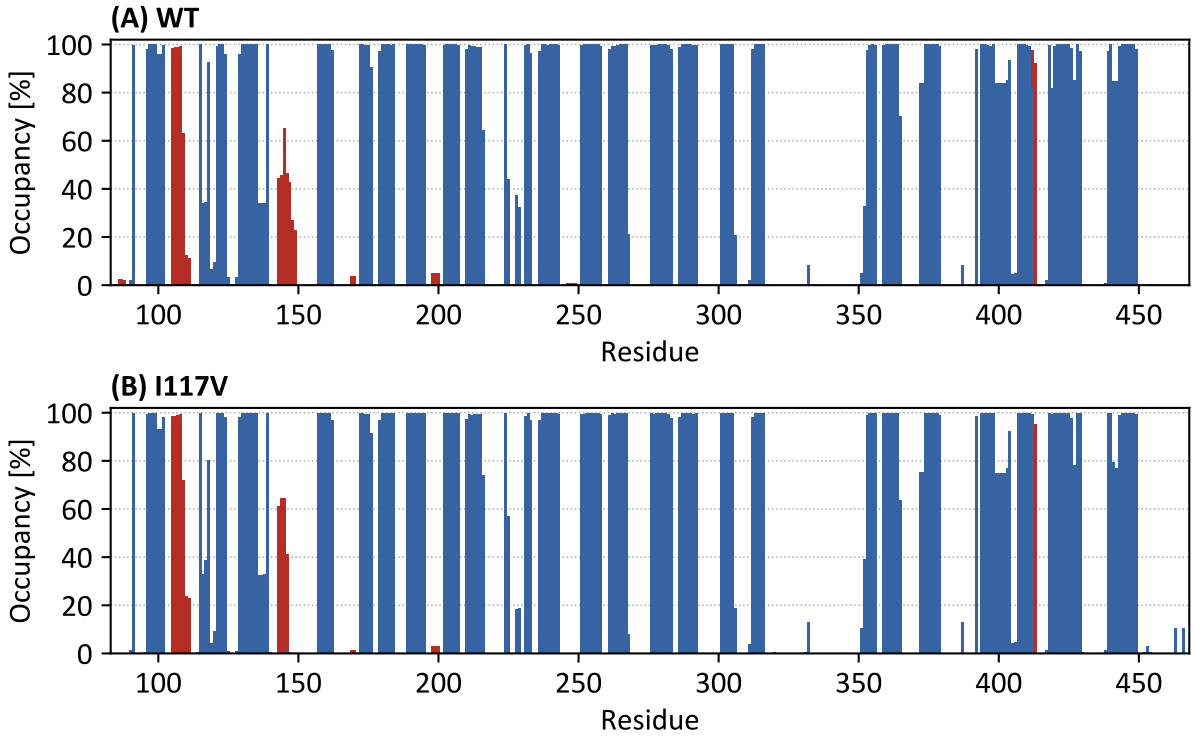

Figure D.2: Secondary structure occupancies of all amino acid residues of neuraminidase in (A) wild type (WT) and (B) I117V mutant neuraminidase-oseltamivir complexes (from *Yadav et al., 2021b*). Three categories (Helix, Sheet & Coil) were used to simplify the secondary structure classification. The helix component is shown by red bars and the sheet component is shown by blue bars, whereas the coil component is represented by the rest. Figure extracted directly from the original article by *Yadav et al.* (*2021b*), without modifications (CC BY 4.0 license, https://creativecommons.org/licenses/by/4.0).

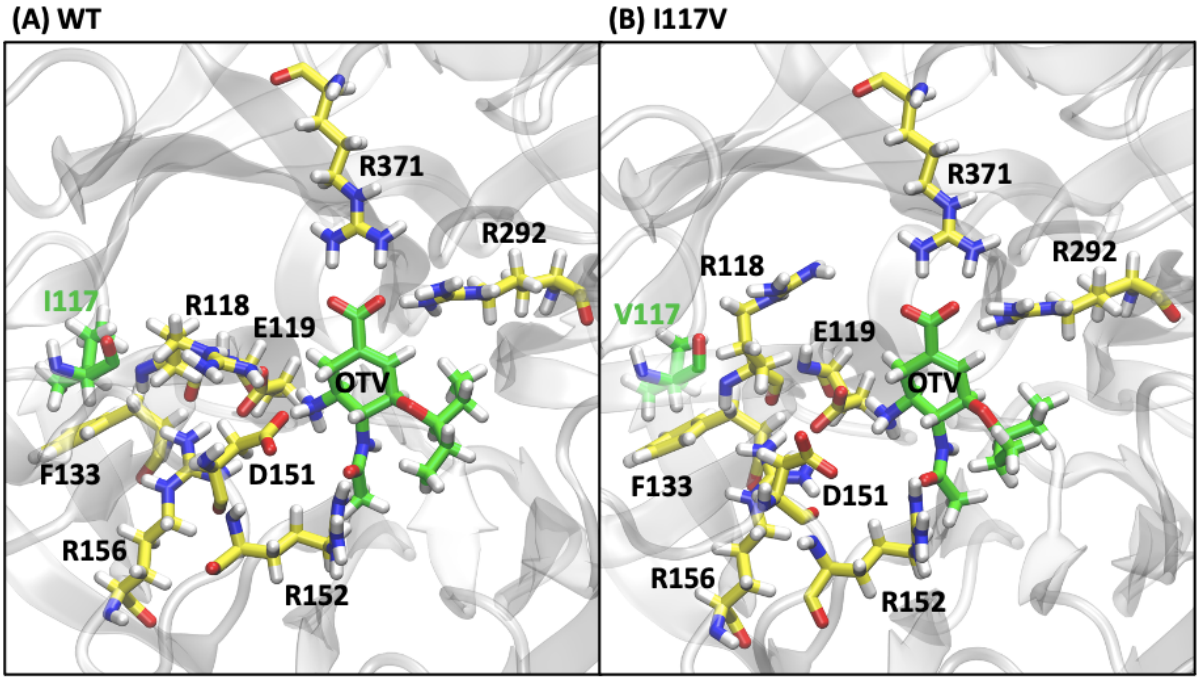

Figure D.3: Snapshot images of (A) wild type (WT) and (B) I117V mutant neuraminidase-oseltamivir complexes. Oseltamivir (OTV) and residue 117 are shown in green and the rest of the residues are shown in yellow.

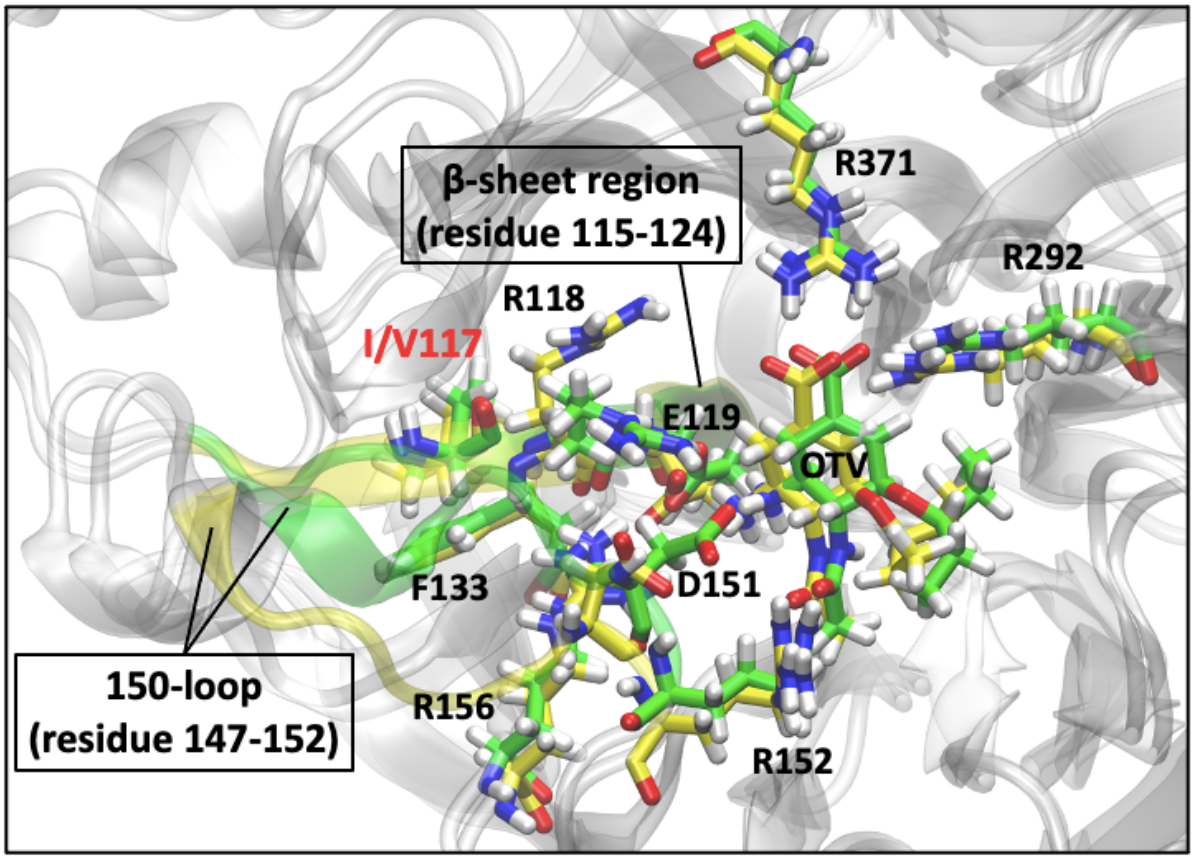

Figure D.4: Superimposed snapshot image of wild type (WT) and I117V mutant neuraminidase-oseltamivir complexes. WT NA-OTV complex is shown in green and I117V mutant NA-OTV complex is shown in yellow. The 150-loop region is formed by residues 147-152. The β-sheet region is formed by residues 115-124.

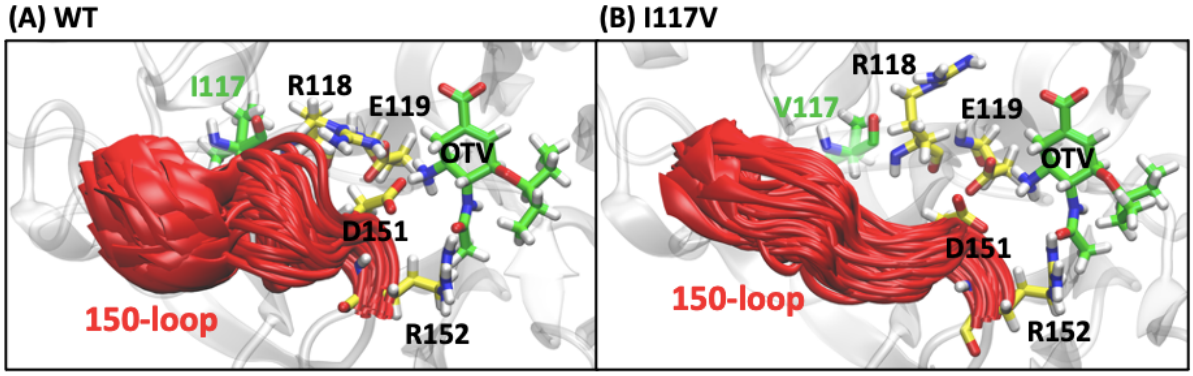

Figure D.5: Snapshot images of the 150-loop region (residues 147-152) of (A) wild type (WT) and (B) I117V mutant neuraminidase-oseltamivir complexes obtained from MD simulations. The 150-loop region of NA is shown in red, and conformational changes are represented by superimposing 100 snapshot images obtained from MD simulation. Oseltamivir (OTV) and residue 117 are shown in green. Rest of the residues are shown in yellow.